I.O.S.

THE PERMEABILITY AND CONSOLIDATION OF DEEP-SEA SEDIMENTS

BY

P. J. SCHULTHEISS AND D. E. GUNN

REPORT NO. 201

1985

OCEAN DISPOSAL OF HIGH LEVEL RADIOACTIVE WASTE
A RESEARCH REPORT PREPARED FOR THE DEPARTMENT
OF THE ENVIRONMENT

NATURAL ENVIRONMENT RESEARCH COUNCIL

INSTITUTE OF OCEANOGRAPHIC SCIENCES

INSTITUTE OF OCEANOGRAPHIC SCIENCES

Wormley, Godalming,
Surrey, GU8 5UB.
(0428 - 79 - 4141)

(Director: Dr. A.S. Laughton FRS)

Bidston Observatory,
Birkenhead,
Merseyside, L43 7RA.
(051 - 653 - 8633)

(Assistant Director: Dr D.E. Cartwright FRS)

Crossway,
Taunton,
Somerset, TA1 2DW.
(0823 - 86211)

(Assistant Director: M.J. Tucker)

When citing this document in a bibliography the reference should be given as follows:-

SCHULTHEISS, P.J. & GUNN, D.E. 1985 The permeability and consolidation of deep-sea sediments. *Institute of Oceanographic Sciences, Report*, No. 201, 94pp.

INSTITUTE OF OCEANOGRAPHIC SCIENCES

WORMLEY

The permeability and consolidation of deep-sea sediments

by

P.J. Schultheiss and D.E. Gunn

I.O.S. Report No. 201

1985

DEPARTMENT OF THE ENVIRONMENT
RADIOACTIVE WASTE MANAGEMENT
RESEARCH PROGRAMME 1982/84

DoE Report No.: DoE/RW 84/202

Contract Title: DoE selection and evaluation of sites for the disposal of high-level radioactive waste

DoE Reference: DGR 481/179

Report Title: The permeability and consolidation of deep sea sediments

Authors: SCHULTHEISS, P.J. and GUNN, D.E.

Date of submission to DoE: 6 December 1984

ABSTRACT

This report presents permeability and consolidation data for a wide range of sediment types. Permeability (also known as hydraulic conductivity when the permeant is water) is one of the two parameters which are needed to directly quantify pore water advection in deep sea sediments (the other is differential pore pressure) and which are being investigated in high-level radioactive waste study areas. While it is desirable that these parameters should be measured in situ it is argued that values of permeability can be measured sufficiently accurately in the laboratory from core samples. Consequently, an apparatus has been developed which enables sediment permeability to be measured at decreasing void ratios during a back-pressured consolidation test. Data presented in this report from over 60 samples has established the major differences in permeability between various sediment types and how permeability changes as a function of burial depth and void ratio. Samples from two study areas in the North Atlantic Ocean, King's Trough Flank (KTF) and Great Meteor East (GME), have been compared with samples of Red Clay (RC) obtained from the NW Pacific Ocean. Typically, the permeability of the nannofossil turbidites in the GME area is 1×10^{-5} mm/s but increases dramatically to 1×10^{-3} mm/s in their silty bases. The marls and oozes in the KTF area generally have higher permeabilities around 5×10^{-5} mm/s. Permeabilities of the RC samples range from 1×10^{-4} near the surface to less than 1×10^{-7} mm/s at a sub-bottom depth of 170 m.

Keywords: Disposal under deep ocean bed (94)
Soil/sediments (131)
Geotechnics (113)
Sediment structure/permeability (117)
Laboratory experiments (123)

This work has been commissioned by the Department of the Environment as part of its radioactive waste management research programme. The results will be used in the formulation of Government policy but, at this stage, they do not necessarily represent Government policy.

CONTENTS

1. INTRODUCTION

Burial of high-level radioactive waste in deep sea sediments would create a series of natural and artifical barriers which would inhibit or delay the transfer of radionuclides back to man (Hinga et al., 1982). These barriers are: the waste form, the waste canister, the sediment surrounding the canister, the benthic boundary layer and the water column.

Within the sediment barrier the mechanisms for transport of radionuclides which have escaped from the canister are by diffusion, advection and convection. The rate of transfer between the canister and the benthic boundary layer will also depend largely on the sorption of radionuclides onto solid sediment particles. The work described in this report is concerned with the evaluation of natural pore water fluxes in deep sea sediments (i.e. advection). It is not concerned with the problems of disturbance to the sedimentary environment which will undoubtedly result from the emplacement of the canister (near field); it is concerned solely with the far field environment where there would originally be no disturbance.

The only known natural steady-state driving forces for pore-water movement within deep-sea sediments are compaction and geothermal heating (Hollister et al., 1981). Pore water movement caused by compaction can probably be regarded as negligible in deep-sea sediments where the accumulation rates are very slow (<2 cm/1000 years) and the sediments have consolidated normally. It has been suggested that vertical convection of pore fluid through the sedimentary layer is an important component of the total heat transfer through the sea floor and may exist over one-third of the world's ocean floor (Anderson et al., 1979). There is, however, a large discrepancy (up to three orders of magnitude) between the upward advection rates calculated from non-linear temperature profiles and those calculated from pore water chemistry profiles (Crowe and McDuff, 1979). The non-linear temperature profiles give the higher advection rates. The curvature of the non-linear temperature profiles is quite insensitive to advection rates; a resolution of 20 cm/year is probably the best that can be achieved with a 5-metre long lance (Noel, 1984). Noel (1983) discusses mechanisms other than pore water advection which would cause non-linear temperature profiles. His analysis sheds some doubt on interpretations of such profiles which are based solely on the mechanism of pore water advection. In order to resolve the uncertainties surrounding the calculation of pore water fluxes, another measurement technique is needed.

2. PORE WATER FLUXES

Deep sea sediments consist of a framework of particles with widely-differing shapes and sizes in sea water. The interconnecting network of pore spaces renders the sediments permeable. Any mass transfer of water through these pore spaces can only occur if a non-hydrostatic pressure gradient exists in the pore water.

The flow of fluids through permeable media was investigated by Henry Darcy in 1856. From his experiments on sand samples he concluded that the rate of flow (volume per unit time) Q is proportional to the cross-sectional area of the sample (A) and the hydraulic gradient, i. The non-dimensional hydraulic gradient is the non-hydrostatic pressure head per unit length of the sample. Darcy's Law can, therefore, be written as

$$Q = kiA \qquad (1)$$

The constant of proportionality, k, is the permeability of the system and has the units of velocity. Permeability defined in this way is dependent on the characteristics of both the fluid and solid phases. It is most often expressed this way in hydrology and soil mechanics because only one permeant (water) is usually considered. In this case, it is also known as hydraulic conductivity. An absolute permeability, K (which has units of area), of a material is independent of the permeant and is obtained using

$$K = k\mu/\gamma \ (m^2) \qquad (2)$$

where μ = viscosity of permeant (centipoise, Pa.s)
γ = density of permeant (kg m^{-2})

To correct laboratory measured values of permeability to in-situ values the following equation should, therefore, be used

$$k_i = k_l \frac{\mu_l}{\mu_i} \frac{\gamma_i}{\gamma_l}$$

where the subscript, i, denotes in-situ values and the subscript, l, denotes laboratory values. For most laboratory measurements made at ~20°C and atmospheric pressure the corrected in-situ permeability value k_i for sediments at ~5000m would be

$$k_i = 0.7\ k_l$$

It is often useful to express the velocity, v, of an element of water approaching the sediment in a water column; in this case, from equation 1

$$V = Q/A = ki \qquad (3)$$

The velocity of an element of water in the sediment (seepage velocity, V_s) is given by

$$V_s = \frac{v}{n} \qquad \text{where n is the porosity}$$

therefore

$$V_s = \frac{ki}{n} \qquad (4)$$

The importance of this simple expression for calculating the seepage velocity is that it provides the vertical component of migration velocity for pore water and radionuclides through a sediment under a given hydraulic gradient.

In equation 4, three parameters are required to calculate the seepage velocity V_s; these are the permeability, k, the hydraulic gradient, i, and the porosity, n. The hydraulic gradient can only be measured in situ and a probe for making this measurement has been developed at IOS (Schultheiss et al., 1984).

The IOS research programme to calculate pore water advection in deep-sea sediments from pore pressures, permeability and porosity is shown as a flow chart in Figure 1. This report deals only with those aspects of the flow chart which involve the determination of permeability in the laboratory.

3. PERMEABILITY OF DEEP SEA SEDIMENTS

The overall objective of this research project is to assess natural flow rates of pore water in deep sea sediments. An essential component of this project is to define accurately the in-situ permeability profiles of the sediments that exist in appropriate study areas. In order to achieve this, the programme of work being followed by IOS includes the following:

1. Obtain relatively undisturbed samples of a wide range of sediment types.
2. Measure the permeability of these sediments at decreasing void ratios in the laboratory.
3. Develop an in-situ permeability capability in order to assess the validity of the laboratory measurements.

Permeability measurements of terrestrial soils have, in general, been found to exhibit large differences between in-situ and laboratory measurements. The major discrepancy arises as a result of unrepresentative sampling rather than physical disturbance to the sample. Although there is no directly comparable data for deep-sea sediments, it is probable that the situation may, at least in many areas, be different from the terrestrial experience. Many areas of deep-sea sediments probably do not exhibit the inhomogeneities, such as fractures and

fissures, which drastically effect the permeability of terrestrial soils. Consequently, high-quality sampling and laboratory-determined permeabilities of deep-sea sediments may represent much more closely the in-situ permeability than similar techniques have found on land. It is this reasoning that has determined the rationale of the research programme, whereby the laboratory assessment of permeability takes priority over in-situ testing. However, the observation of open burrows (Weaver and Schultheiss, 1983) illustrates that, even in the deep sea, the effects of unrepresentative sampling must still be carefully considered.

The soil mechanics and soil science literatures contain many references relating to the measurement of permeability in the laboratory. Lambe and Whitman (1979) provide a clear discussion of fluid flow through permeable media and discuss the falling and constant head methods. Olsen and Daniel (1981) provide an excellent summary of both laboratory and field techniques for determining the permeability of fine-grained soils. The main laboratory methods are the constant head method, the falling head method (both direct measurements) and the one-dimensional consolidation testing method (in direct method; permeability is calculated using Terzaghi's theory (Terzaghi, 1925, 1943) from the coefficient of consolidation, the volume compressibility and void ratio).

Published data on the permeability characteristics of deep-sea sediments is limited. Bryant et al. (1975) present data from a large number of natural marine sediment samples from the Gulf of Mexico. This permeability data was calculated from consolidation tests on a variety of samples ranging from clays to sandy clays and silts. The strongest correlation was obtained between the coefficient of permeability and the porosity among groups sorted according to grain size. Nickerson (1978) conducted both consolidation and constant head permeability tests on ten samples from the central North Pacific Ocean. The coefficient of permeability calculated from consolidation theory correlated poorly with the values obtained directly from the constant head tests. In nearly all cases, the permeability values obtained from Terzaghi's consolidation theory were lower than those obtained from direct measurements. It was concluded that the permeability values obtained from consolidation theory were not very reliable. Clukey and Silva (1982) found a similar discrepancy between calculated and measured values of permeability on sediments from the East Bermuda Rise and Blake Bahama Ridge. Silva et al. (1981) describe a consolidation system allowing direct permeability measurements to be made under back pressures of up to 3100 kPa with hydraulic gradients ranging from 2 to over 10,000. They present data for different deep-sea sediment types (see Figure 60) showing permeabilities ranging from

2×10^{-4} mm/s (for a calcareous nanno ooze at a void ratio of 1.6) to
6×10^{-8} mm/s (for a smectite clay at a void ratio of 3).

The system, designed and built at IOS to measure consolidation and permeability directly, was influenced by the type of equipment used in some of the above references and is described in the following section.

4. THE IOS CONSOLIDATION AND PERMEABILITY APPARATUS

The apparatus used to measure the consolidation and permeability characteristics of sediments at IOS is shown schematically in Figure 2. The system is based on a consolidation cell (Fig. 3) which has the following features:

1. Corrosion-resistant materials enables the cell to be saturated with sea water and a back pressure of up to 700 kPa can be applied to ensure that any free gas in the sample or in the cell is forced back into solution.
2. Either 50-mm or 75-mm diameter samples 20 mm in height can be tested in the cell. The samples are taken in a 'teflon' coated stainless steel sampling ring direct from the core. These are stacked under sea water during transport and are stored at 4°C until ready for testing. The sampling ring fits directly into the consolidation cell which alleviates any further disturbance to the sample when it is being loaded for a test.
3. Drainage through thin, sintered, porous stainless steel discs from both the top and/or bottom of the samples enable both consolidation and direct permeability tests to be performed.
4. The complete system is enclosed in a constant temperature room which is kept at 27°C ± 0.25°C. Temperature stability is necessary in order that rapid (1-2 hours) permeability measurements can be made in clays. Temperature changes cause differential expansion in the system which would cause an apparent flow in the volume change unit.

Consolidation of the sample is achieved using a consolidation frame with a lever ratio of 10:1. Loads are applied in incremental steps while the sample thickness is monitored using a dial gauge. The size of each incremental step depends on the type of sample being tested. It is normally half of the existing load but never exceeds the existing load. At the end of each loading step the lever arm can be locked in position to prevent any creep while the permeability test is performed. The system diagram (Figure 2) illustrates how a constant head permeability test is performed. Back pressure is supplied from an air compressor and regulator which feeds two bladder-type air/water interchange units. The back pressure is monitored by a pressure gauge next to the priming system which enables

the system to be bled. The air/water interface units are connected to the top and bottom drainage ports of the sample cell via two de-aired water/paraffin/salt-water interchange units. These units ensure that salt water is confined to the sample area only and does not contaminate the rest of the system. A constant head permeability test is performed by adjusting the relative heights of the air/water interface units. The difference in height between the two units (Δh) is the head of water which causes flow around the system and through the sample; it is measured using a differential pressure transducer accurate to 0.05 kPa. Hydraulic gradients used in the permeability tests varied between 2 and 100. No significant variation in permeability was observed by using different hydraulic gradients between these limits.

The rate of water flow during the permeability test is measured using a high precision capillary tube volume change unit. This unit consists of a set of horizontal parallel glass capillary tubes with a coloured paraffin/water interface in each. Internal tube diameters range from 0.25 mm to 2.0 mm and each tube is approximately 1m long. A reversing valve enables the flow in the tubes to be in either direction irrespective of the flow direction in the system. Selection of tubes is achieved with a multiway valve depending on the flow rate during the test. A volume change resolution as little as 5×10^{-5} cm^3 is achievable using the 0.25-mm diameter tube. This enables the permeability test to be performed relatively rapidly (a few minutes to two hours, depending on the permeability) even at small hydraulic gradients. It is normal for the flow rate to be assessed at several different hydraulic gradients in both directions in order to calculate the permeability. The consolidation of the samples is monitored using a Linear Variable Displacement Transformer (LVDT) to obtain the height of the sample and a differential pressure transducer to obtain the pressure difference across the sample. Voltage readings from these transducers are taken during a single scan which is controlled by a microcomputer. Scan rates can be set as fast as four per minute. The data logged in this way is presented on the printer as tables or as graphs for any channel.

Apart from the data obtained using the IOS apparatus data from two other sources is incorporated in this report. Samples were provided with the Universities of North Wales and Oxford (UCNW and OX). The consolidation technique used by UCNW is an incremental loading one without the application of a back pressure (standard consolidation test); no direct permeability data is available from this test. The Oxford consolidation test provides a continuous stress-strain curve by using a flow restrictor to control the rate of drainage.

Permeability, at any time during the test, is calculated from the rate of flow and the pressure difference across the sample. A report on this contract is provided in Appendix A.

5. RESULTS

Data from all the consolidation and permeability tests are presented graphically in Figures 7-58 in the same order as they appear in Table 1. Where the data set is complete for each sample three graphs are presented. Graph 1 (bottom-left) is an e-log σ' plot (void ratio [e] versus log [vertical effective stress (σ')]); this graph depicts the consolidation behaviour of the sample. and Graph 2 (bottom-right) is an e-log k plot (void ratio versus log [permeability]); this graph characterises the permeability of the sediment type throughout the range of void ratios in the consolidation test. Graph 3 (top-right) is a σ-log k plot (vertical effective stress versus log [permeability]); this graph illustrates the change in permeability with increasing overburden pressure assuming normal consolidation.

A summary of the pertinent consolidation and permeability parameters are given in Table 1. Samples tested at Oxford, University College of North Wales IOS are designated OX, UCNW and IOS respectively. Orientation refers to the axis of the sample; hence, V (vertical) implies that the consolidation direction and the water flow was parallel to the core axis; H (horizontal) implies that the flow and the consolidation are normal to the core axis. R is a remoulded sample. Sediment type is given by a broad definition based on carbonate analysis and microscope observation. The following broad classification has been used:

Per cent carbonate	
100 - 70	- ooze
70 - 30	- marl
30 - 5	- calcareous clay
5 - 0	- clay

The carbonate fraction is divided up into percentages of forams and nannofossils:

Percent forams	Percent nannofossils	
100 - 70	0 - 30	foram
70 - 30	30 - 70	foram nanno
30 - 0	70 - 100	nanno

Hence the following initials represent the sediment types shown below:

NM - nanno marl
FNM - foram nanno marl
FNO - foram nanno ooze
CPC - calcareous pelagic clay
ARC - Atlantic red clay
PRC - Pacific red clay

SUB-BOT DEPTH is the depth from the top of the core which is assumed to be the sediment surface. e_0 is the initial void ratio. OCR is the over-consolidation ratio given by σ'_c/σ'_0 where σ'_c is an estimate of the maximum past preconsolidation stress obtained from the e-log σ' curve using the technique proposed by Casagrande (1936), and σ'_0 is the vertical effective stress on the sample in situ (calculated by integrating the bulk density profile to the required depth). It is not unusual for deep sea sediments to exhibit an over-consolidated behaviour with having been subjected to any excess overburden stresses. This 'apparent' overconsolidation appears to be characteristic of sediments having a very low rate of accumulation (Richards & Hamilton, 1967). C_c is the compressibility index for the 'straight line' part of the e-log σ' plot where C_c is given by

$$C_c = - \frac{\Delta e}{\Delta(\log \sigma')}$$

C_c is thus the change in void ratio per logarithmic cycle of stress.

The estimated in-situ permeability (ignoring temperature and hydrostatic pressure effects) of the sample at σ'_c (k at σ'_c) is obtained from the e-log k plot where e corresponds to the appropriate value of σ'_c.

k_c is the permeability index which is defined by

$$k_c = \frac{\Delta e}{\Delta(\log k)}$$

and is taken from a straight line estimated from the e-log k plot. k_c is thus the change in void ratio per logarithmic cycle of permeability.

The locations and water depths from which the cores were taken are shown in Table 2. The area is given for convenience with reference to the study sites for high-level radioactive waste disposal (Searle, 1979; Anderson, 1981). These are:

is interesting to compare both the consolidation and permeability data obtained from all the red clay samples with the values inferred at σ'_o from individual samples (Fig. 5). Values of C_c for the individual samples range from 1.0 to 3.0 with an average of 1.75. This compares favourably with the value 2.1 obtained from the σ'_o plot. Values of k_c for the individual samples range from 1.0 to 2.2 with an average of 1.35. This again compares favourably with the value 1.2 obtained from the σ'_o plot. It can be concluded, therefore, that the individual consolidation and permeability characteristics which are measured over a period of only 2 to 3 weeks are comparable with the consolidation process which occurs naturally over millions of years in Pacific Red clays.

6.2 GME Sediments

The GME study area (Searle et al., 1984) is dominated by a sequence of distal nannofossil turbidites named a, b, c, ... g, Fig. 6) which are discussed by Weaver and Kuijpers (1983); thicknesses of individual turbidites vary between a few centimetres and a few metres. The bases of some of the turbidites contain sands and silts which thin and eventually disappear as the unit becomes more distal (i.e. in the west of the area). Between each turbidite unit a thin pelagic interval of marl or calcareous clay is present and is typically only a few centimetres thick.

Figure 42 (10965/2/14) is typical of the consolidation and permeability behaviour of the nannofossil turbidites. It exhibits a high void ratio and has a high compressibility index (1.1). Samples from the same turbidite (b) in core S126/4 exhibit even higher void ratios towards the top (up to 5.2) with C_c values as high as 1.5.

At the base of some turbidites (in particular b, e and f) the silt component increases rapidly with a consequent increase in the permeability and decrease in the compressibility index. Figure 47 (10695/8/16) illustrates the behaviour of a very silty base. The void ratio is below 2 with a C_c value of only 0.5. To illustrate the change in permeability that occurs the profile for core 10695 is shown in Figure 6. It should be noted that the permeability in the silty bases can be over two orders of magnitude higher than in the bulk of the turbidite unit.

6.3 Permeability Anisotropy and Open Burrows

It is possible that both depositional and post-depositional processes can result in permeability anisotropy. During deposition the grain structure can become orientated in such a way that the tortuosity in one direction is

systematically greater than in another direction with a consequent difference in permeability. In addition to this, bioturbation effects could preferentially effect the permeability in a given direction by either creating filled burrows with a different permeability or by creating open burrows. Evidence to support the existence of both these processes has been found in the samples tested. Samples D10316/3 and 4 (foram nanno marl) are shown together in Figure 22. The horizontal permeability (k_h) is greater than the vertical permeability at high void ratios ($k_h/k_v \approx 3$) but this ratio decreases as the sample is consolidated. Samples D10321/6 and 7 are calcareous pelagic clays (Figure 28) and exhibit no significant permeability anisotropy.

In turbidite (b) in core S126/4 open burrows were observed on freshly fractured surfaces (Weaver & Schultheiss, 1983). One type of burrow, which is only about 0.5 mm in diameter and extends vertically down to 1.7 m was numerous (approximately 1 per 2 cm^2). Samples tested in this burrowed region (S126/4-5 and 6) are shown in Figure 53 and reveal a greater permeability in the direction of burrowing (vertically). Compare this with the samples tested in the same turbidite but below the zone of burrowing (S126/4-9 and 10) in Figure 54. In this case, the horizontal permeability is slightly greater than the vertical permeability. It should be noted that the permeability anisotropy discussed in this section is relatively small compared with the change in permeability caused by different sediment types.

6.4 Comparison of IOS and Oxford data

The samples tested in the Engineering Science department at Oxford University employed an unconventional consolidation technique which is described in Appendix A. It is, therefore, instructive to compare the data obtained from this technique and the more conventional technique used at IOS.

Although many of the samples tested at Oxford and IOS can be considered to be similar, only a few can be considered to be practically identical. This is because only they were taken adjacent to one another in the core. The three pairs of samples considered to be most similar are shown in Table 3 and are plotted for ease of comparison in Figures 9, 14 and 29.

The most striking feature about the two sets of data is the difference between the e-log σ' curves; the Oxford data shows a consistent offset on the stress axis from the IOS data but with similar compressibility indices. The most obvious conclusion to be drawn is that there is an error in the calculation of the vertical effective stress for the Oxford data. This is because the OCRs for all

Core	Sample	Tested at	OCR	C_c	k_c	k at σ'_c mm/s $x^{-6}10$
D10298	9	OX	18.0	1.5	2.5	11.0
D10298	10	IOS	4.0	1.3	1.8	70.0
D10314	5	OX	9.1	1.3	1.3	16.0
D10314	6	IOS	1.5	1.0	1.4	18.0
D10321	10	OX	11.0	0.8	0.9	10.0
D10321	11	IOS	2.9	0.8	1.2	20.0

Table 3 - Consolidation and permeability data from six samples to compare the differences between the Oxford and IOS data.

the Oxford data are generally much higher than the IOS and UCNW values and are much higher than would be expected. However, despite having checked the data and method, no such error can be found. It must be concluded, on the basis of the data available from this study that the differences observed between the two consolidation techniques require that further, more controlled, comparative tests on identical samples are undertaken.

Permeability versus void ratio plots in Figures 9, 14 and 29 show the IOS data to have consistently higher values of permeability by a factor of between 2 and 7 compared with the Oxford data. The combined effects of the differences in the e-log σ' and e-log k graphs causes both the IOS and Oxford data in the σ'-log k graph to be comparable.

6.5 Comparison of Different Sediment Types

One of the primary objectives of this study is to compare the permeabilities of different sediment types. While the data has already been presented it is instructive to make a direct comparison by plotting different sediment types on the same graph. Consequently, the following samples have been chosen as being representative of the different types of sediments tested:

Pacific Red clay	GC576A 3-5
Atlantic Red clay	D10314/15
Calcareous Pelagic clay	D10321/11
Foram Nanno ooze	D10333/7
Nanno Fossil marl (turbidite)	D10695/2-14
Silt (base of turbidite)	D10695/8-16

They have been plotted for comparison in Figure 59. It is clear that the permeability void ratio relationships for these six sediment types varies considerably. At one end of the spectrum the red clays with their very fine-grain sizes have the lowest permeability with the Pacific Red clay being less permeable than the Atlantic Red clay for the same void ratio. However, it should be noticed that because of the large compressibility index and the high initial void ratio the permeability changes very rapidly in the first 50 m of burial. The calcareous pelagic clay, the nanno fossil turbidite and the foram nanno marl increase in permeability in that order, as expected. The silty base to the turbidite has the greatest permeability being some 100,000 times more permeable than the red clays. It is probable that the permeability of this silty base will increase, possibly by another 10 or 100 times as it is traced to less distal parts of the GME area where the grain size increases. A comparison has been made in Figure 60 between the permeability data from Figure 59 and the permeability data of Silva et al., 1981. It can be seen that, while the samples chosen from this study do not cover the higher void ratios, the overall pattern of the data is very similar.

CONCLUSIONS

1. The consolidation characteristics obtained from samples of Pacific red clay and measured in a period of only two to three weeks are comparable with the consolidation process which occurs naturally over millions of years.
2. The permeability of the Pacific red clay rapidly decreases by more than three orders of magnitude in the top 160 metres below the sea floor. Surface values lie between 1×10^{-4} and 1×10^{-5} mm/s whle at 160 metres values between 1×10^{-7} and 1×10^{-8} mm/s have been measured.
3. Below about 20 metres below the sea floor the Pacific red clays are normally consolidated. Above this they exhibit an apparent over-consolidated behaviour.
4. The permeability profile of the sediments in the GME area is dominated by the silty bases at the base of some turbidites. Permeability values in the pelagic units and the major part of the fine-grained turbidites are about 1×10^{-5} mm/s whereas is the silts this value can be as high as 1×10^{-3} mm/s.
5. The ratio of horizontal permeability (k_h) to vertical permeability (k_v) was found to be small. Values of k_h/k_v ranged from 0 to 3.
6. The consolidation data from the Oxford tests produces over-consolidation

ratios that are much higher than those obtained from the IOS and UCNW values and are higher than expected. Further controlled tests are required to compare the differences in the two consolidation techniques.

7. Permeabilities from the IOS tests are generally higher than the Oxford data by a factor of between 2 and 7.
8. The permeabilities measured in all the tests is very large and ranges from 1×10^{-3} mm/s for the silts at the base of the turbidite units to 1×10^{-8} mm/s for Pacific red clays.

ACKNOWLEDGEMENTS

The authors would like to thank G. Sills (Oxford) and Mike Lovel (UCNW) for performing some of the tests in their laboratories and for providing comments on the interpretation of the data. Thanks are extended to R. Schuttenhelm at the State Geological Service of the Netherlands (RGD) who kindly provided us with two samples from core 80PC04. We also appreciate the valuable comments made by R.B. Whitmarsh and T.J.G. Francis who reviewed this manuscript.

REFERENCES

Anderson, D.R. (Ed.) 1981. Proceedings of the sixth annual NEA - seabed working group meeting, Paris. Sandia National Laboratories, SAND 81-0427.

Anderson, R.N., Hobart, M.A. and Langseth, M.G., 1979. Geothermal convection through oceanic crust and sediments in the Indian Ocean. Science, 204, 828-832.

Bryant, W.R., Hoffman, W. and Trabant, P., 1975. Permeability of unconsolidated and consolidated marine sediments, Gulf of Mexico. Marine Geotechnology, 1, 1, pp. 1-14.

Casagrande, A., 1936. The determination of the preconsolidation load and its practical significance. Proc. 1st Int. Conf. Soil Mech. Found. Eng., Cambridge, Mass., p. 60.

Clukey, E.C. and Silva, A.J., 1982. Permeability of deep sea clays: Northwestern Atlantic. Marine Geotechnology, 5, 1, pp. 1-26.

Crowe, J. and McDuff, R.E., 1979. Temperature and pore-water chemistry profiles of sediments in the equatorial Pacific: incompatible results? EOS, Trans. Am. geophys. Un., 60, 863.

Hinga, K.R., Heath, G.R., Anderson, D.R. and Hollister, C.D., 1982. Disposal of high-level radioactive wastes by burial in the seafloor. Environmental Science and Technology, 16, 1, pp. 28A-37A.

Hollister, C.D., Anderson, D.R. and Heath, G.R., 1981. Subseabed disposal of nuclear wastes. Science, 213, 4514, 1321-1326.

Lambe, T.W. and Whitman, R.V., 1979. Soil Mechanics. John Wiley, N.Y., 553 pp.

Nickerson, C.R., 1978. Consolidation and permeability characteristics of deep-sea sediments: North Central Pacific Ocean. M.Sc. Thesis, Worcester Polytechnic Institute, Worcester, Mass., U.S.A., 212 pp.

Noel, M.J., 1983. Origins and significance of non-linear temperature profiles in deep-sea sediments. Geophysical Journal, 76, 673-690.

Noel, M.J., 1984. Pers. comm.

Olsen, R.E. and Daniel, D.E., 1981. Measurement of the hydraulic conductivity of fine-grained soils. In: Permeability and Groundwater Contaminant Transport, T.F. Zimmie and C.O. Riggs (Eds.), ASTM, STP 746, pp. 18-64.

Richards, A.F. and Hamilton, E.L., 1967. Investigation of deep-sea sediment cores: 3 - Consolidation. In: A.F. Richards (ed.), Marine Geotechnique, Univ. Illinois Press, Urbana, Illinois, U.S.A., pp. 93-117.

Searle, R.C., 1979. Guidelines for the selection of sites for disposal of

radioactive waste on or beneath the ocean floor. IOS Report No. 91, 37 pp.

Searle, R.C., Schultheiss, P.J., Weaver, P.P.E., Noel, M.J., Kidd, R.B., Jacobs, C.L. and Huggett, Q.J., 1984. Great Meteor East (Distal Madeira Abyssal Plain): Geological studies of its suitability for disposal of heat-emitting radioactive wastes. IOS report (in press).

Silva, A.J., Hetherman, J.R. and Calnan, D.I., 1981. Low-gradient permeability testing of fine-grained marine sediments. In: Permeability and Groundwater Contaminant Transport, ASTM STP 746, T.F. Zimmie and C.O. Riggs (Eds.), American Society for Testing and Materials, pp. 121-136.

Schultheiss, P.J., McPhail, S.D., Packwood, A.R. and Hart, B. An instrument to measure differential pore pressures in deep-sea sediment. IOS report (in preparation).

Terzaghi, K., 1925. Principles of Soil Mechanics: III - Determination of Permeability of Clay. Engineering New Record, Vol. 95.

Terzaghi, K., 1943. Theoretical Soil Mechanics. John Wiley and Sons, New York.

Weaver, P.P.E. and Kuijpers, A., 1983. Climatic control of turbidite deposition on the Madeira Abyssal plain. Nature, 306, 5941, pp. 360-363.

Weaver, P.P.E. and Schultheiss, P.J., 1983. Vertical open burrows in deep-sea sediments 2 m in length. Nature, 301, 5898, pp. 329-331.

FIGURE CAPTIONS

FIGURE CAPTIONS continued

FIGURE CAPTIONS continued

APPENDIX A

Final contract report from Oxford University, Department of Engineering Science by G.C. Sills (co-ordinator)

STRESS STRAIN RELATIONSHIPS FOR DEEP SEA CORES - Report of conclusion of contract

1. Introduction

A new consolidation test has been developed at Oxford University to provide a continuous stress-strain curve over any required range of loading in a period of not more than 10 hours. Permeability values can also be obtained from the test.

This current programme of tests is the first substantial one to be undertaken. As a result, some minor problems have occurred, highlighting one or two experimental weaknesses. These are discussed later in this report but, nevertheless, the test has been proved to be generally successful.

2. The Restricted Flow Consolidation Test

The soil sample is laterally confined, with drainage permitted from only one face of the sample. The total required load is applied in one increment and water from the drained face passes through a flow restrictor connected into the back pressure system so that only a small proportion of the total pressure drop occurs across the soil sample. The pore pressures are measured on both the undrained and drained faces, represented respectively by u_1 and u_2. The closer u_1 and u_2 are in magnitude, the more uniform is the pore pressure distribution across the sample and, therefore, the more uniform is the effective stress $\sigma' = \sigma - \frac{1}{3}(2u_1 + u_2)$, assuming a parabolic distribution of pore pressure. A measure of the non-uniformity of the effective stress is given by the difference between the two pore pressure values. During the course of a test, the effective stress changes continuously from an initial zero value to a final value equal to the total stress. By monitoring the settlement of the soil sample, the corresponding void ratio changes can also be calculated and a continuous effective stress-void ratio relationship produced.

It is also possible to calculate the permeability from the pore pressure and settlement measurements. At the drained face, the pore pressure gradient $du/dx = 2(u_1 - u_2)/h$ where h is the current sample thickness. If the velocity of water flow, v, is measured from the settlement of the sample surface in a given time, then the permeability is given by $k = v(du/dx)$.

3. Experimental details

The soil sample is placed in a Rowe cell, modified to take the cutting rings supplied by I.O.S. With drainage lines closed, a total stress of 1700 kPa is applied. If the system is thoroughly de-aired and the soil sample is fully saturated, the pore pressures increase immediately to the value of the total applied stress, giving a condition of zero effective stress. The drainage line is opened through the flow restrictor to a back pressure of magnitude 700 kPa and, as pore pressures dissipate, the sample consolidates. The values of pore pressure, total stress and displacement are all recorded on a chart recorder and logged digitally.

Both the back pressure of 700 kPa (required to ensure saturation of the soil) and the total stress of 1700 kPa were higher than the conditions that had been used in a number of previously successful tests and, with hindsight, some modifications should be made in the measurement techniques. Previously, sufficient accuracy of the differential pore pressure measurement had been obtained by subtracting the value measured on the drained face from that measured on the undrained face. However, using transducers of a higher range reduced their sensitivity and the permeability values are not individually as accurate as a direct differential measurement would achieve. This is particularly marked at the beginning and end of a test, when the pore pressures are closest: at the start, a few minutes elapse before the flow is established through the flow restrictor and, during this time, the pore pressures are very close. Nevertheless, little consolidation occurs during this stage so that little change in void ratio takes place. Similarly, at the end of the test when the pore pressures have practically dissipated to the back pressure level, little change occurs in the void ratio. Thus, with the exception of three tests, permeability values have been obtained for most of the range of void ratios for each sample.

Restriction of the drainage flow was achieved using a Millipore filter system. This was not designed for the high-line pressures of these tests but, nevertheless, performed satisfactorily in most of the tests. Alternative restrictors were tested initially but not found to be as reliable as the Millipore.

The calculation of void ratio was found to be very sensitive to the quality of the samples. A number of these were found to contain visible depressions and holes - presumably due in part to the problems associated with sampling from great depths of water. No attempt was made to allow for these in the overall calculations of void ratio as they were very difficult to quantify. In the worst

case (sample number 10298/1) the soil did not occupy the full height of the ring and allowing for this could reduce the calculated initial void ratio by as much as 0.3.

4. Data Analysis

The data is analysed making appropriate corrections for the salt content in the calculation of void ratio and specific gravity. However, the specific gravity was not measured for each sample so that the correction was based on the wet weight W_w and the dry weight W_d at the end of the consolidation test (the ones used for moisture content determinations). Thus, the mineral weight W_m was obtained from the calculation,

$$W_m = W_d - 0.035(W_w - W_d)$$

and the specific gravity was corrected by multiplication by the factor $W_m W_d$ where the specific gravity was not measured directly, the representative value of 2.69 was used. It is apparent that the value of the void ratio is sensitive to small changes in the salt corrections.

The results have been plotted in terms of void ratio against the logarithm of effective stress and void ratio against the logarithm of permeability. They are marked as discrete points since a discrete analysis has been used. However, since the raw data is available in analogue form, as many points as required can be calculated and sufficient values have been taken to identify a continuous relationship. With the graphs for each sample is included a note of such characteristics as initial and final moisture contents, and the dry weight of the sample.

The effective stress/void ratio curves show clearly the stress/strain behaviour. Two tests appeared to contain a small quantity of air in the system despite a careful de-airing routine, as is shown by a high minimum effective stress but, apart from this, the test seems to have produced reliable, consistent data. As already mentioned, the permeability data is somewhat less satisfactory, although reasonable results have been obtained for all but three samples (Nos. 10298/13, 10333/9, 10333/10).

The samples themselves showed a range of characteristics, with colour ranging from almost white through pale beige and pink to brown. Dry weights varied from a minimum of 38.0 gms. to a maximum of 79.6 gms.

5. Conclusions

The new consolidation test has produced good results for the stress/strain characteristics and acceptable results for the permeability measurements for the deep-sea samples provided by I.O.S. Clearly, better permeability values could, and should, have been provided by the use of direct differential pore pressure measurement. However, the measurement of permeability in the laboratory is often difficult to relate to field conditions due to sample disturbance, anisotropy, fissures, bioturbation, etc., so that the present values should provide an adequate guide.

There are a number of inherent advantages and disadvantages with the new test. The major advantages are two-fold: its speed; since a complete test, including swell-back, is achieved in well under 24 hours; and its accuracy of definition of the effective stress/void ratio curve. The disadvantages lie in the fact that data collection must be reliably automated and that a failure in the mechanical or electrical part of the experiment can lead to almost complete loss of information. For example, malfunction of the flow restrictor prevented the collection of adequate permeability data on three samples. In the traditional test, there is less to go wrong during each load increment and measurements are required only for the equilibrium condition. Nevertheless, a high price is paid for the duration of the test.

In the light of this experience, a number of developments have been undertaken. A new flow restrictor has been designed and is being tested and a new cell has also been designed. This will allow constant head permeability tests to be undertaken at the beginning and end of a test and, if required, at intermediate points. Differential pore-pressure measurement is also incorporated as an option.

TABLE 1

FIGURE No.	CORE	SAMPLE	TESTED AT	ORIENTATION	SEDIMENT TYPE	SUB-BOTTOM DEPTH m	e_o	OCR	C_c	k_c	k at $'_c$ mm/s x 10^{-6}
7	D10298	3	OX	V	NM	1.80	4.60	9.6	1.7	1.9	80.0
8		4	OX	V	NM	1.72	4.60	27.0	1.5	2.9	10.0
9		9	OX	H	NM	1.32	4.64	18.0	1.5	2.5	11.0
9		10	IOS	H	NM	1.31	4.52	4.0	1.3	1.8	70.0
10		11	IOS	V	NM	1.06	4.23	-	1.3	1.8	200.0
11		13	OX	V	FNM	0.42	4.37	23.0	1.2	-	-
12		14	IOS	V	FNM	0.25	3.17	3.0	0.8	1.7	16.0
13	D10302	1	OX	V	FNM	0.35	2.80	54.0	1.0	0.7	50.0
14	D10314	5	OX	H	NM	1.84	4.21	9.1	1.3	1.3	16.0
14		6	IOS	H	NM	1.83	4.01	1.5	1.0	1.4	18.0
15		7	OX	V	NM	1.66	4.09	13.0	1.0	2.5	0.8
16		8	OX	V	NM	1.58	3.98	6.0	1.3	1.0	100.0
17		10	OX	H	NM	1.09	3.20	33.0	1.1	1.5	2.5
18		12	OX	V	NM	1.00	3.50	3.8	1.1	-	2.0
19		13	OX	V	NM	0.84	5.42	45.0	1.5	2.5	0.8
20		15	IOS	V	ARC	0.75	3.81	4.2	1.0	1.0	200.0
21		18	OX	V	ARC	0.58	2.61	64.0	1.0	0.9	2.0
22	D10316	3	OX	V	FNM	0.28	2.42	54.0	0.6	1.7	5.0
22		4	OX	H	FNM	0.28	2.43	108.0	0.6	1.7	16.0
23		7	OX	V	CPC	0.45	2.72	167.0	1.0	0.9	10.0
24		8	OX	V	FNM	0.53	2.42	154.0	1.0	0.8	5.0
25		11	OX	H	CPC	0.95	2.63	7.0	0.8	0.7	20.0
26		13	OX	V	CPC	1.05	2.28	8.3	0.6	0.4	40.0
27		18	OX	V	FNM	1.31	2.51	11.0	0.8	2.0	0.9

TABLE 1 - continued 2

FIGURE No.	CORE	SAMPLE	TESTED AT	ORIENTATION	SEDIMENT TYPE	SUB-BOTTOM DEPTH m	e_o	OCR	C_c	k_c	k at $'_c$ mm/s x 10^{-6}
28	D10321	6	OX	V	CPC	0.52	3.59	38.0	1.3	1.7	3.0
28		7	OX	H	CPC	0.52	3.38	29.0	1.2	1.9	2.0
29		10	OX	V	CPC	0.92	2.69	11.0	0.8	0.9	10.0
29		11	IOS	V	CPC	0.92	2.67	2.9	0.8	1.2	20.0
30		16	OX	V	FNM	1.46	2.42	12.0	0.5	0.6	10.0
31	D10325	4	OX	V	FNM	0.20	3.08	50.0	1.1	1.1	10.0
32		5	IOS	V	FNM	0.28	2.49	117.0	0.9	1.0	150.0
33		7	IOS	V	FNM	0.44	2.54	6.3	0.8	0.9	21.0
34		12	OX	V	CPC	1.01	2.98	3.4	0.9	0.8	40.0
35	D10333	2	OX	V	FNO	0.28	2.66	31.0	0.6	0.7	8.0
36		7	IOS	V	FNM	0.76	2.43	2.0	0.4	1.5	45.0
37		9	OX	V	FNM	0.92	2.25	2.3	0.2	-	-
37		10	OX	V	FNO	1.08	2.21	5.9	0.4	-	-
38		11	OX	R	FNO	1.08	2.25	-	0.2	0.2	200.0
39		12	OX	V	FNO	1.24	2.43	1.7	0.3	-	-
39	D10406	1	UCNW	V	FNM	0.21	5.19	1.0	1.0	-	-
40		3	UCNW	V	NM	0.51	4.60	7.1	1.4	-	-
40		7	UCNW	V	NM	1.04	5.34	2.6	1.8	-	-
41		11	UCNW	V	FNO	1.86	3.21	2.9	1.2	-	-
41		20	UCNW	V	FNM	3.04	2.10	1.8	0.5	-	-

TABLE 1 - continued 3

FIGURE No.	CORE	SAMPLE	TESTED AT	ORIENTATION	SEDIMENT TYPE	SUB-BOTTOM DEPTH m	e_o	OCR	C_c	κ_c	κ at $'_c$ mm/s x 10^{-6}
42	D10695	2-14	IOS	V	NM	1.68	3.55	1.1	1.1	1.6	26.0
43		2-69	IOS	R	SILT	2.23	0.95	-	0.1	0.4	250.0
44		3-82	IOS	V	NM	3.90	3.00	1.1	0.9	1.4	5.5
45		5-46	IOS	V	SNM	6.60	1.70	1.0	0.4	0.7	22.0
46		6-28	IOS	V	NM	7.94	3.68	0.2	1.2	1.4	6.5
47		8-16	IOS	V	SILT	10.77	1.74	2.1	0.5	0.5	900.0
48	80PC04	1	OX	V	FNO	1.10	2.17	-	0.3	0.6	2.0
49		3	OX	V	FNO	0.20	2.62	-	0.3	0.9	1.5
50	S126/2	1	UCNW	V	NM	0.44	5.43	1.0	1.2	-	-
51		3	IOS	V	FNM	0.62	2.43	7.0	0.5	1.5	85.0
50		4	UCNW	V	FNM	0.70	3.44	10.0	0.8	-	-
52	S126/4	4	IOS	V	NM	0.74	4.76	18.0	1.4	1.4	150.0
53		5	IOS	V	NM	1.02	5.20	5.5	1.5	1.8	160.0
53		6	IOS	H	NM	1.02	5.46	5.5	1.5	2.2	70.0
54		9	IOS	H	NM	3.44	3.54	2.3	1.2	1.8	30.0
54		10	IOS	V	NM	3.44	3.73	5.0	1.2	1.8	30.0
55	S126/15	4	UCNW	V	CPC	1.66	2.22	5.0	0.7	-	-
55		11	UCNW	V	CPC	1.79	2.54	1.8	0.7	-	-

TABLE 1 - continued 4

FIGURE No.	CORE	SAMPLE	TESTED AT	ORIENTATION	SEDIMENT TYPE	SUB-BOTTOM DEPTH m	e_o	OCR	C_c	κ	κ at $'_c$ mm/s x 10^{-6}
56	GC576A	1-1	IOS	V	RC	1.45	6.12	8.5	2.5	2.2	64.00
56		1-5	IOS	V	RC	7.45	4.56	2.2	1.8	1.2	25.00
56		2-3	UCNW	V	RC	13.15	5.04	3.5	3.0	-	-
56		2-5	IOS	V	RC	16.15	4.61	2.1	2.6	1.2	13.00
56		3-3	IOS	V	RC	22.65	3.65	1.2	1.4	1.0	1.2
56		3-5	IOS	V	RC	25.65	3.10	1.8	1.5	1.2	0.70
56		4-3	IOS	V	RC	32.15	4.11	1.1	2.1	1.8	0.80
56		5-3	IOS	V	RC	41.65	3.22	0.5	1.3	1.4	0.25
56		5-5	UCNW	V	RC	44.65	2.88	0.8	1.4	-	-
56		6-1	IOS	V	RC	48.15	3.62	0.7	1.9	1.5	0.20
56		7-3	IOS	V	RC	60.65	2.84	0.9	1.5	1.3	0.14
56	GC578A	17-4	IOS	V	RC	153.25	2.70	1.2	1.8	1.1	0.05
56		19-2	IOS	V	RC	169.25	1.65	1.1	1.0	1.0	0.03
57	GC577A	3-4	UCNW	V	FNO	24.90	1.84	1.7	0.5	-	-
57		4-6	IOS	V	FNO	37.40	1.59	1.6	0.3	-	-
58		8-4	IOS	V	FNO	72.40	1.33	1.7	0.3	-	-
58		9-2	UCNW	V	FNO	78.90	1.24	1.4	0.4	-	-

TABLE 2 - Core locations and water depth.
GMW - Great Meteor West; GME - Great Meteor East; KTF - King's Trough Flank;
PAC - Pacific.

CORE	WATER DEPTH	POSITION		AREA
	m	LATITUDE	LONGITUDE	
D10298	5547	36°24'.7N	18°20'.0W	
D10302	5035	34°19'.9N	21°34'.2W	
D10314	6130	25°38'.3N	30°57'.3W	
D10316	4966	26°13'.2N	26°59'.1W	
D10321	4978	31°04'.8N	25°49'.3W	GME
D10325	5407	30°22'.9N	24°05'.8W	GME
D10333	4133	41°07'.3N	22°57'.1W	KTF
D10406	5268	32°34'.7N	22°27'.3W	
D10695	5433	31°23'.7N	24°46'.3W	GME
80PC04	4188	30°22'.5N	20°20'.3W	GMW
S126/2	5446	31°32'.2N	24°50'.5W	GME
S126/4	5446	31°31'.7N	24°25'.3W	GME
S126/15	5330	30°22'.0N	23°35'.0W	GME
GC576	6217	32°21'.4N	164°16'.5E	$PAC1/E_2$
GC577	2675	32°26'.5N	157°43'.4E	
GC578	6010	33°55'.6N	151°37'.7E	$PAC1/B_1$

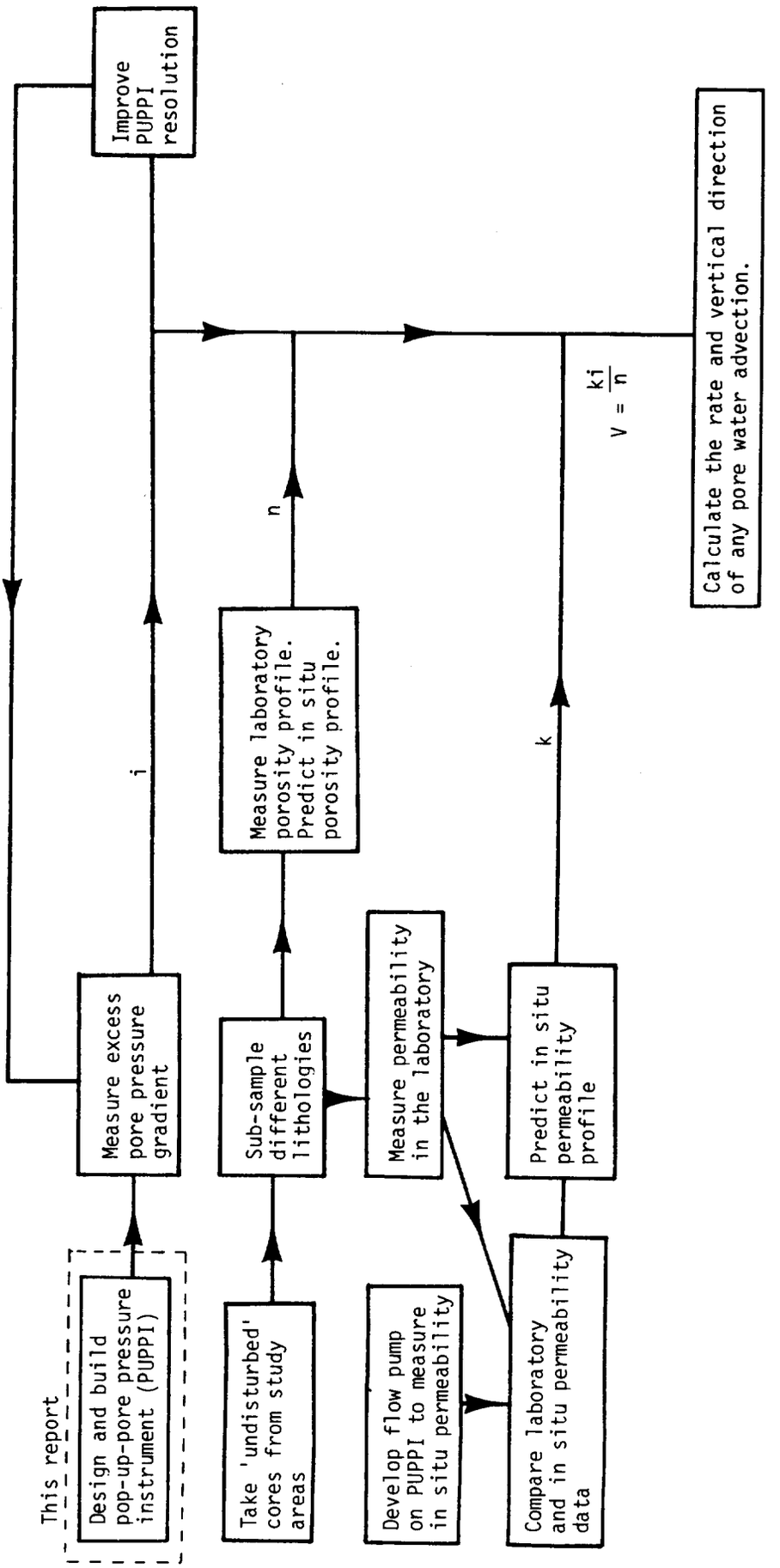

FIG. 1 Flow chart of IOS programme to measure pore water fluxes in deep sea sediments.

IOS CONSOLIDATION/PERMEABILITY SYSTEM FOR DEEP SEA SEDIMENTS

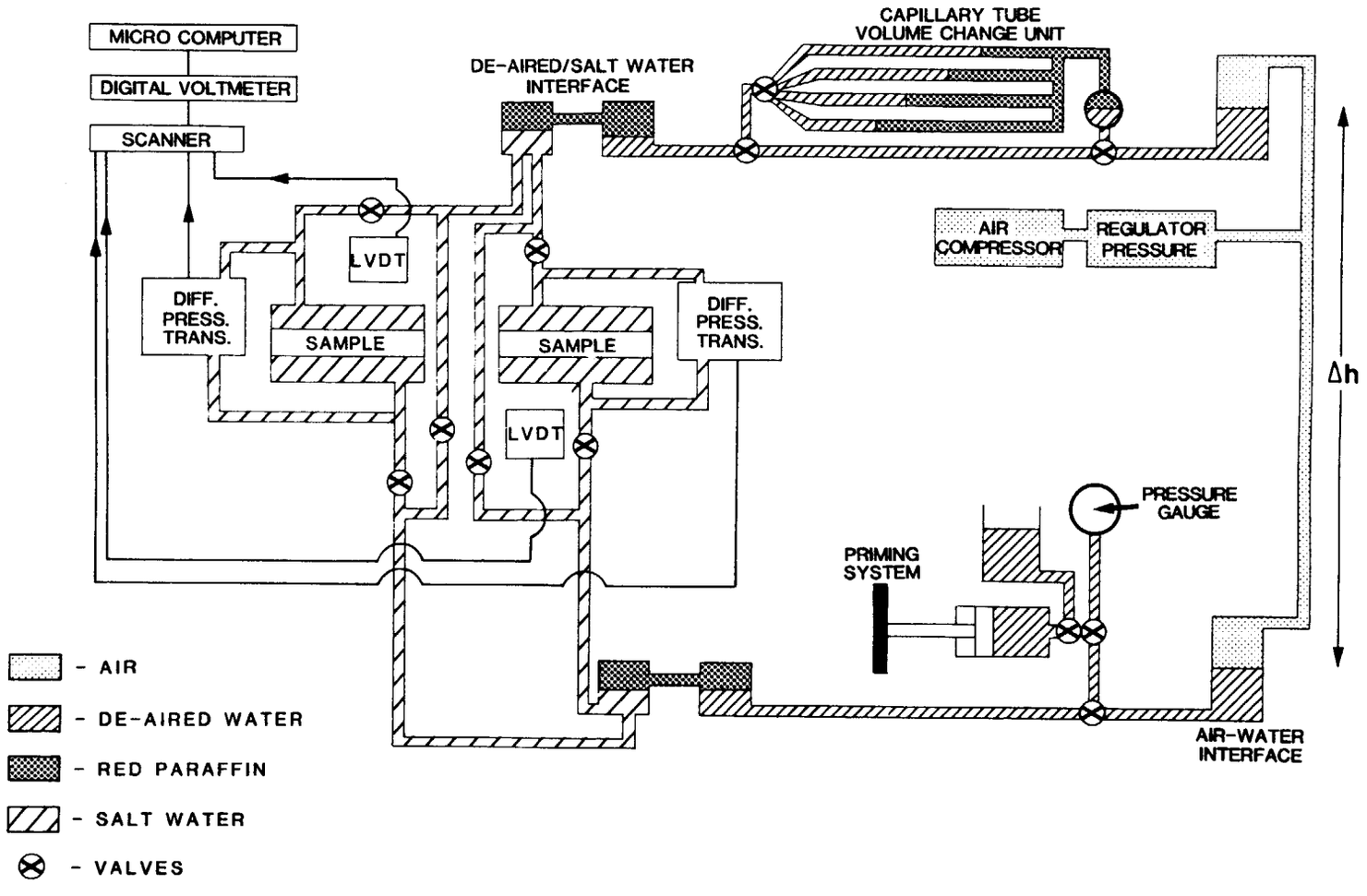

Fig. 2. Schematic diagram of the apparatus used to measure the consolidation and permeability characteristics of sediments.

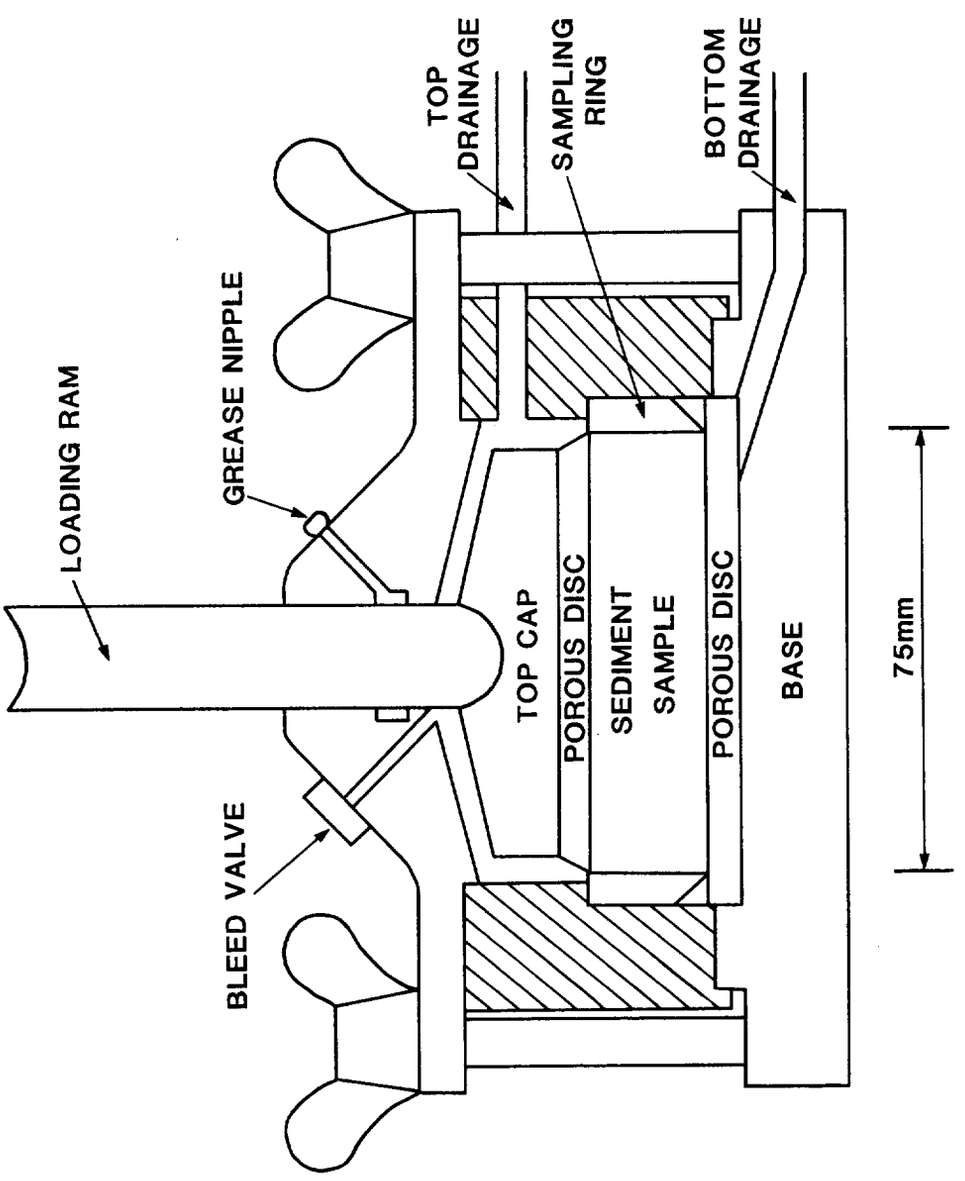

FIG. 3. Schematic diagram of the back pressurised consolidation cell

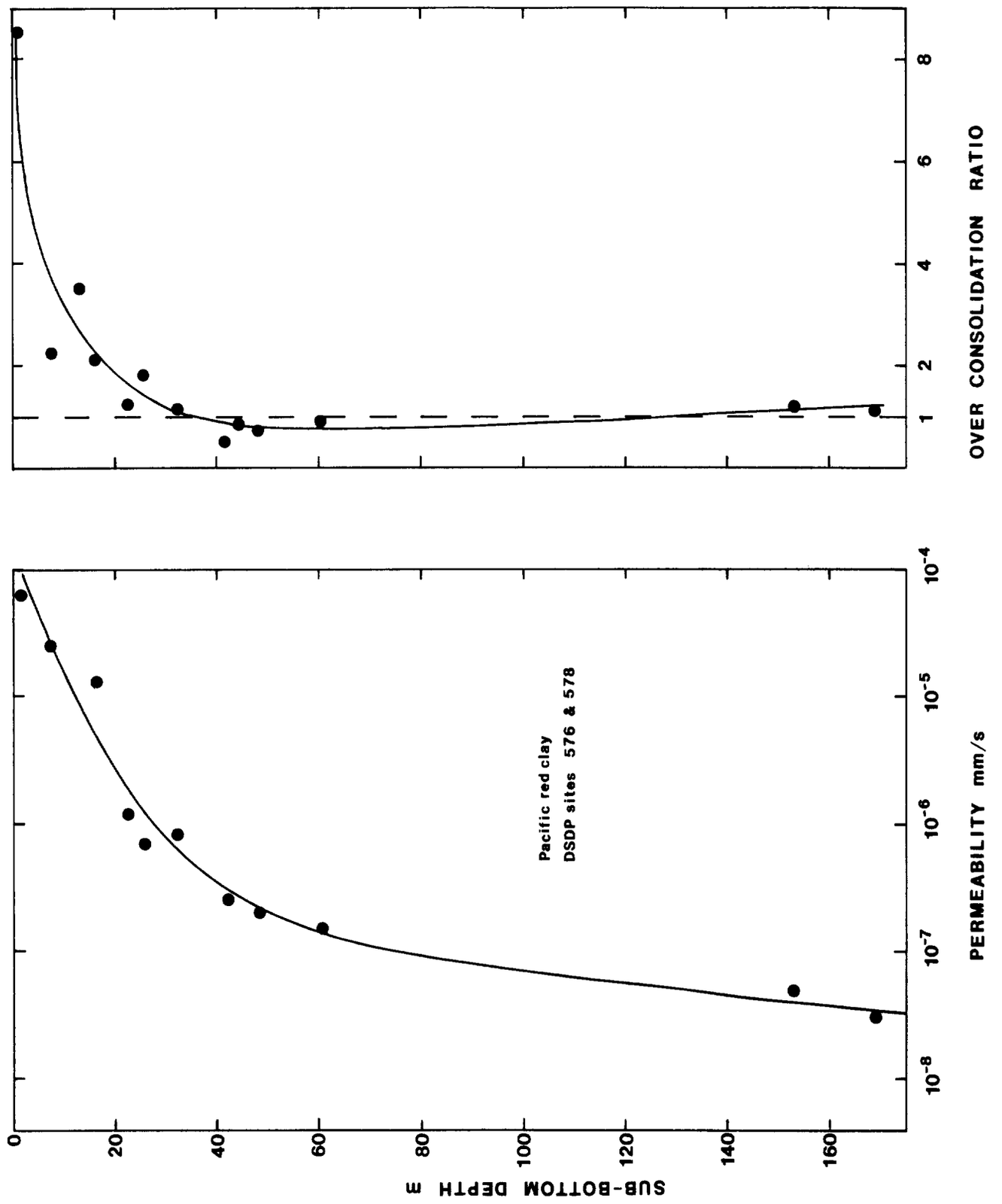

FIG. 4. Permeability and over consolidation ratio profiles for Pacific red clay

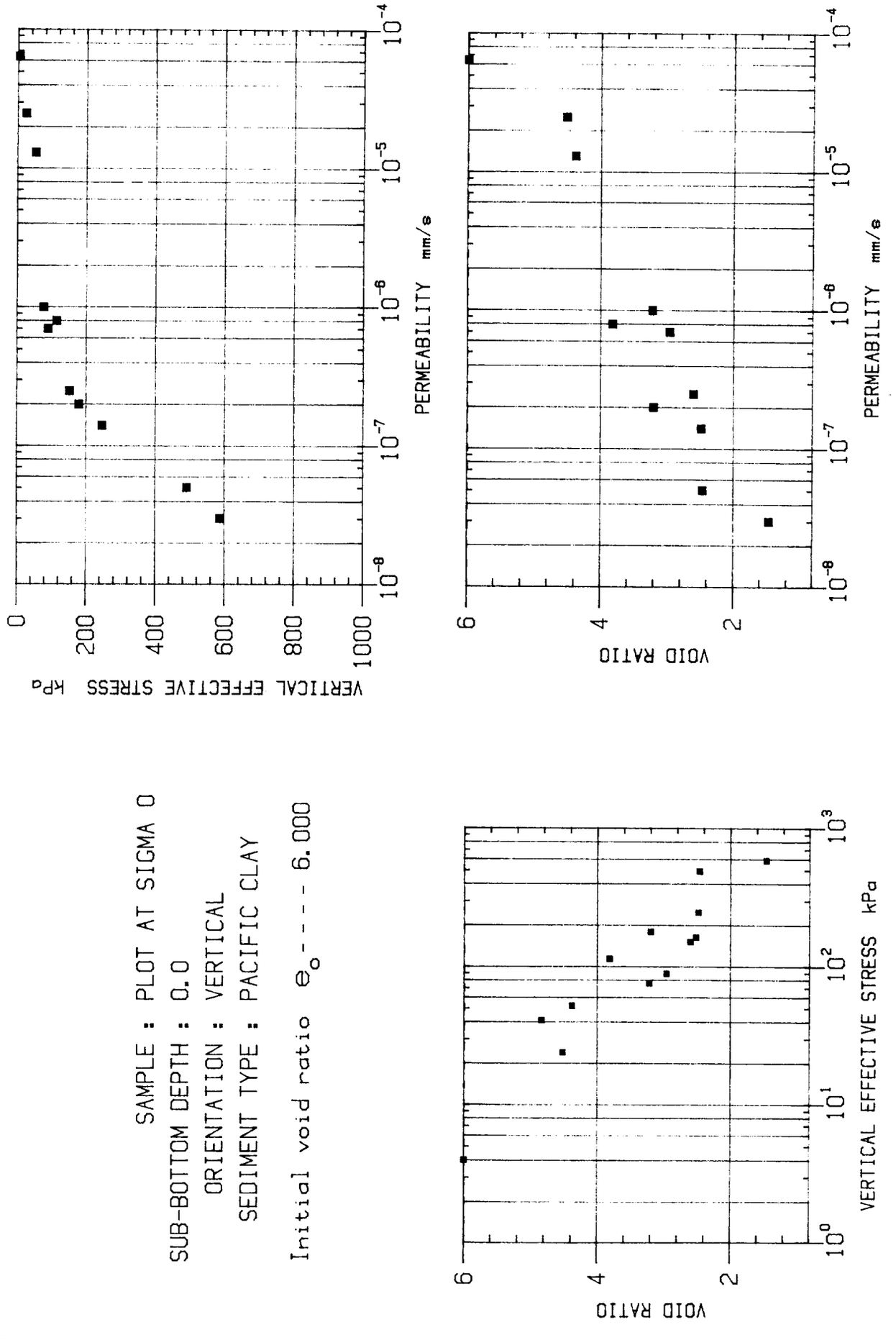
SAMPLE : PLOT AT SIGMA 0
SUB-BOTTOM DEPTH : 0.0
ORIENTATION : VERTICAL
SEDIMENT TYPE : PACIFIC CLAY
Initial void ratio e_o - - - - 6.000
VERTICAL EFFECTIVE STRESS kPa
0
200
400
600
800
1000
PERMEABILITY mm/s
10^{-4}
10^{-5}
10^{-6}
10^{-7}
10^{-8}
VOID RATIO
2
4
6
VERTICAL EFFECTIVE STRESS kPa
10^{0}
10^{1}
10^{2}
10^{3}

Fig. 5

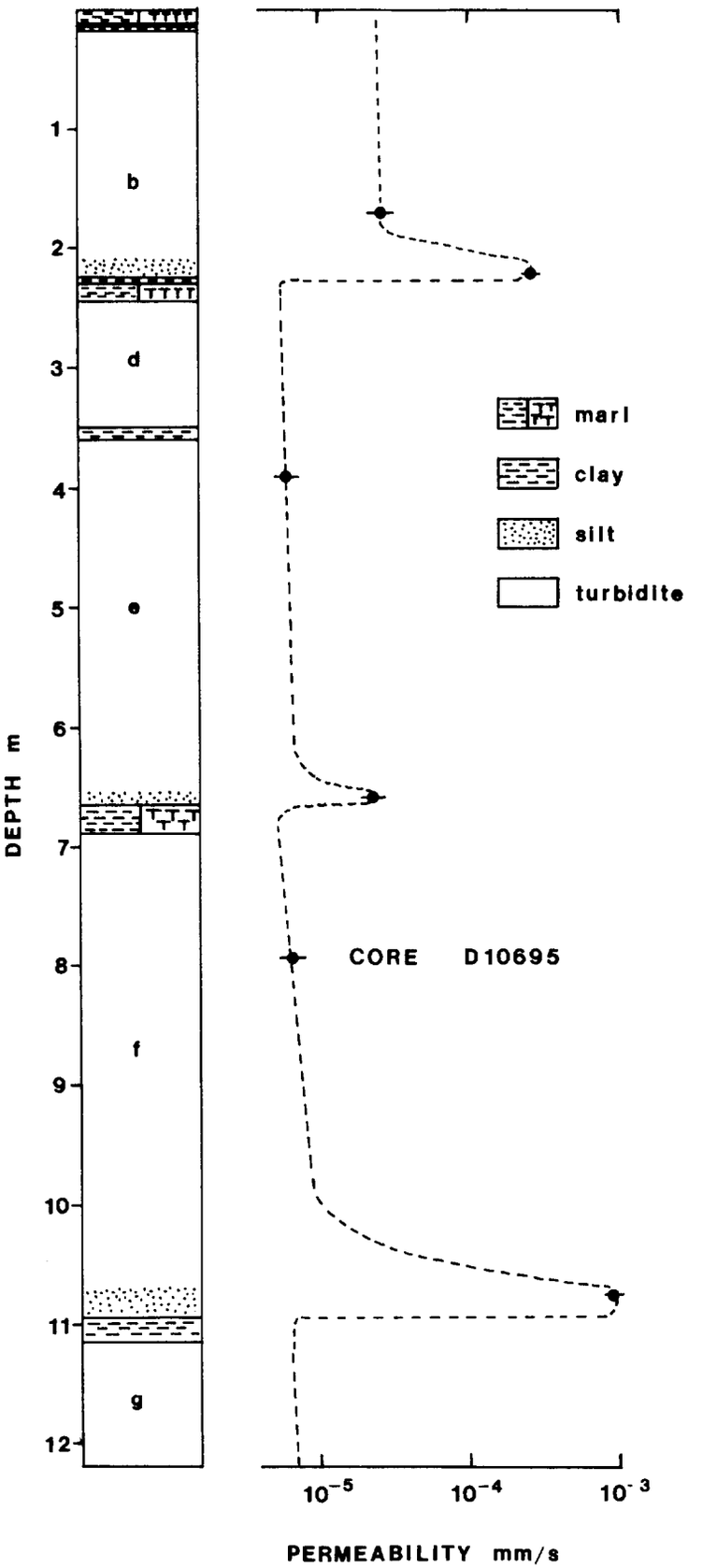

Fig. 6 **Permeability profile of the turbidite sequence in the GME study area (core D10695).**

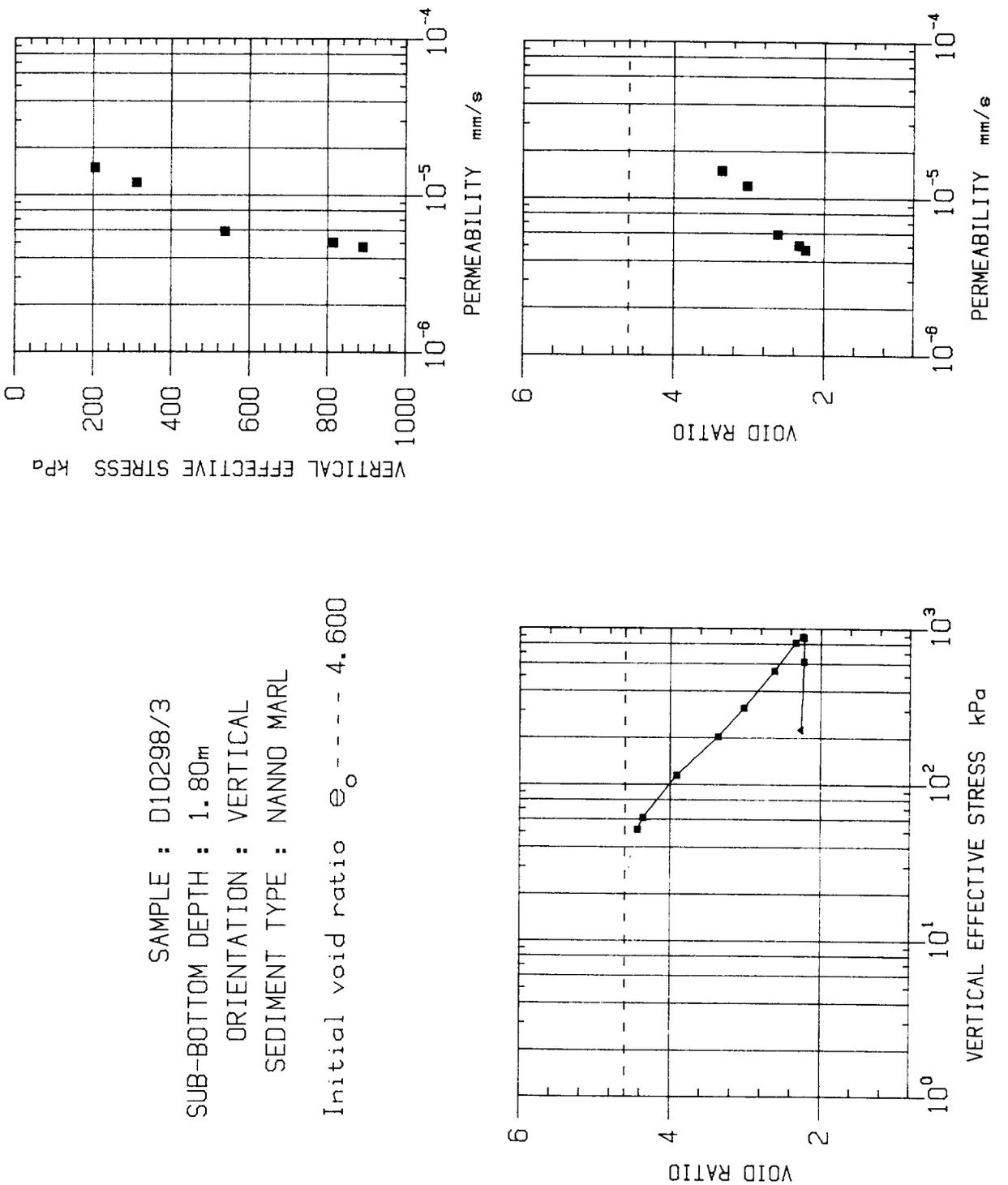
SAMPLE : D10298/3
SUB-BOTTOM DEPTH : 1.80m
ORIENTATION : VERTICAL
SEDIMENT TYPE : NANNO MARL
Initial void ratio e_o ---- 4.600
VERTICAL EFFECTIVE STRESS kP_a
0
200
400
600
800
1000
10^{-6}
10^{-5}
10^{-4}
PERMEABILITY mm/s
VOID RATIO
2
4
6
10^{0}
10^{1}
10^{2}
10^{3}
VERTICAL EFFECTIVE STRESS kPa

Fig. 7

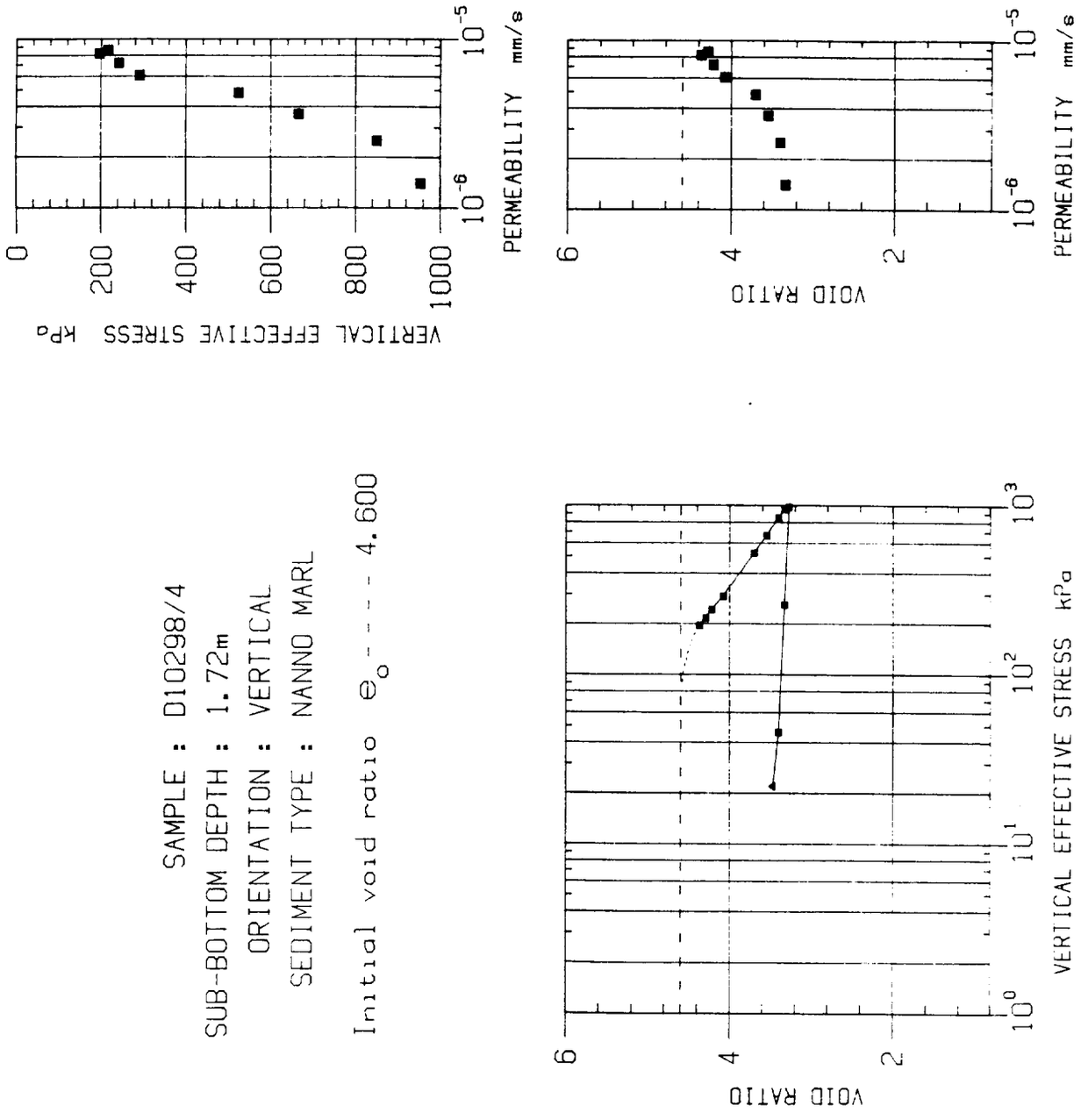
SAMPLE : D10298/4
SUB-BOTTOM DEPTH : 1.72m
ORIENTATION : VERTICAL
SEDIMENT TYPE : NANNO MARL
Initial void ratio e_o - - - - 4.600
VERTICAL EFFECTIVE STRESS kPa
0
200
400
600
800
1000
10^{-6}
10^{-5}
PERMEABILITY mm/s
VOID RATIO
6
4
2
10^{0}
10^{1}
10^{2}
10^{3}
VERTICAL EFFECTIVE STRESS kPa

Fig. 8

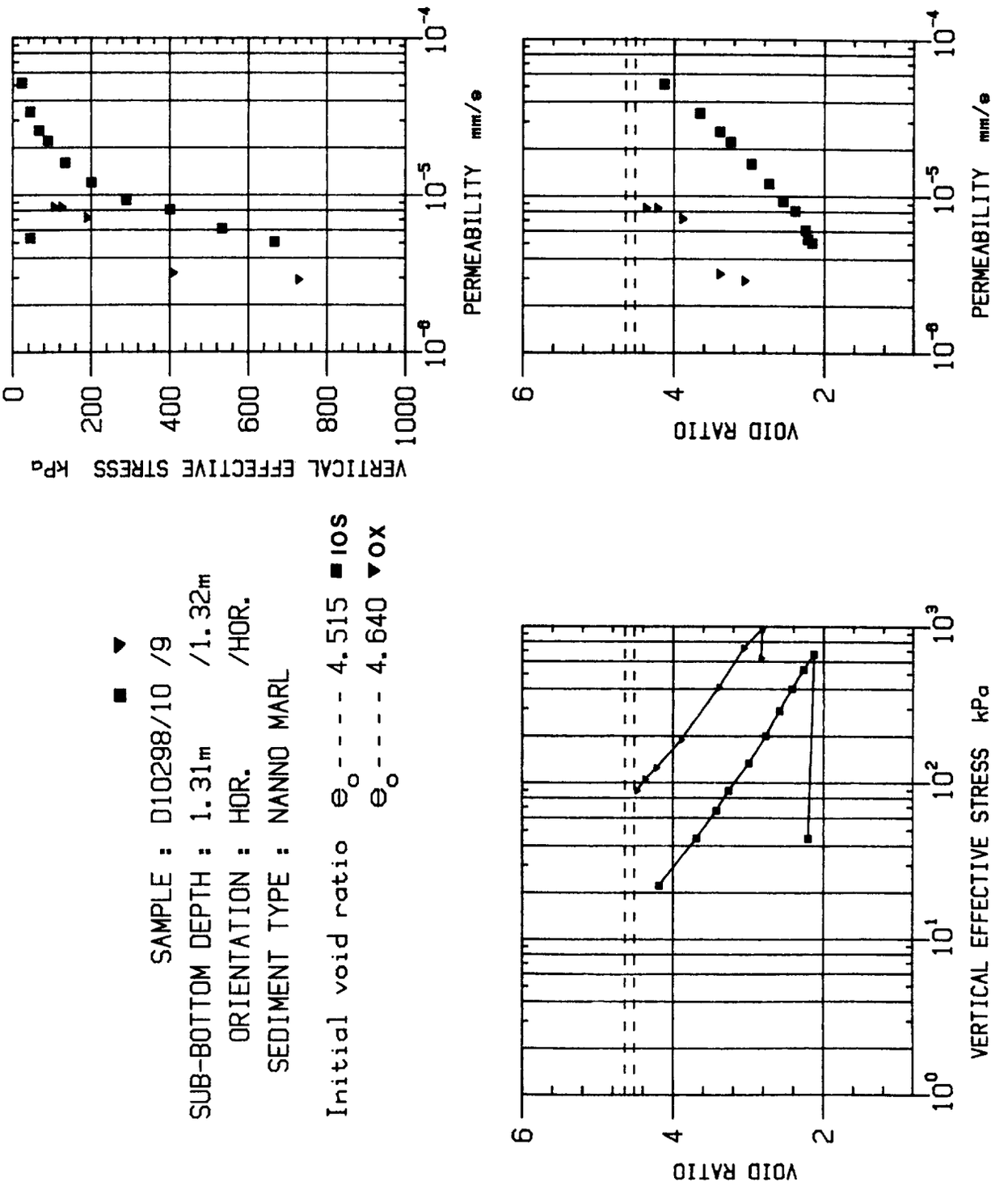
SAMPLE : D10298/10 /9
SUB-BOTTOM DEPTH : 1.31m /1.32m
ORIENTATION : HOR. /HOR.
SEDIMENT TYPE : NANNO MARL
Initial void ratio e_o - - - - 4.515 ■ IOS
e_o - - - - 4.640 ▼ OX
VERTICAL EFFECTIVE STRESS kPa
0
200
400
600
800
1000
PERMEABILITY mm/s
10^{-4}
10^{-5}
10^{-6}
VOID RATIO
6
4
2
10^0
10^1
10^2
10^3

Fig. 9

Fig. 10

SAMPLE : D10298/11
SUB-BOTTOM DEPTH : 1.06m
ORIENTATION : VERTICAL
SEDIMENT TYPE : NANNO MARL

Initial void ratio e_o - - - - 4.230

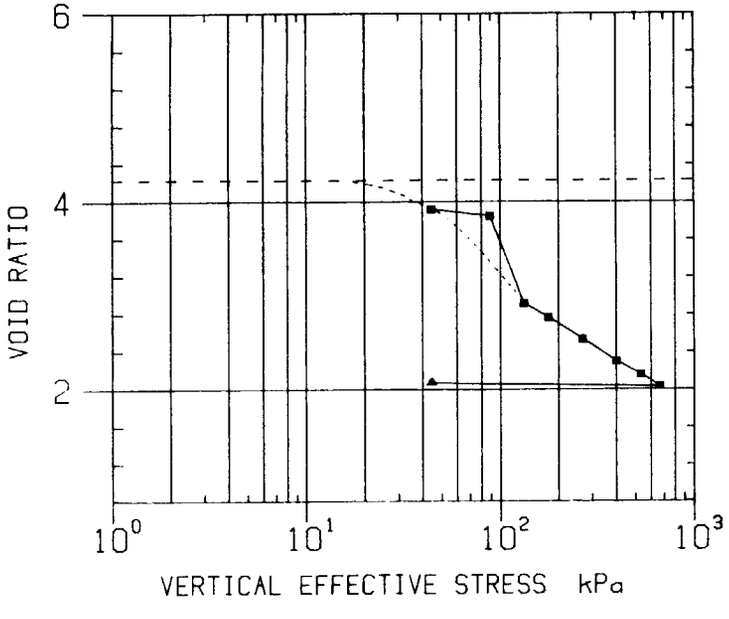

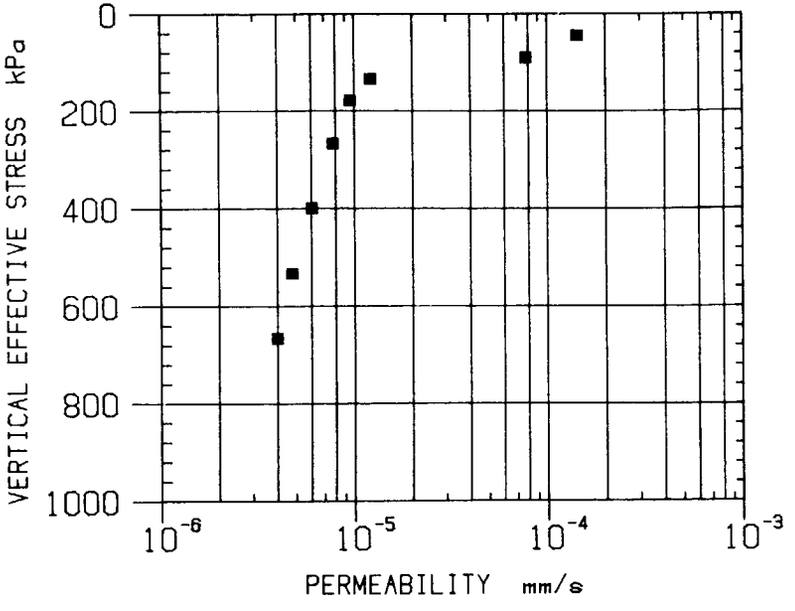

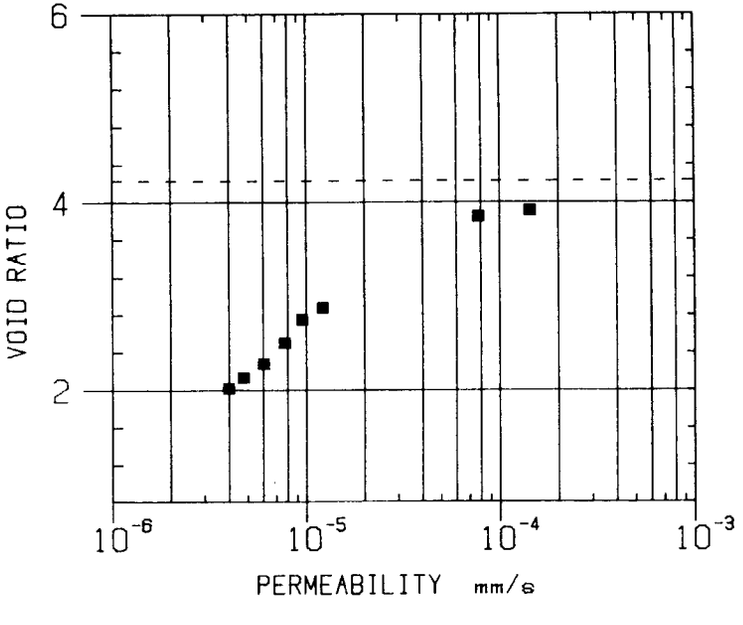

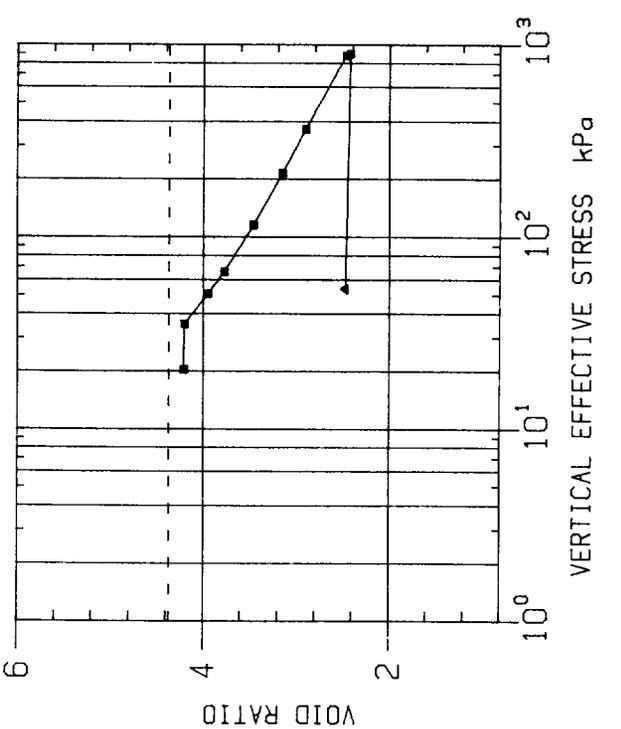
SAMPLE : D10298/13
SUB-BOTTOM DEPTH : 0.42m
ORIENTATION : VERTICAL
SEDIMENT TYPE : FORAM NANNO MARL
Initial void ratio e_o---- 4.370
VOID RATIO
6
4
2
10^0
10^1
10^2
10^3
VERTICAL EFFECTIVE STRESS kPa

Fig. 11

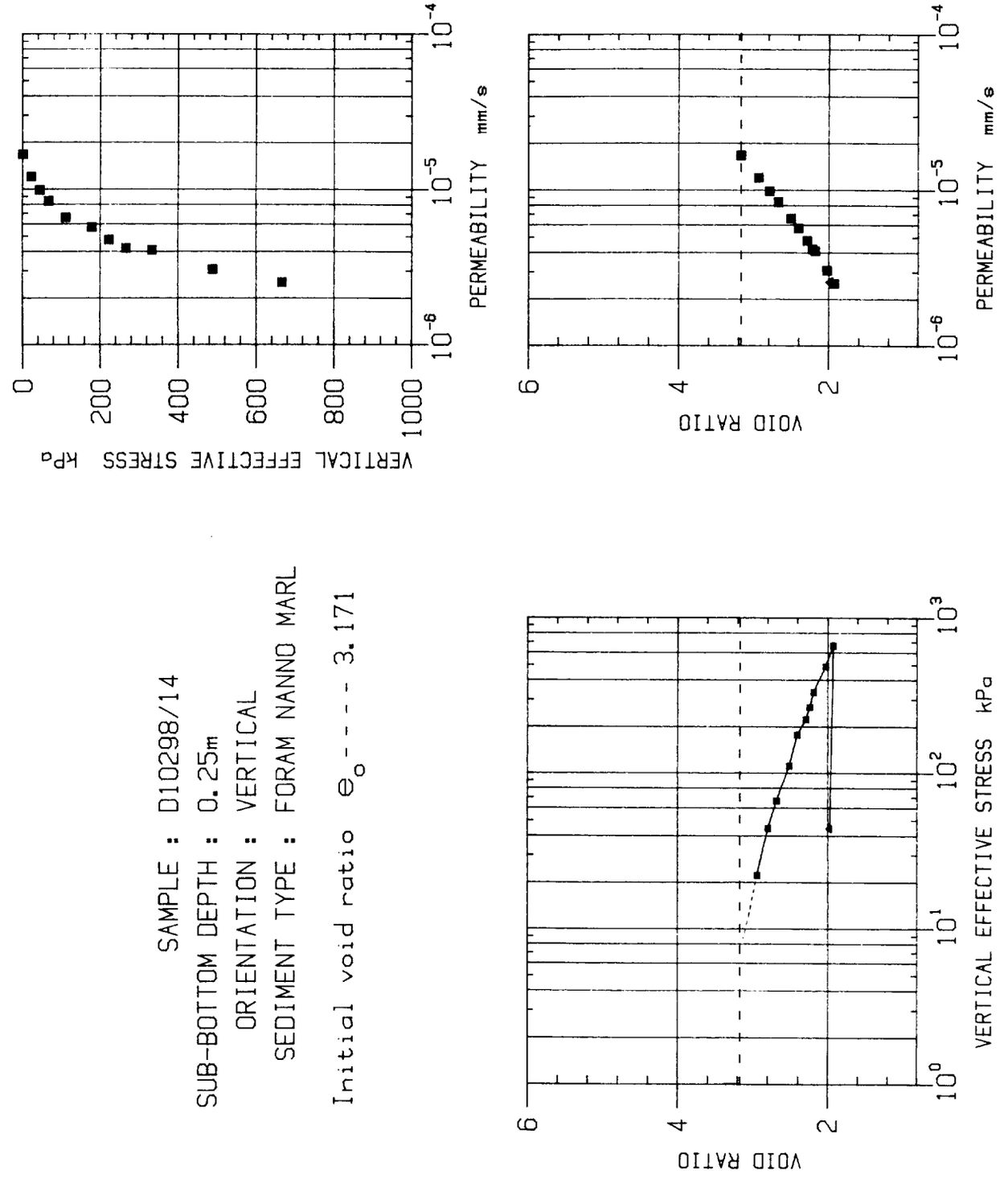
SAMPLE : D10298/14
SUB-BOTTOM DEPTH : 0.25m
ORIENTATION : VERTICAL
SEDIMENT TYPE : FORAM NANNO MARL
Initial void ratio e_o ---- 3.171
VERTICAL EFFECTIVE STRESS kP_a
0
200
400
600
800
1000
10^{-6}
10^{-5}
10^{-4}
PERMEABILITY mm/s
VOID RATIO
2
4
6
VERTICAL EFFECTIVE STRESS kP_a
10^0
10^1
10^2
10^3

Fig. 12

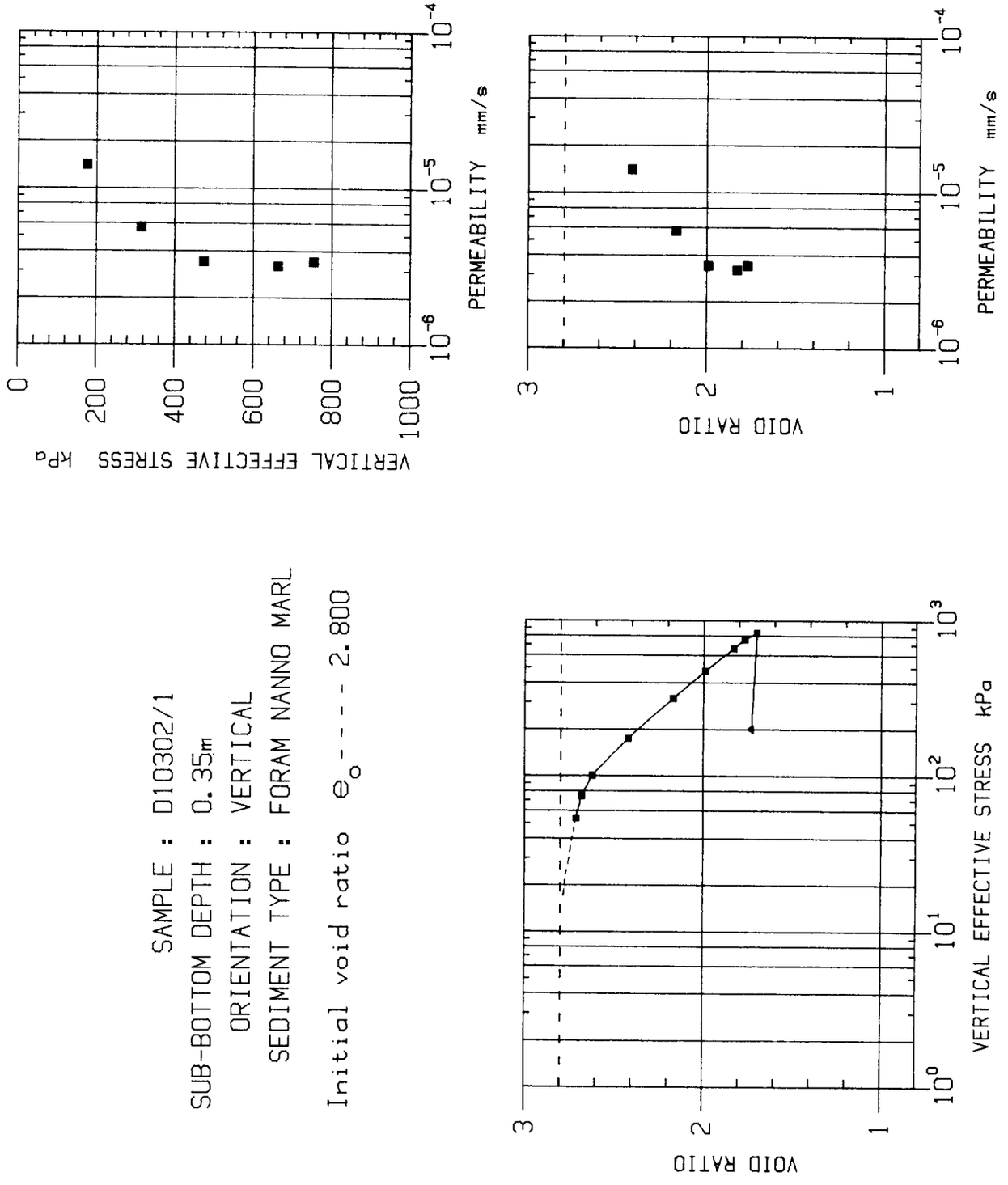
SAMPLE : D10302/1
SUB-BOTTOM DEPTH : 0.35m
ORIENTATION : VERTICAL
SEDIMENT TYPE : FORAM NANNO MARL
Initial void ratio e_o ---- 2.800
VERTICAL EFFECTIVE STRESS kPa
0
200
400
600
800
1000
10^{-6}
10^{-5}
10^{-4}
PERMEABILITY mm/s
VOID RATIO
3
2
1
10^{0}
10^{1}
10^{2}
10^{3}
VERTICAL EFFECTIVE STRESS kPa

Fig. 13

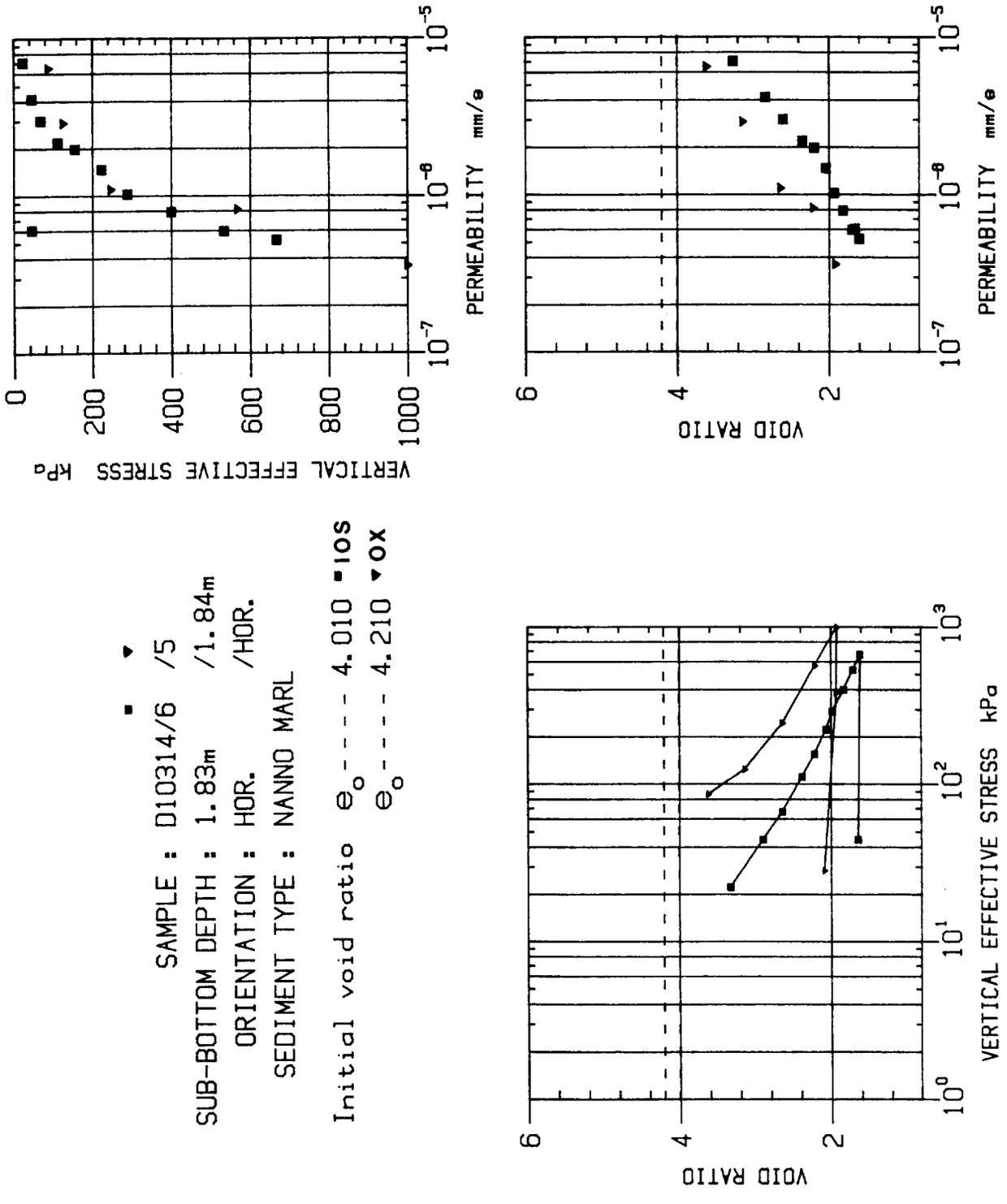
SAMPLE : D10314/6 /5
SUB-BOTTOM DEPTH : 1.83m /1.84m
ORIENTATION : HOR. /HOR.
SEDIMENT TYPE : NANNO MARL
Initial void ratio e_o ---- 4.010 ▪IOS
e_o ---- 4.210 ▾OX
VERTICAL EFFECTIVE STRESS kPa
0
200
400
600
800
1000
PERMEABILITY mm/s
10^{-5}
10^{-6}
10^{-7}
VOID RATIO
2
4
6
VERTICAL EFFECTIVE STRESS kPa
10^{0}
10^{1}
10^{2}
10^{3}

Fig. 14

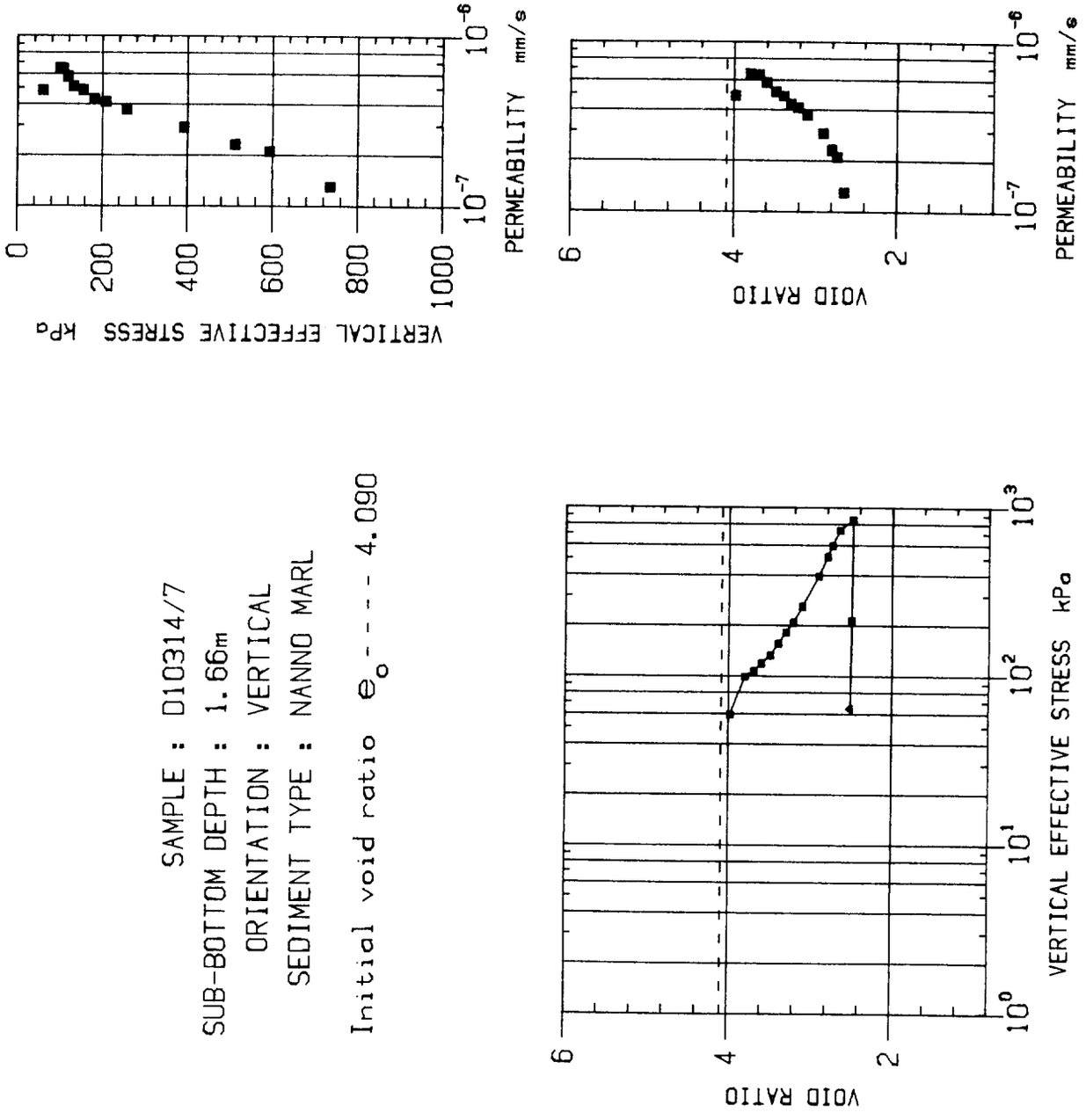
SAMPLE : D10314/7
SUB-BOTTOM DEPTH : 1.66m
ORIENTATION : VERTICAL
SEDIMENT TYPE : NANNO MARL
Initial void ratio e_o ---- 4.090
VERTICAL EFFECTIVE STRESS kPa
0
200
400
600
800
1000
10^{-6}
10^{-7}
PERMEABILITY mm/s
VOID RATIO
6
4
2
10^0
10^1
10^2
10^3
VERTICAL EFFECTIVE STRESS kPa

Fig. 15

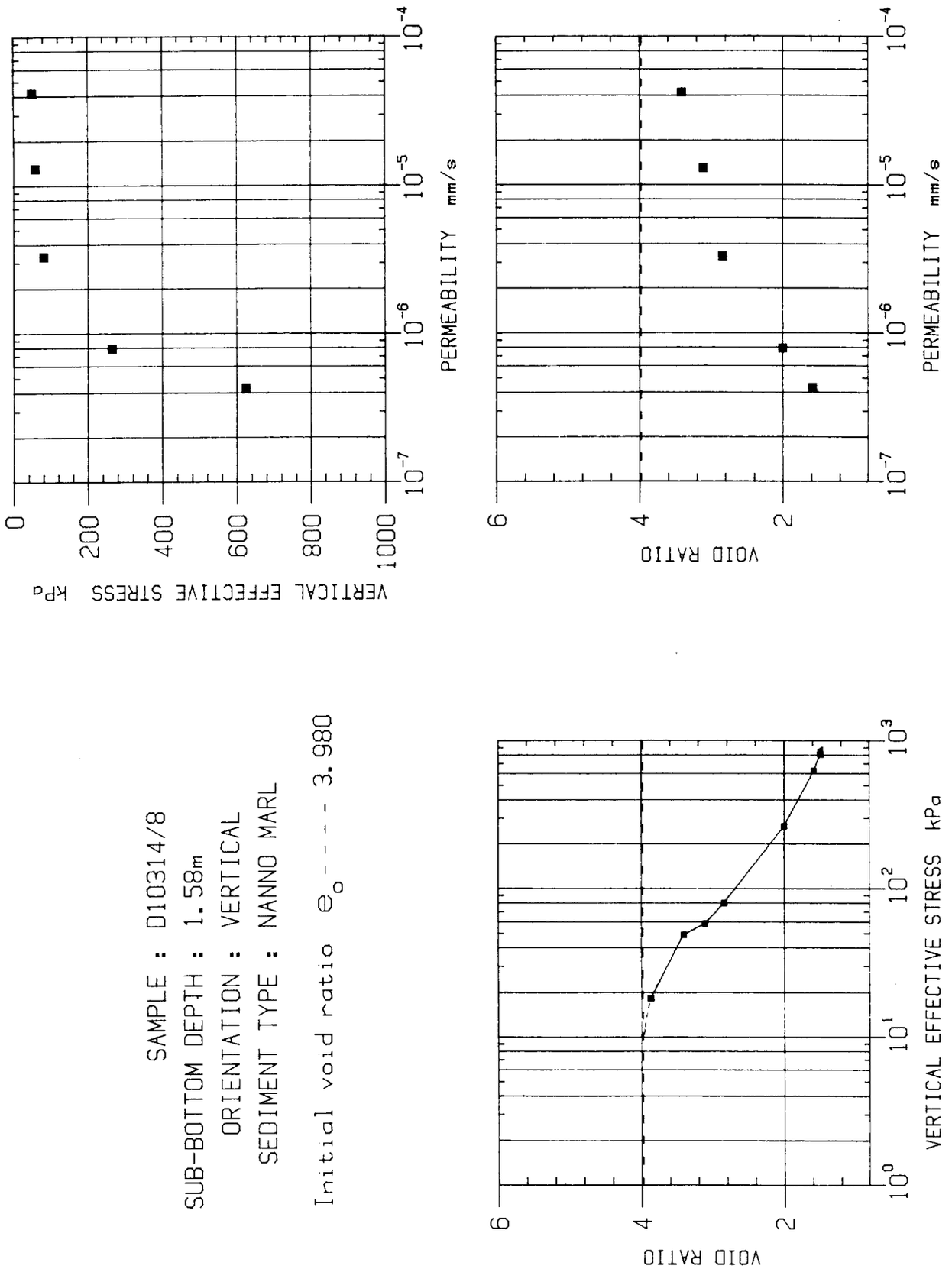
SAMPLE : D10314/8
SUB-BOTTOM DEPTH : 1.58m
ORIENTATION : VERTICAL
SEDIMENT TYPE : NANNO MARL
Initial void ratio e_o - - - - 3.980
VERTICAL EFFECTIVE STRESS kPa
0
200
400
600
800
1000
PERMEABILITY mm/s
10^{-4}
10^{-5}
10^{-6}
10^{-7}
VOID RATIO
6
4
2
PERMEABILITY mm/s
10^{-4}
10^{-5}
10^{-6}
10^{-7}
VOID RATIO
6
4
2
VERTICAL EFFECTIVE STRESS kPa
10^{0}
10^{1}
10^{2}
10^{3}

Fig. 16

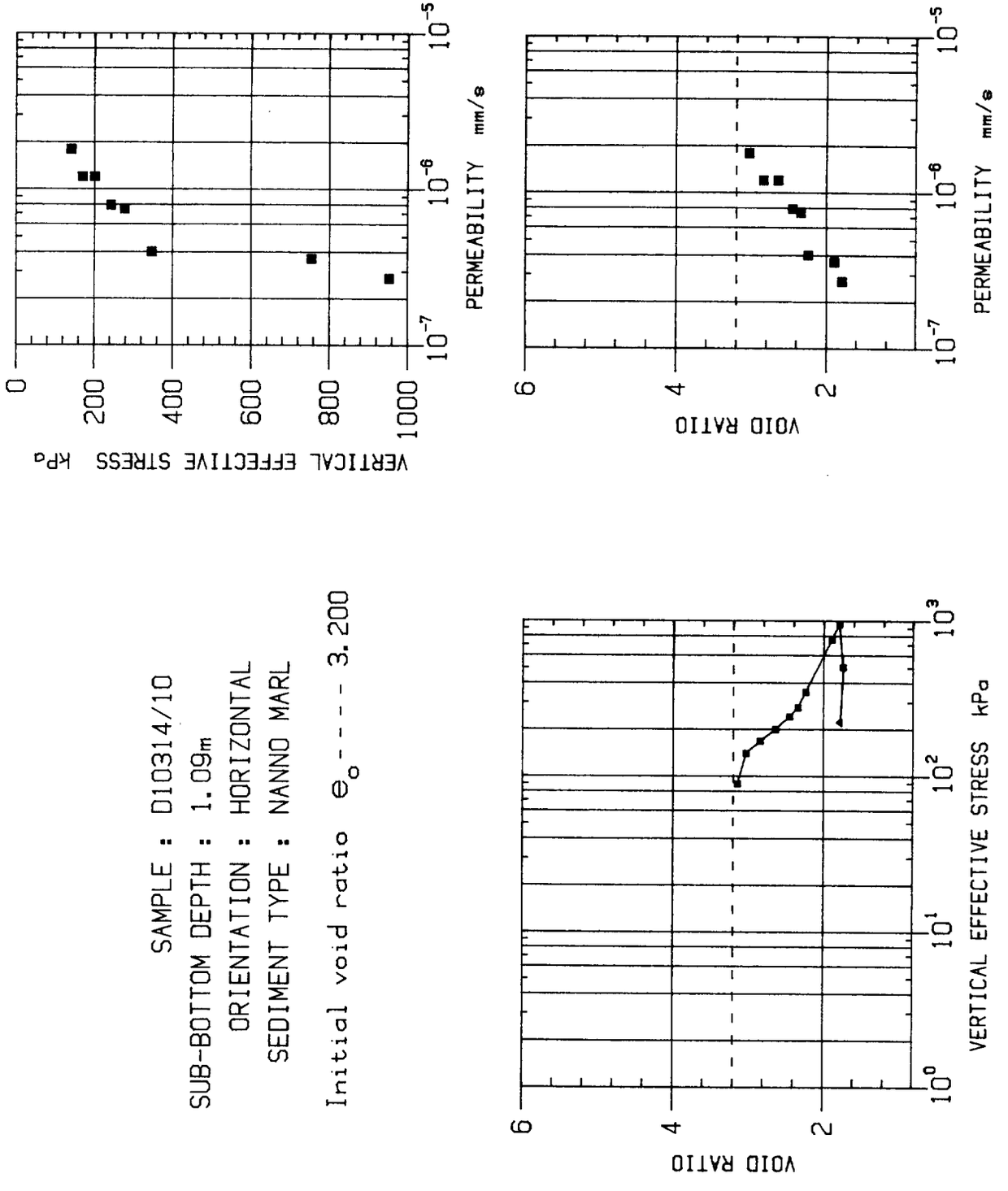
SAMPLE : D10314/10
SUB-BOTTOM DEPTH : 1.09m
ORIENTATION : HORIZONTAL
SEDIMENT TYPE : NANNO MARL
Initial void ratio e_o ---- 3.200
VERTICAL EFFECTIVE STRESS kP_a
0
200
400
600
800
1000
10^{-5}
10^{-6}
10^{-7}
PERMEABILITY mm/s
VOID RATIO
2
4
6
10^0
10^1
10^2
10^3

Fig. 17

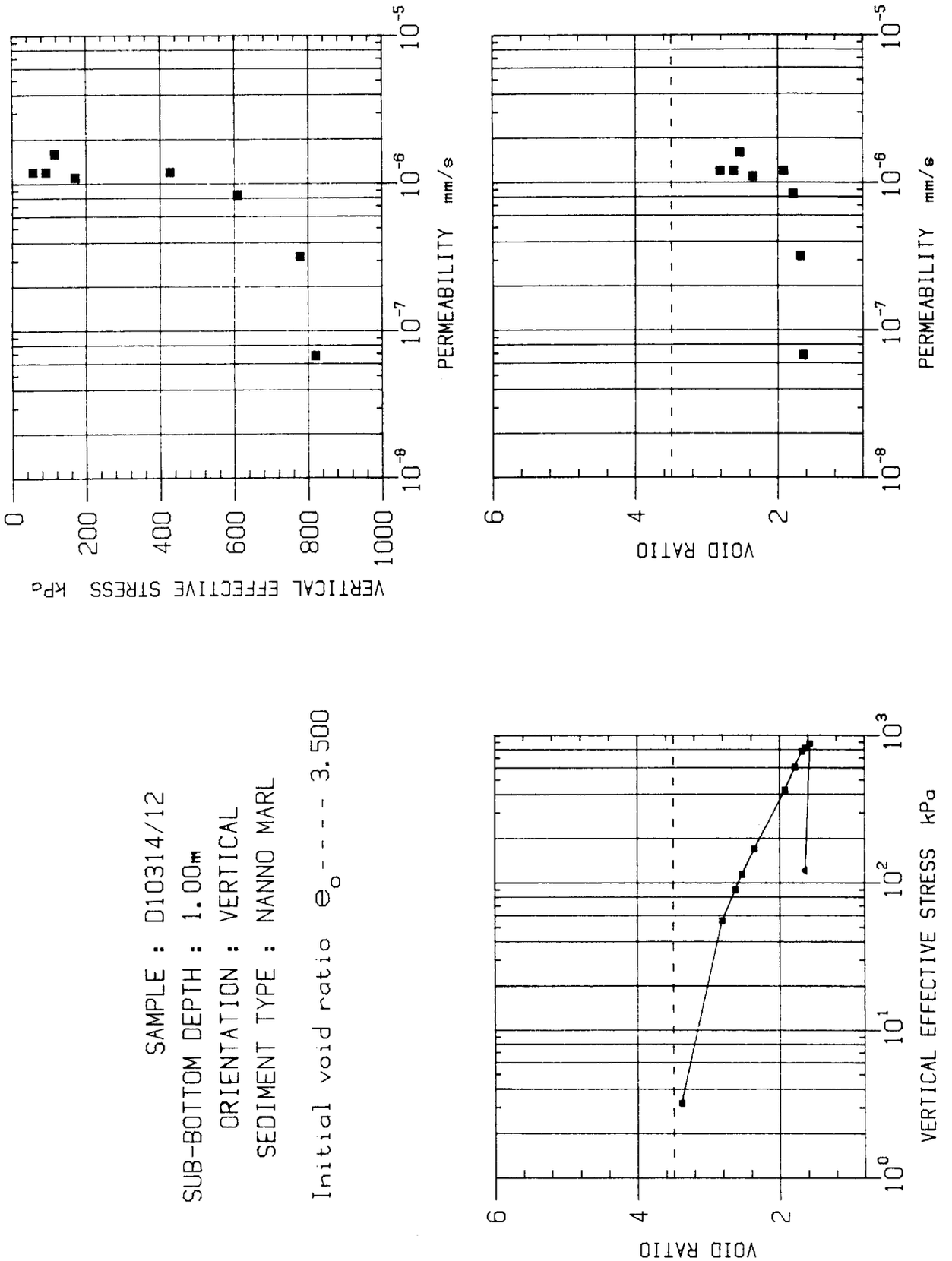
SAMPLE : D10314/12
SUB-BOTTOM DEPTH : 1.00m
ORIENTATION : VERTICAL
SEDIMENT TYPE : NANNO MARL
Initial void ratio e_o - - - - 3.500
VERTICAL EFFECTIVE STRESS kPa
0
200
400
600
800
1000
PERMEABILITY mm/s
10^{-8}
10^{-7}
10^{-6}
10^{-5}
VOID RATIO
2
4
6
VERTICAL EFFECTIVE STRESS kPa
10^{0}
10^{1}
10^{2}
10^{3}

Fig. 18

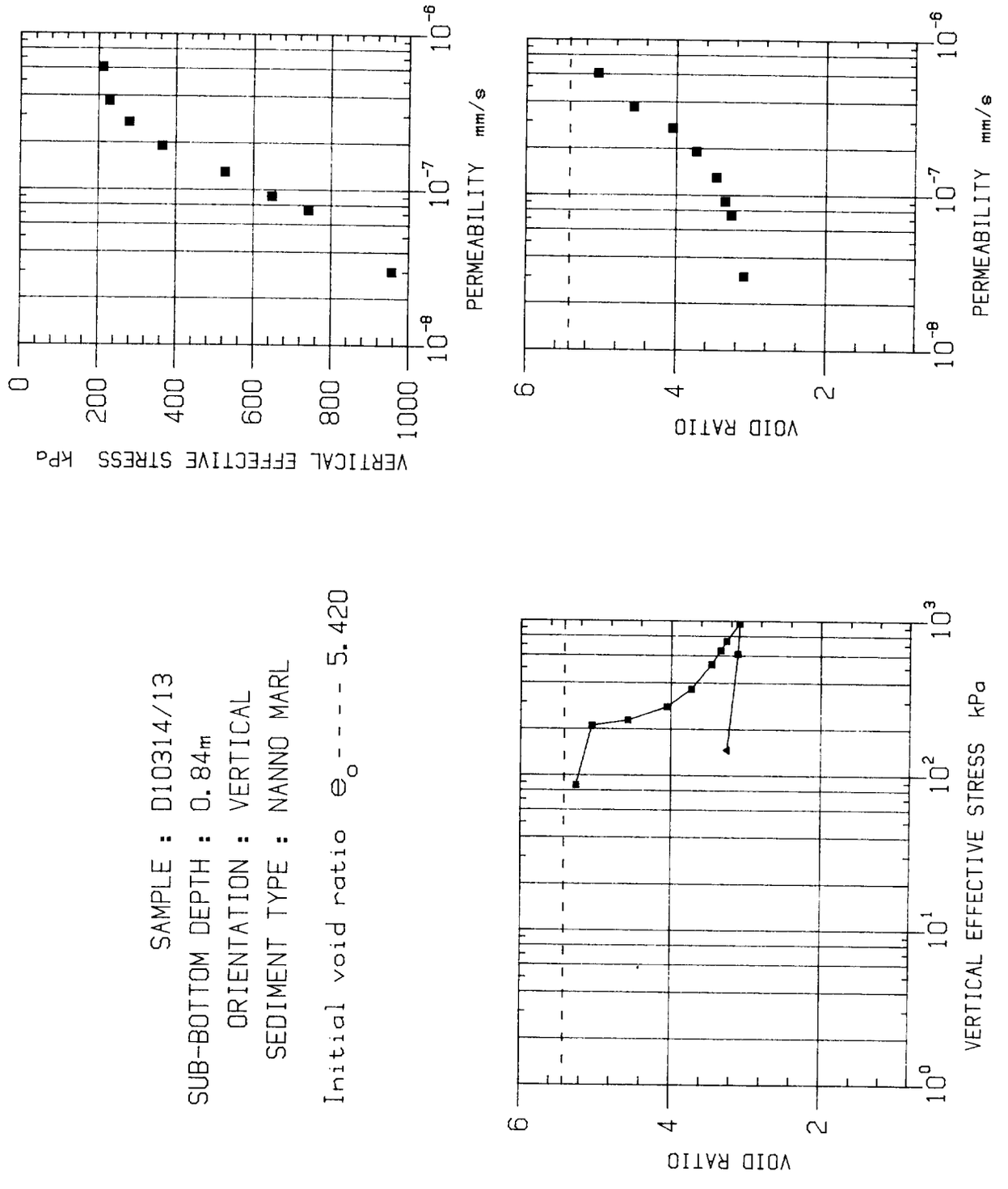
SAMPLE : D10314/13
SUB-BOTTOM DEPTH : 0.84m
ORIENTATION : VERTICAL
SEDIMENT TYPE : NANNO MARL
Initial void ratio e_o - - - - 5.420
VERTICAL EFFECTIVE STRESS kP_a
0
200
400
600
800
1000
10^{-6}
10^{-7}
10^{-8}
PERMEABILITY mm/s
VOID RATIO
2
4
6
10^{0}
10^{1}
10^{2}
10^{3}
VERTICAL EFFECTIVE STRESS kPa
PERMEABILITY mm/s

Fig. 19

Fig. 20

SAMPLE : D10314/15
SUB-BOTTOM DEPTH : 0.75m
ORIENTATION : VERTICAL
SEDIMENT TYPE : ATLANTIC RED CLAY

Initial void ratio e_o - - - - 3.808

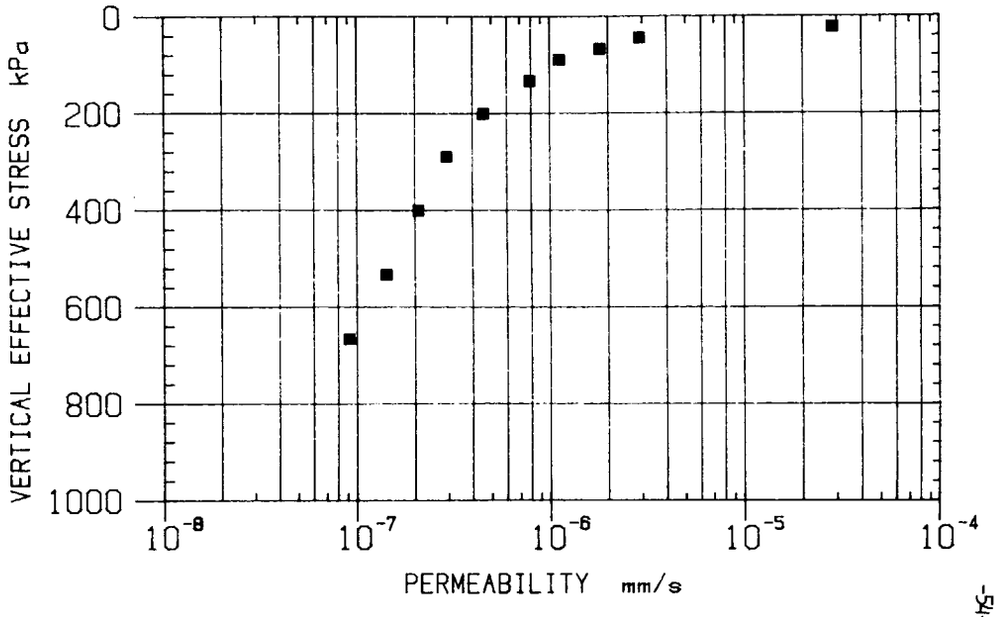

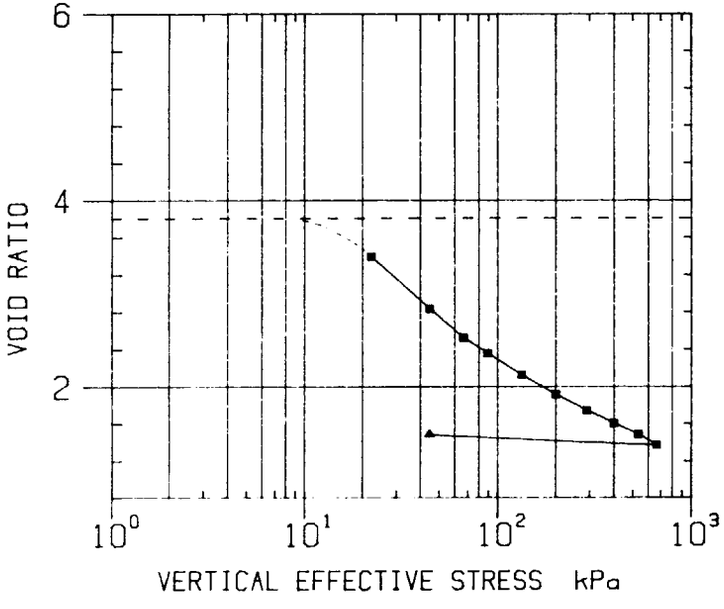

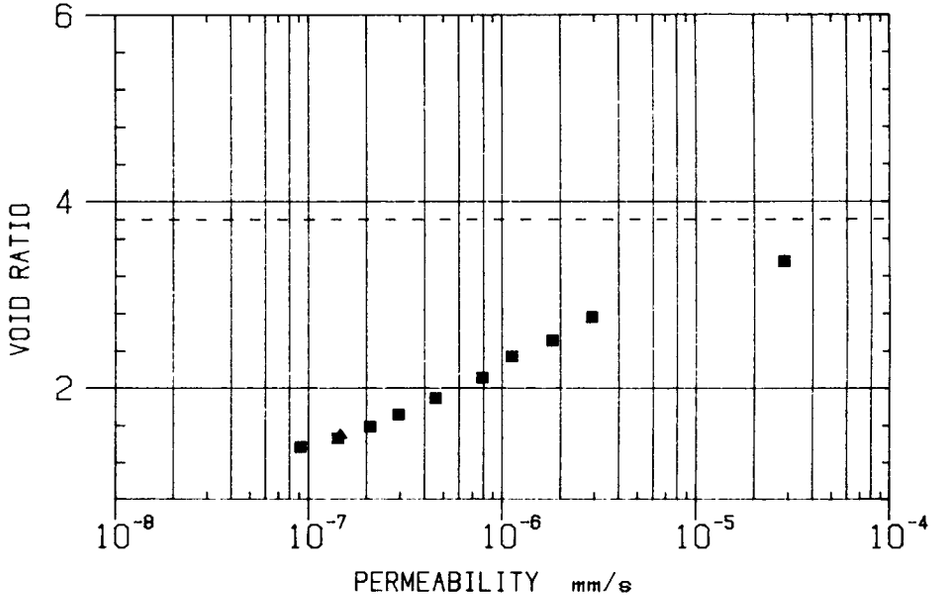

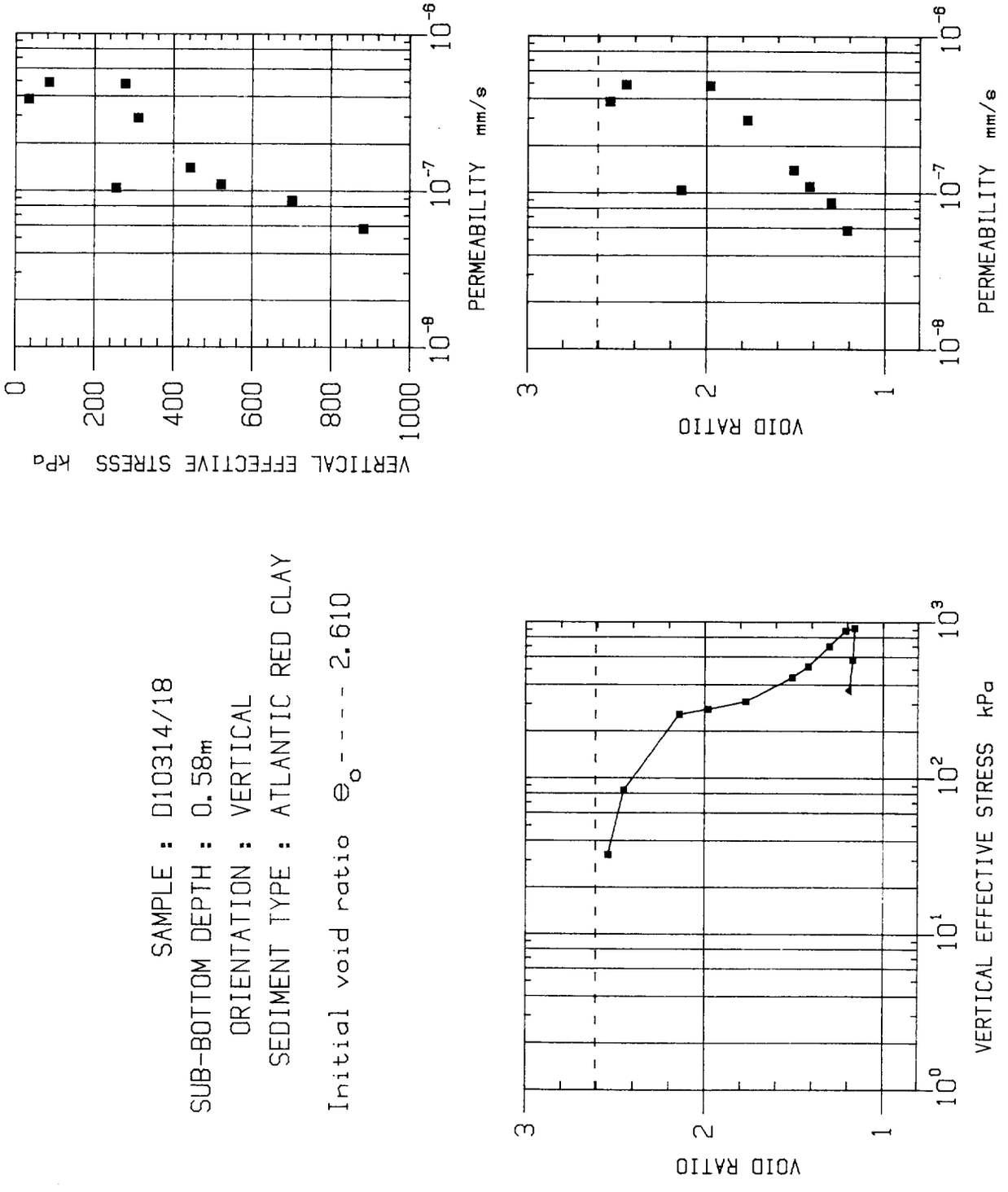
SAMPLE : D10314/18
SUB-BOTTOM DEPTH : 0.58m
ORIENTATION : VERTICAL
SEDIMENT TYPE : ATLANTIC RED CLAY
Initial void ratio e_o - - - - 2.610
VERTICAL EFFECTIVE STRESS kPa
0
200
400
600
800
1000
PERMEABILITY mm/s
10^{-8}
10^{-7}
10^{-6}
VOID RATIO
3
2
1
VERTICAL EFFECTIVE STRESS kPa
10^{0}
10^{1}
10^{2}
10^{3}

Fig. 21

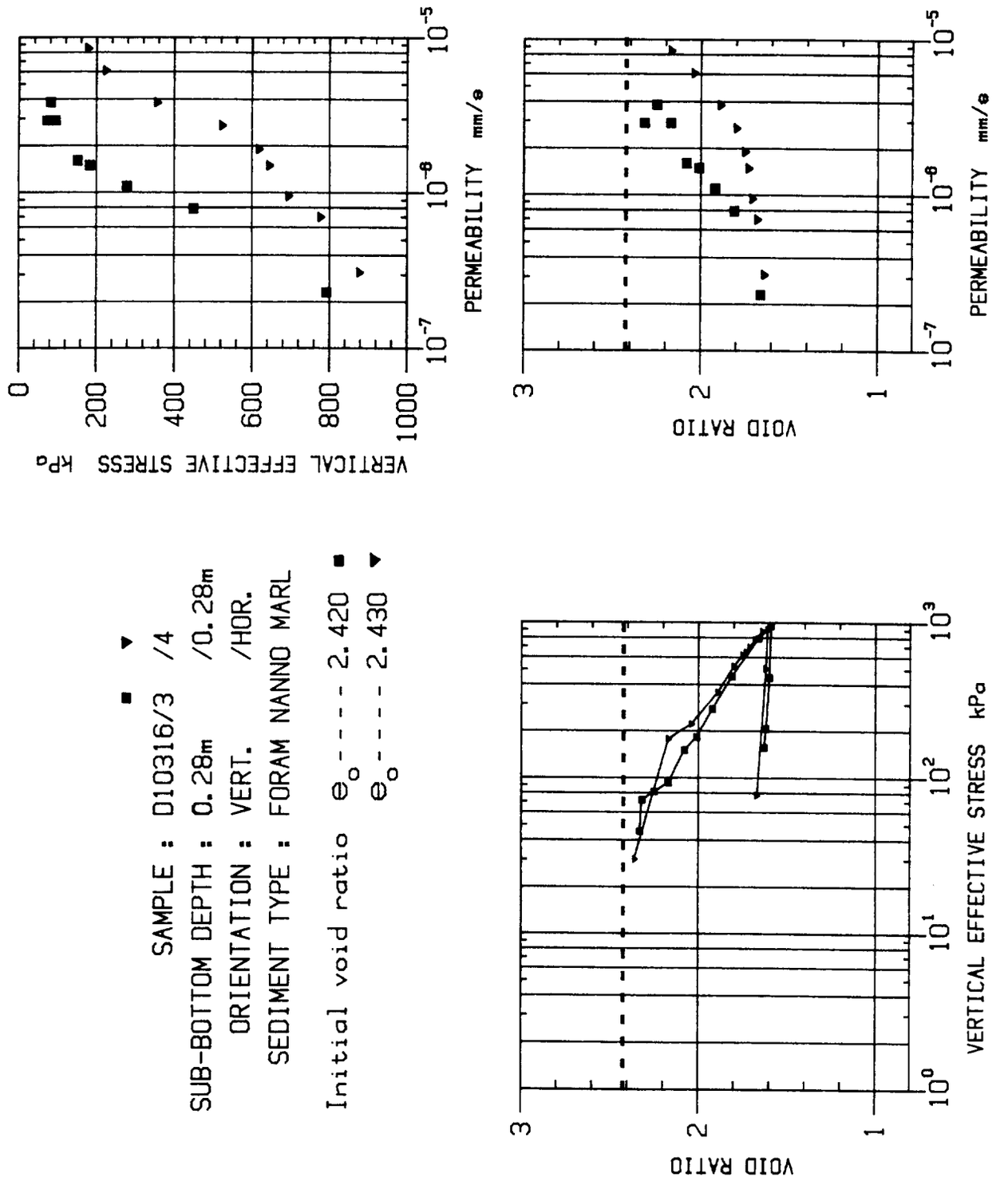
SAMPLE : D10316/3 /4
SUB-BOTTOM DEPTH : 0.28m /0.28m
ORIENTATION : VERT. /HOR.
SEDIMENT TYPE : FORAM NANNO MARL
Initial void ratio e_o ---- 2.420 ■
e_o ---- 2.430 ▼
VERTICAL EFFECTIVE STRESS kPa
VOID RATIO
PERMEABILITY mm/s
VERTICAL EFFECTIVE STRESS kPa
VOID RATIO
PERMEABILITY mm/s

Fig. 22

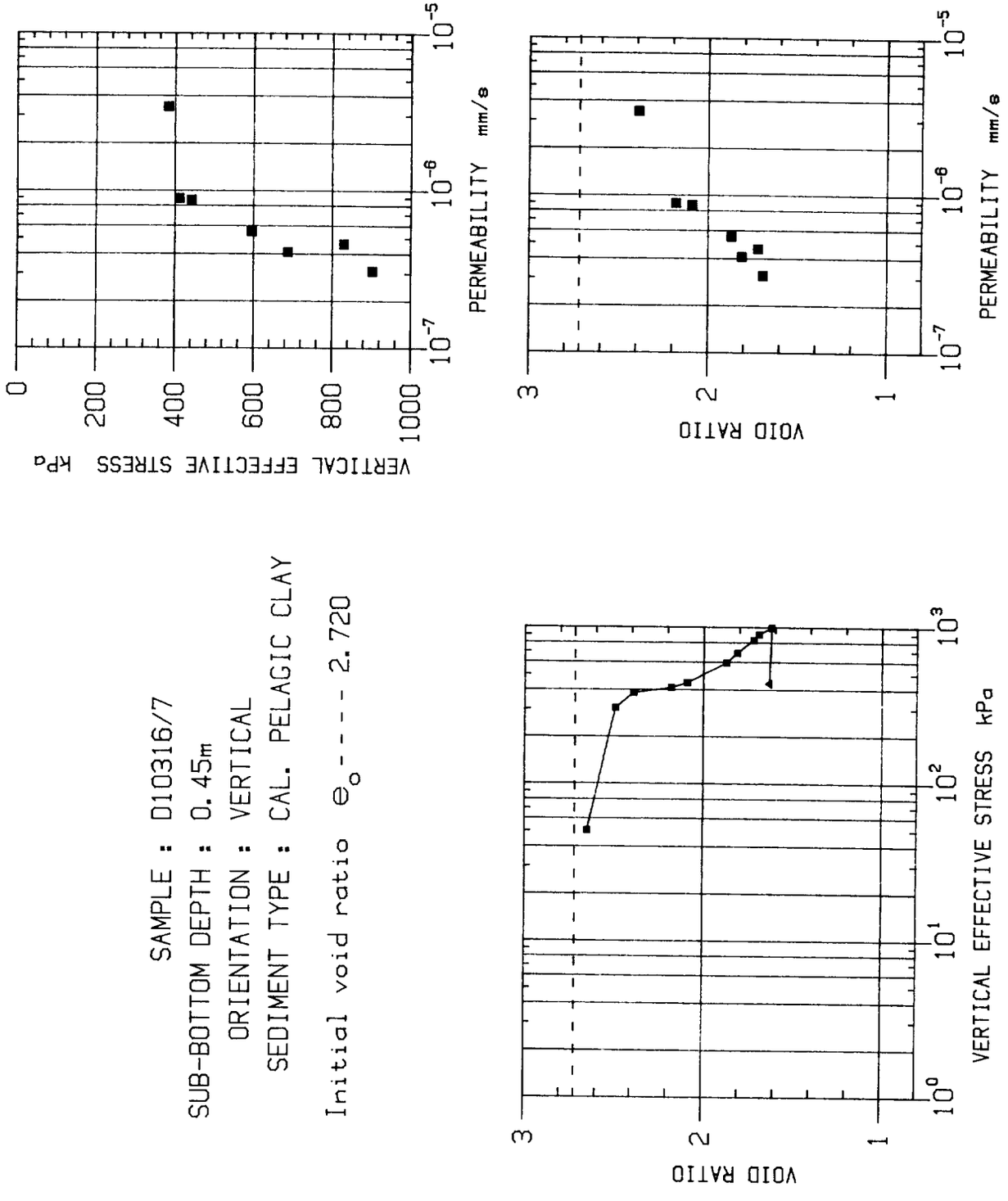
SAMPLE : D10316/7
SUB-BOTTOM DEPTH : 0.45m
ORIENTATION : VERTICAL
SEDIMENT TYPE : CAL. PELAGIC CLAY
Initial void ratio e_o ---- 2.720
VERTICAL EFFECTIVE STRESS kP_a
0
200
400
600
800
1000
10^{-5}
10^{-6}
10^{-7}
PERMEABILITY mm/s
VOID RATIO
3
2
1
10^{-5}
10^{-6}
10^{-7}
PERMEABILITY mm/s
VOID RATIO
3
2
1
10^{0}
10^{1}
10^{2}
10^{3}
VERTICAL EFFECTIVE STRESS kPa

Fig. 23

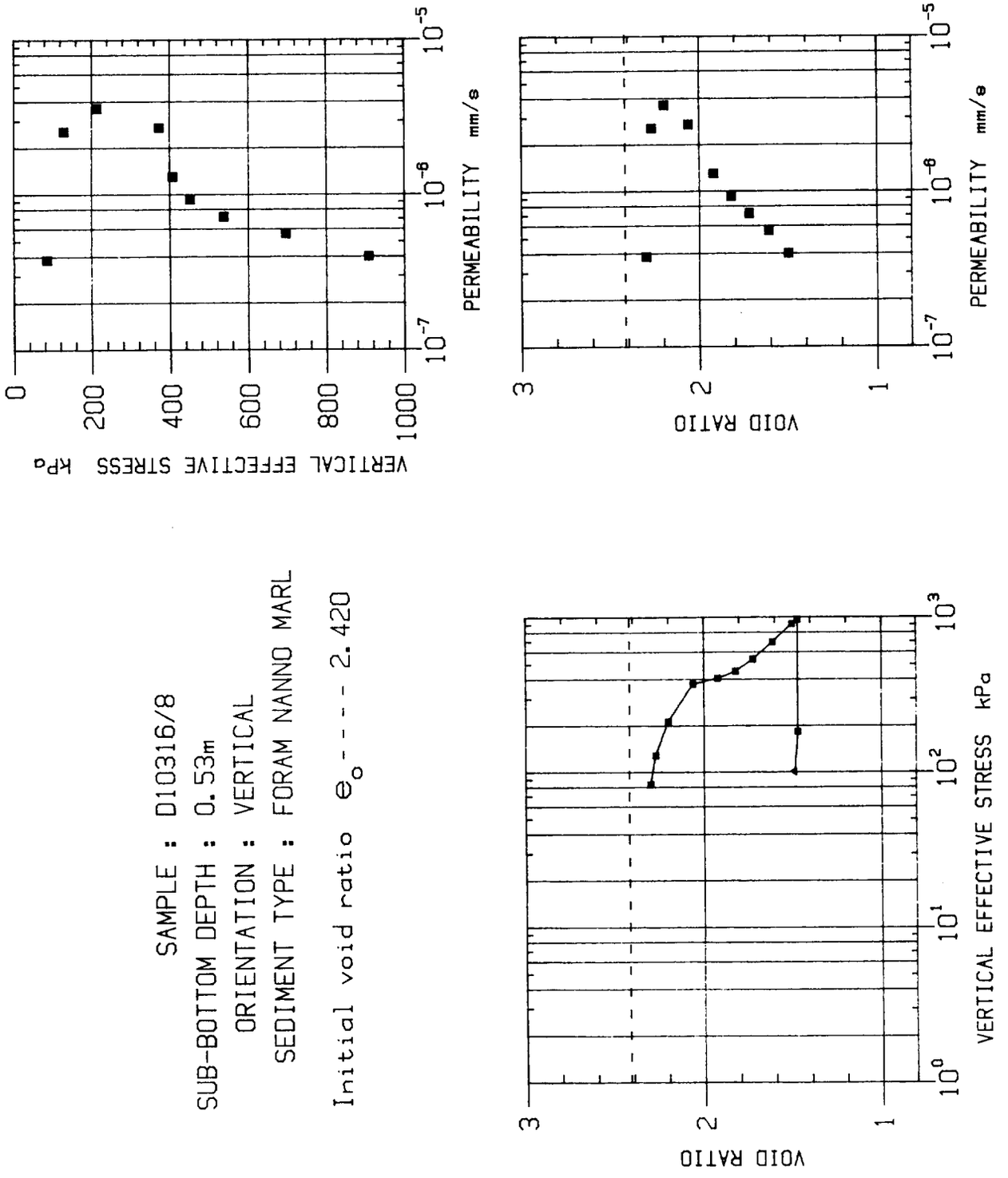
SAMPLE : D10316/8
SUB-BOTTOM DEPTH : 0.53m
ORIENTATION : VERTICAL
SEDIMENT TYPE : FORAM NANNO MARL
Initial void ratio e_o ---- 2.420
VERTICAL EFFECTIVE STRESS kPa
0
200
400
600
800
1000
PERMEABILITY mm/s
10^{-5}
10^{-6}
10^{-7}
VOID RATIO
3
2
1
VERTICAL EFFECTIVE STRESS kPa
10^{0}
10^{1}
10^{2}
10^{3}

Fig. 24

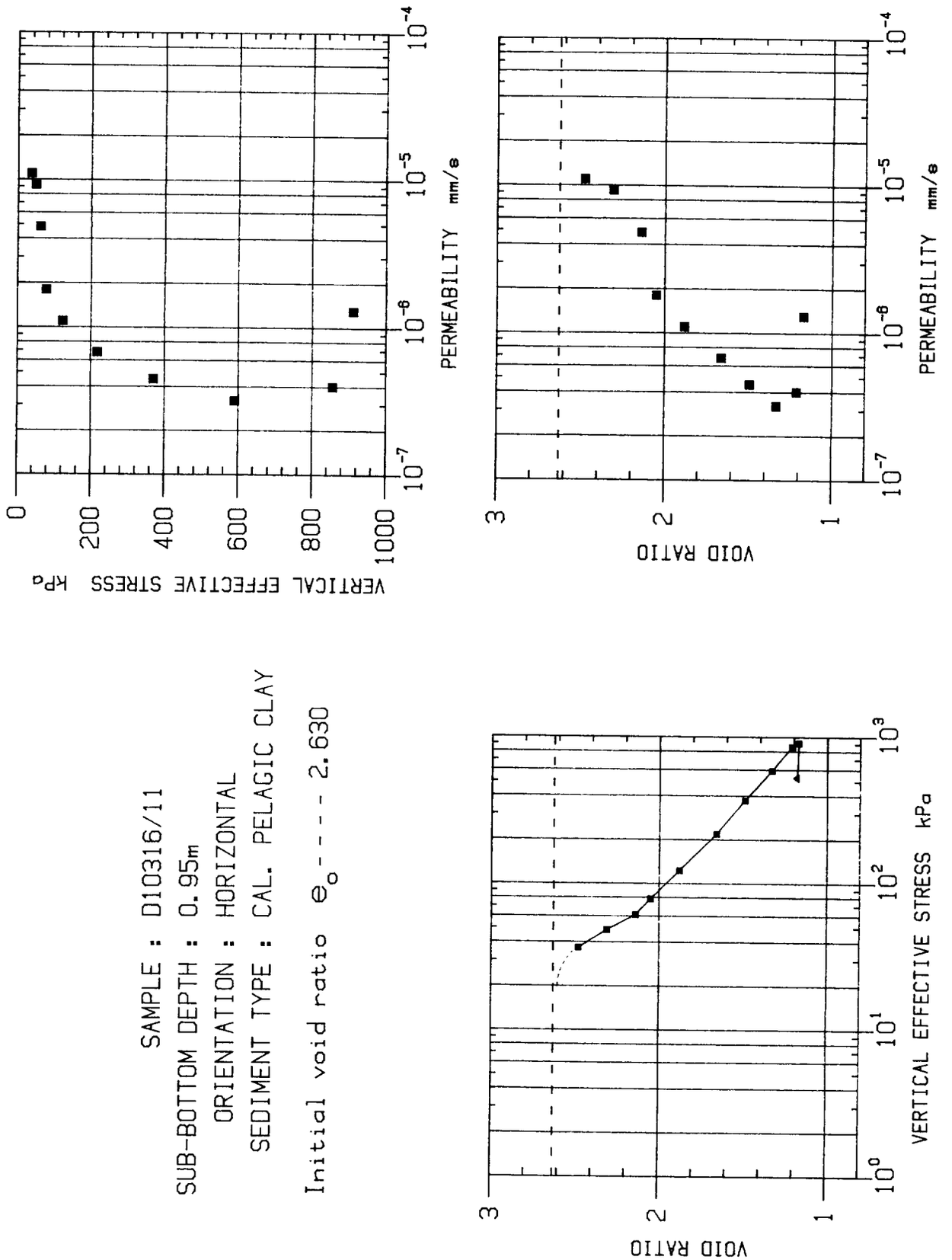
SAMPLE : D10316/11
SUB-BOTTOM DEPTH : 0.95m
ORIENTATION : HORIZONTAL
SEDIMENT TYPE : CAL. PELAGIC CLAY
Initial void ratio e_o ---- 2.630
VERTICAL EFFECTIVE STRESS kPa
0
200
400
600
800
1000
PERMEABILITY mm/s
10^{-4}
10^{-5}
10^{-6}
10^{-7}
VOID RATIO
1
2
3
VERTICAL EFFECTIVE STRESS kPa
10^{0}
10^{1}
10^{2}
10^{3}

Fig. 25

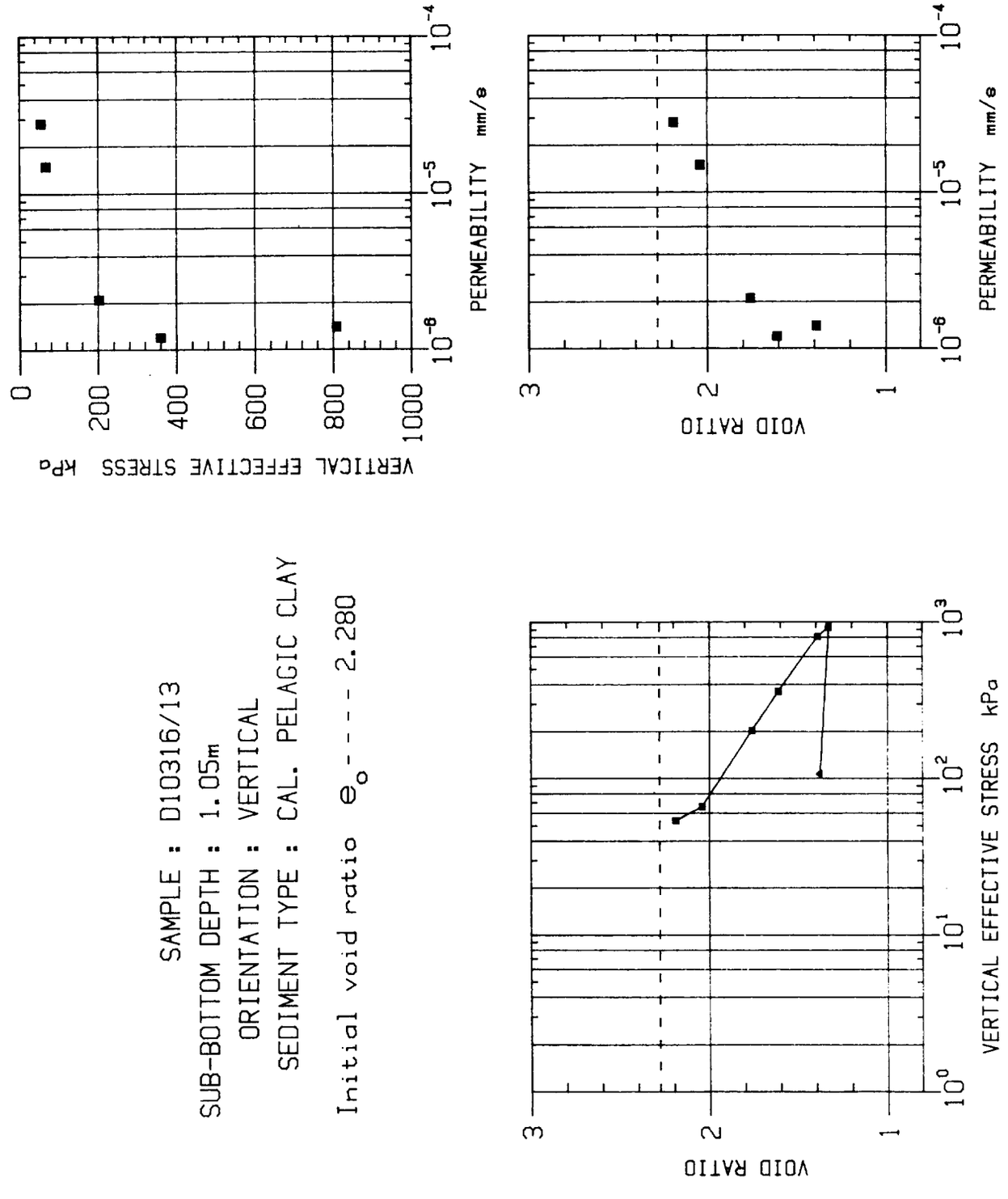
SAMPLE : D10316/13
SUB-BOTTOM DEPTH : 1.05m
ORIENTATION : VERTICAL
SEDIMENT TYPE : CAL. PELAGIC CLAY
Initial void ratio e_o - - - - 2.280
VERTICAL EFFECTIVE STRESS kPa
0
200
400
600
800
1000
PERMEABILITY mm/s
10^{-4}
10^{-5}
10^{-6}
VOID RATIO
3
2
1
VERTICAL EFFECTIVE STRESS kPa
10^{0}
10^{1}
10^{2}
10^{3}

Fig. 26

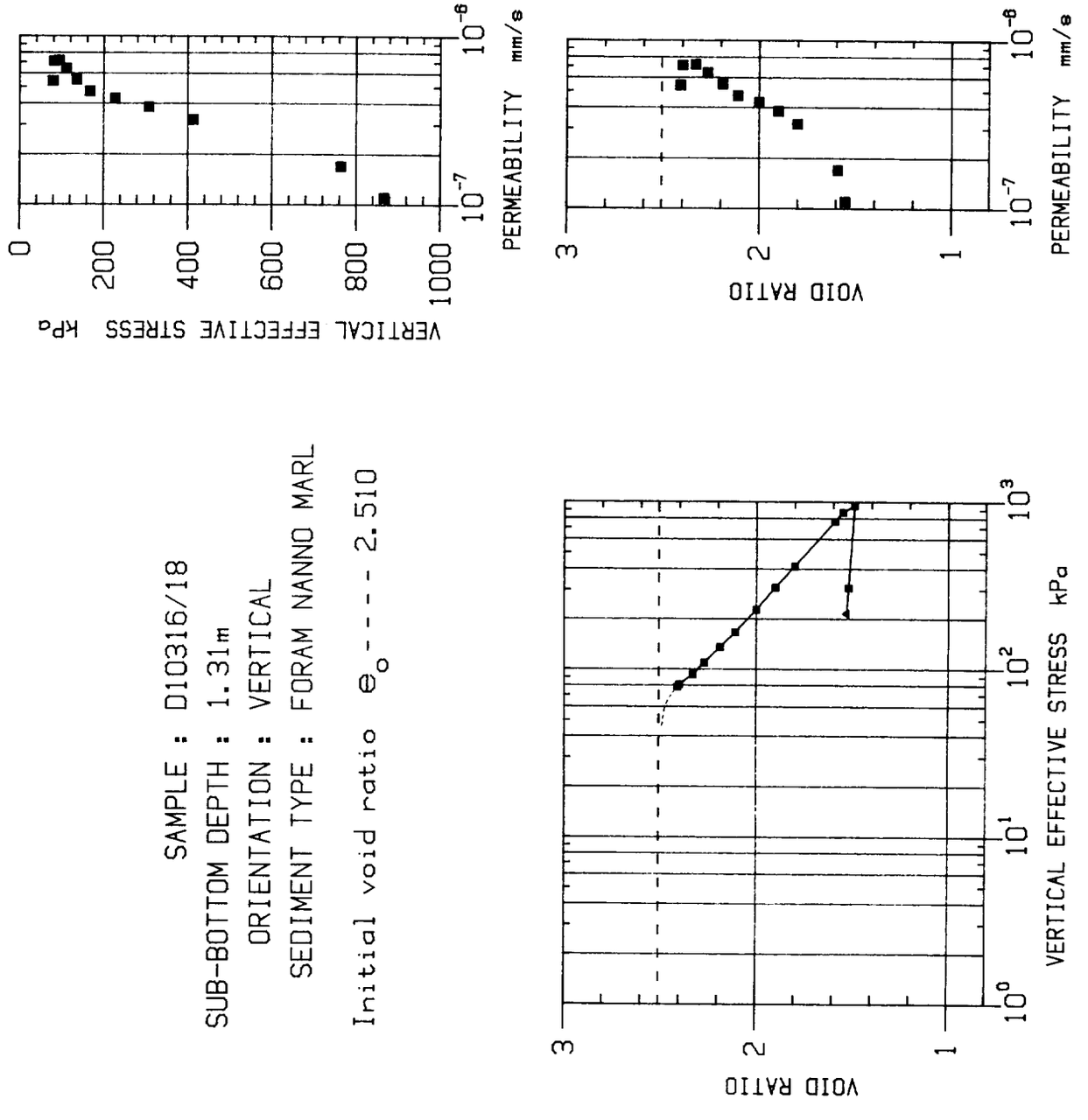
SAMPLE : D10316/18
SUB-BOTTOM DEPTH : 1.31m
ORIENTATION : VERTICAL
SEDIMENT TYPE : FORAM NANNO MARL
Initial void ratio e_o - - - - 2.510
VERTICAL EFFECTIVE STRESS kPa
0
200
400
600
800
1000
PERMEABILITY mm/s
10^{-6}
10^{-7}
VOID RATIO
3
2
1
VERTICAL EFFECTIVE STRESS kPa
10^0
10^1
10^2
10^3

Fig. 27

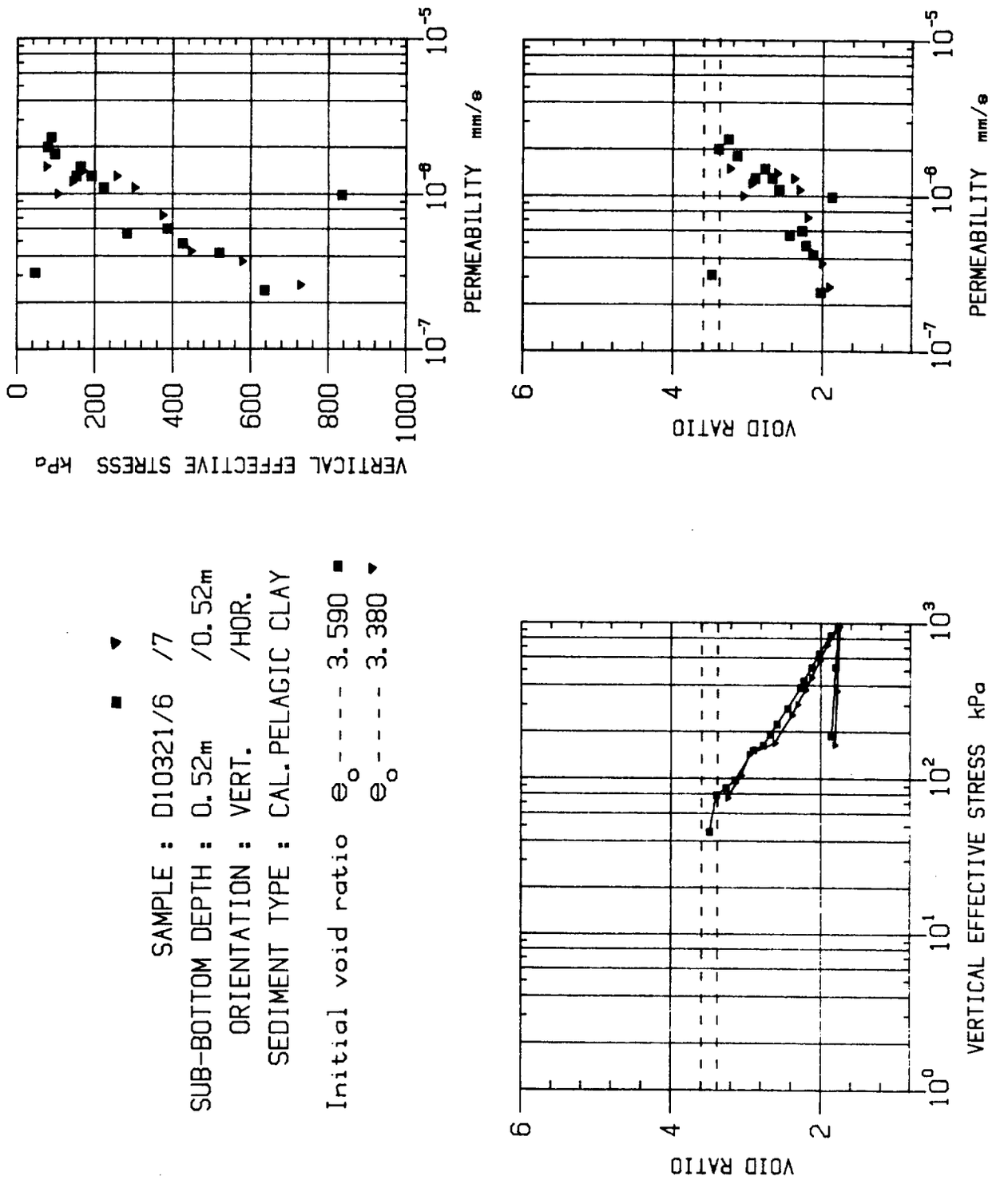
SAMPLE : D10321/6 /7
SUB-BOTTOM DEPTH : 0.52m /0.52m
ORIENTATION : VERT. /HOR.
SEDIMENT TYPE : CAL.PELAGIC CLAY
Initial void ratio e_o ---- 3.590 ■
e_o ---- 3.380 ▼
VERTICAL EFFECTIVE STRESS kPa
PERMEABILITY mm/s
VOID RATIO
VERTICAL EFFECTIVE STRESS kPa
PERMEABILITY mm/s
VOID RATIO

Fig. 28

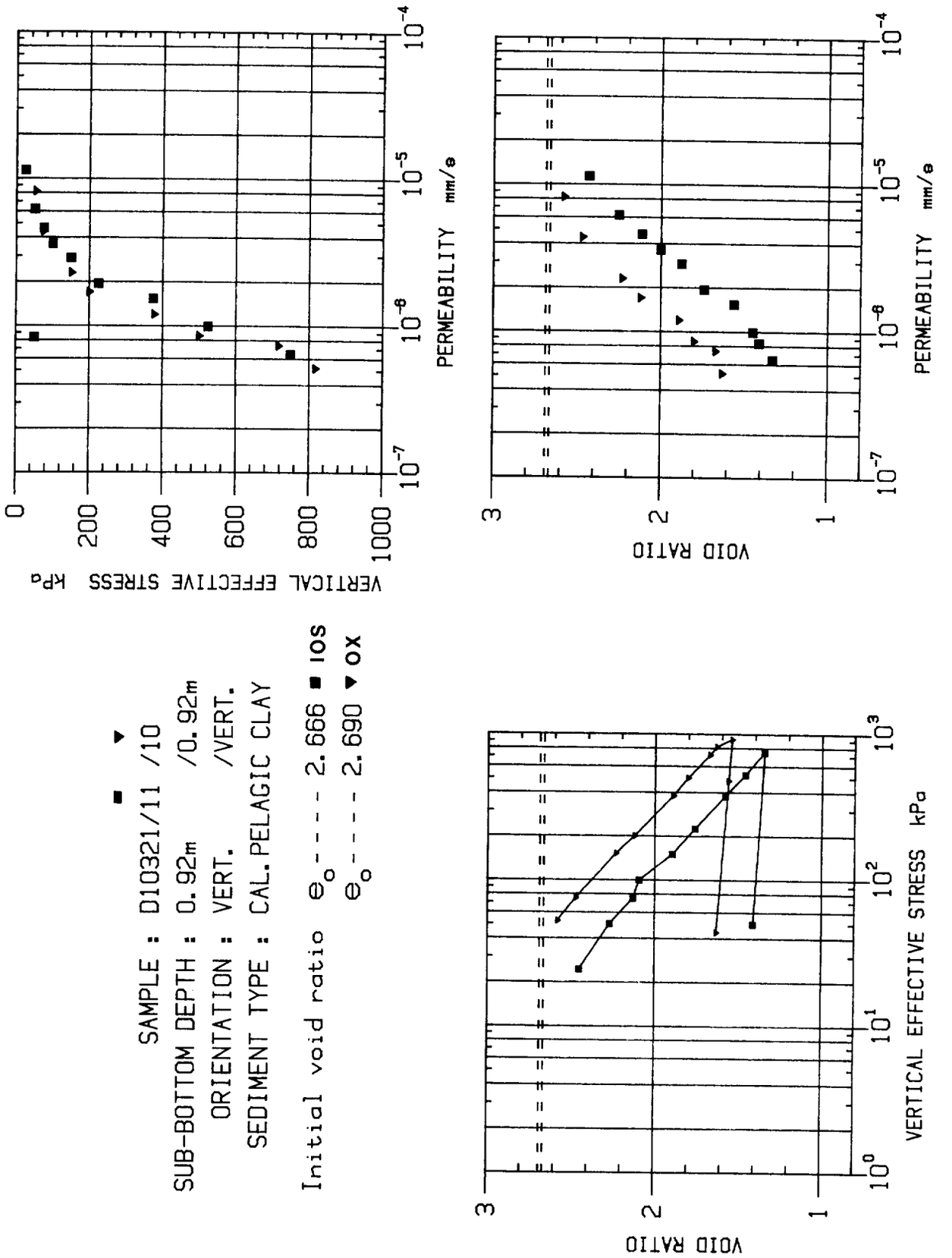
SAMPLE : D10321/11 /10
SUB-BOTTOM DEPTH : 0.92m /0.92m
ORIENTATION : VERT. /VERT.
SEDIMENT TYPE : CAL.PELAGIC CLAY
Initial void ratio e_o ---- 2.666 ■ IOS
e_o ---- 2.690 ▼ OX
VERTICAL EFFECTIVE STRESS kPa
PERMEABILITY mm/s
VOID RATIO
VERTICAL EFFECTIVE STRESS kPa

Fig. 29

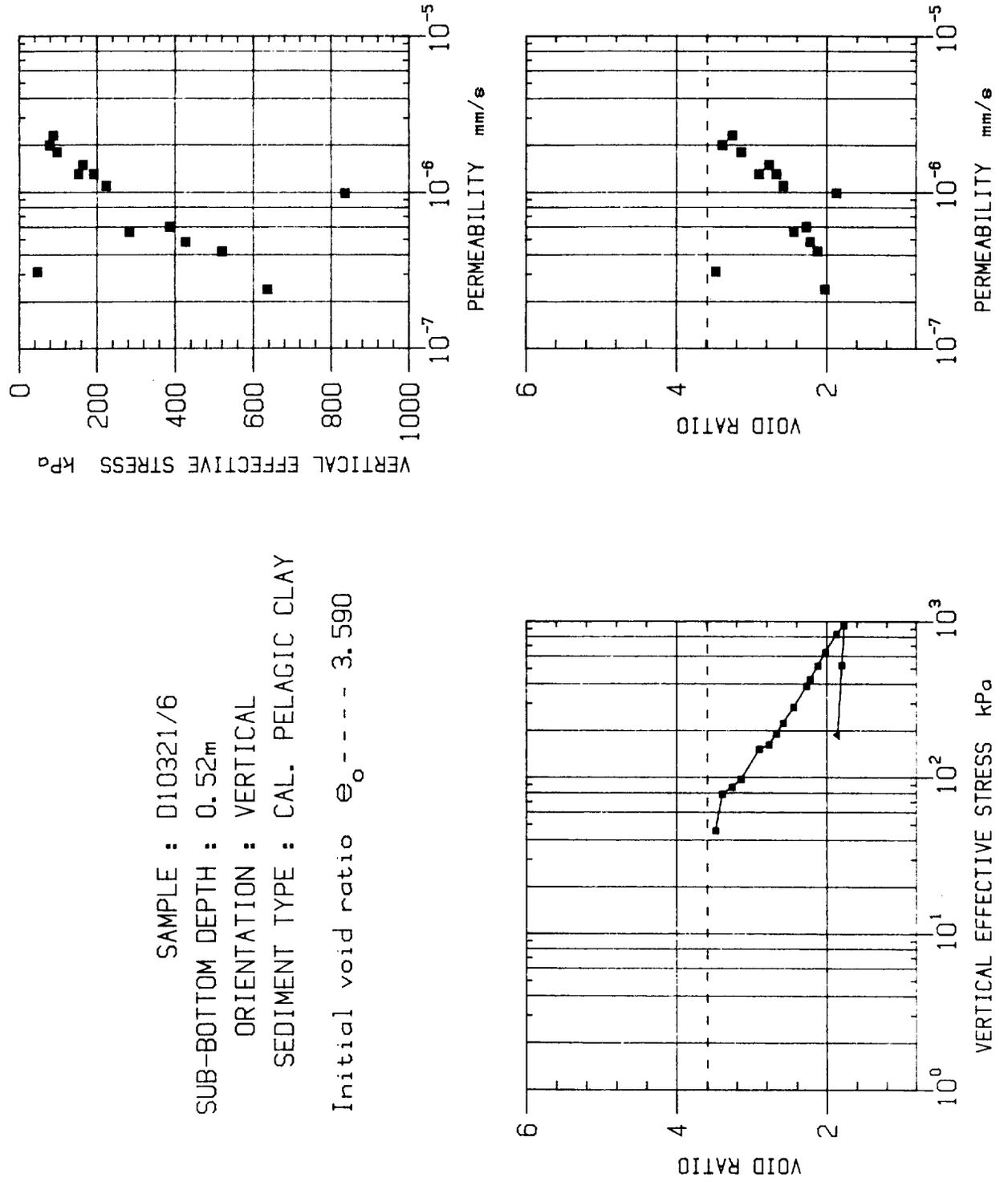
SAMPLE : D10321/6
SUB-BOTTOM DEPTH : 0.52m
ORIENTATION : VERTICAL
SEDIMENT TYPE : CAL. PELAGIC CLAY
Initial void ratio e_o - - - - 3.590
VERTICAL EFFECTIVE STRESS kPa
0
200
400
600
800
1000
PERMEABILITY mm/s
10^{-5}
10^{-6}
10^{-7}
VOID RATIO
2
4
6
VERTICAL EFFECTIVE STRESS kPa
10^{0}
10^{1}
10^{2}
10^{3}

Fig. 30

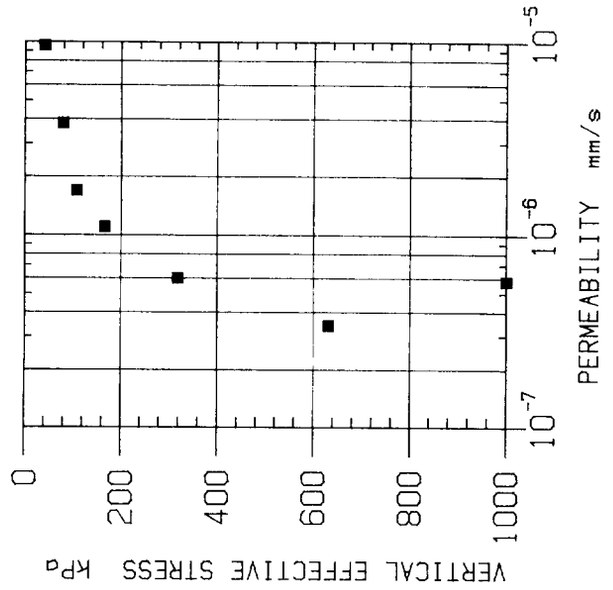

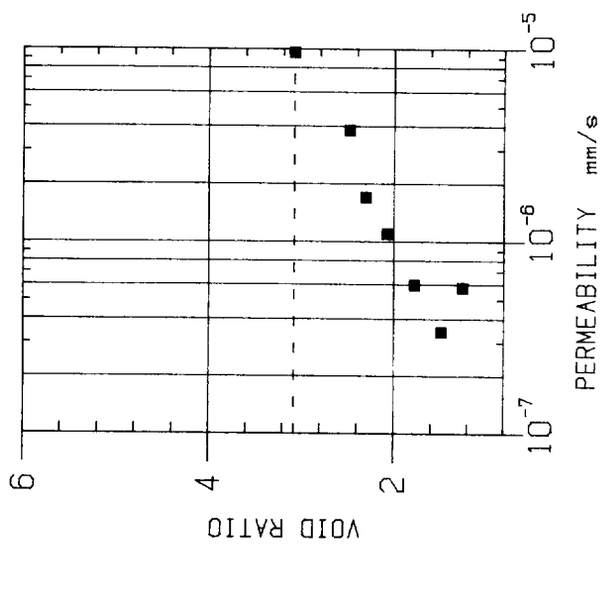

SAMPLE : D10325/4
SUB-BOTTOM DEPTH : 0.20m
ORIENTATION : VERTICAL
SEDIMENT TYPE : FORAM NANNO MARL

Initial void ratio e_o ---- 3.080

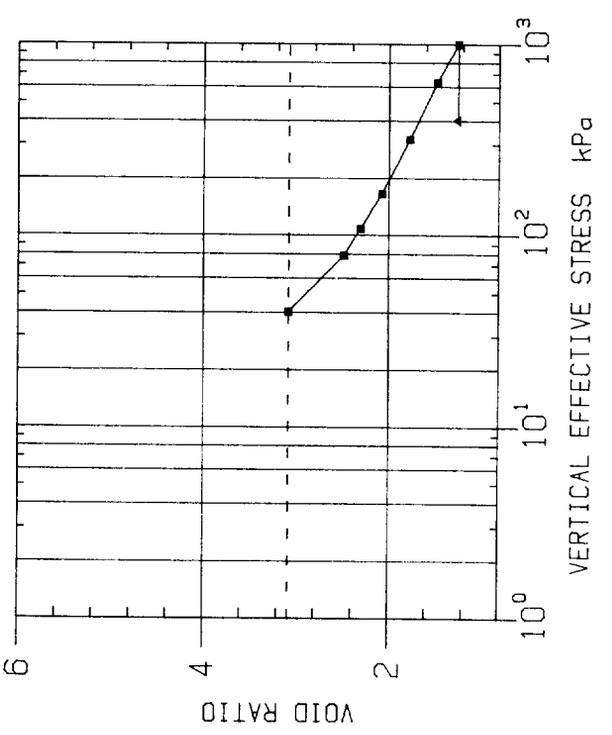

Fig. 31

Fig. 32

SAMPLE : D10325/5
SUB-BOTTOM DEPTH : 0.28m
ORIENTATION : VERTICAL
SEDIMENT TYPE : FORAM NANNO MARL

Initial void ratio e_o - - - - 2.491

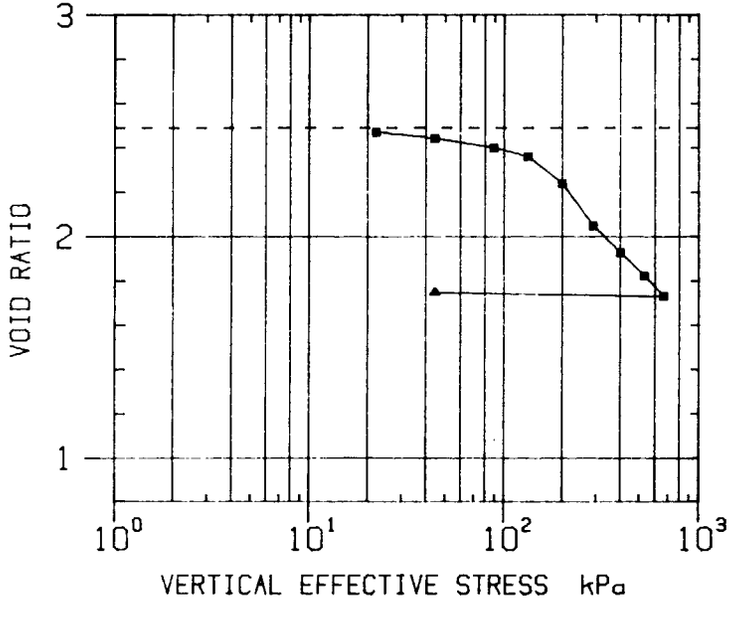

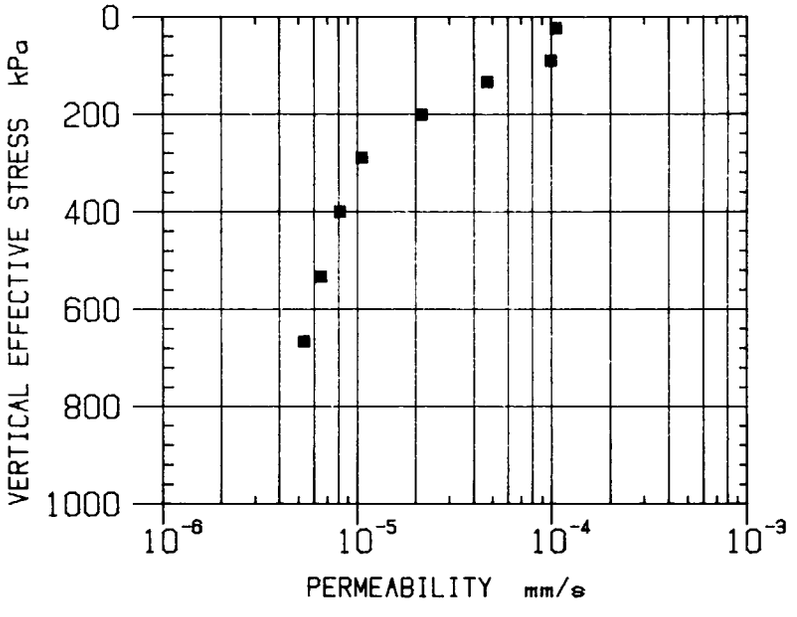

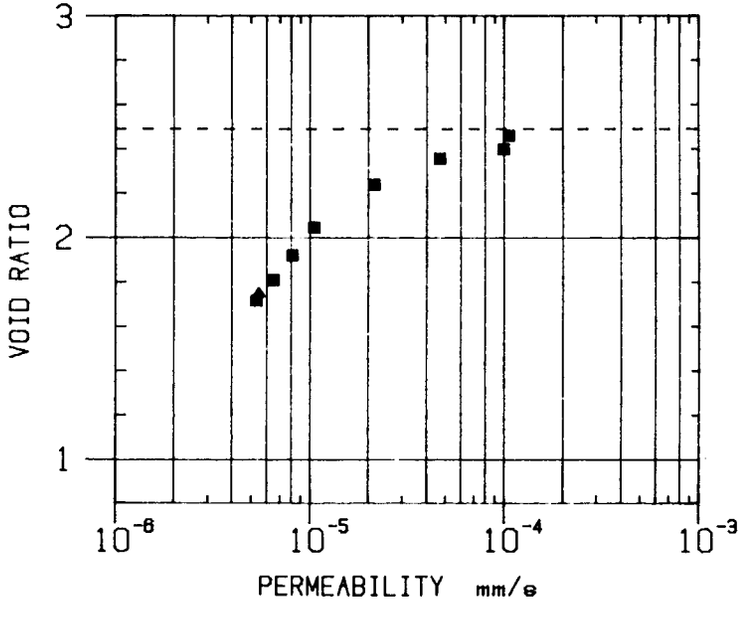

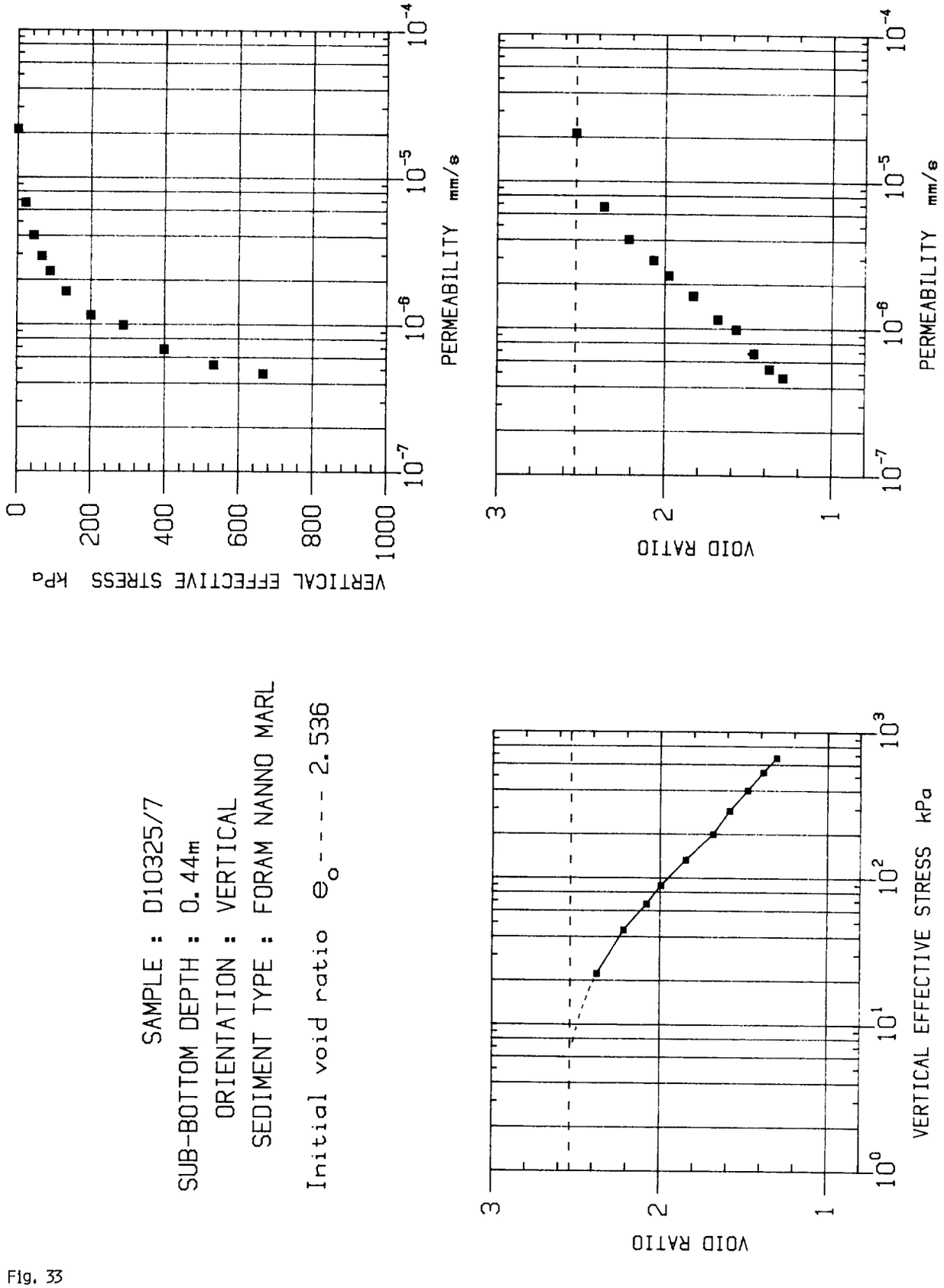
SAMPLE : D10325/7
SUB-BOTTOM DEPTH : 0.44m
ORIENTATION : VERTICAL
SEDIMENT TYPE : FORAM NANNO MARL
Initial void ratio e_o - - - - 2.536
VERTICAL EFFECTIVE STRESS kPa
0
200
400
600
800
1000
PERMEABILITY mm/s
10^{-4}
10^{-5}
10^{-6}
10^{-7}
VOID RATIO
3
2
1
PERMEABILITY mm/s
10^{-4}
10^{-5}
10^{-6}
10^{-7}
VOID RATIO
3
2
1
VERTICAL EFFECTIVE STRESS kPa
10^{0}
10^{1}
10^{2}
10^{3}

Fig. 33

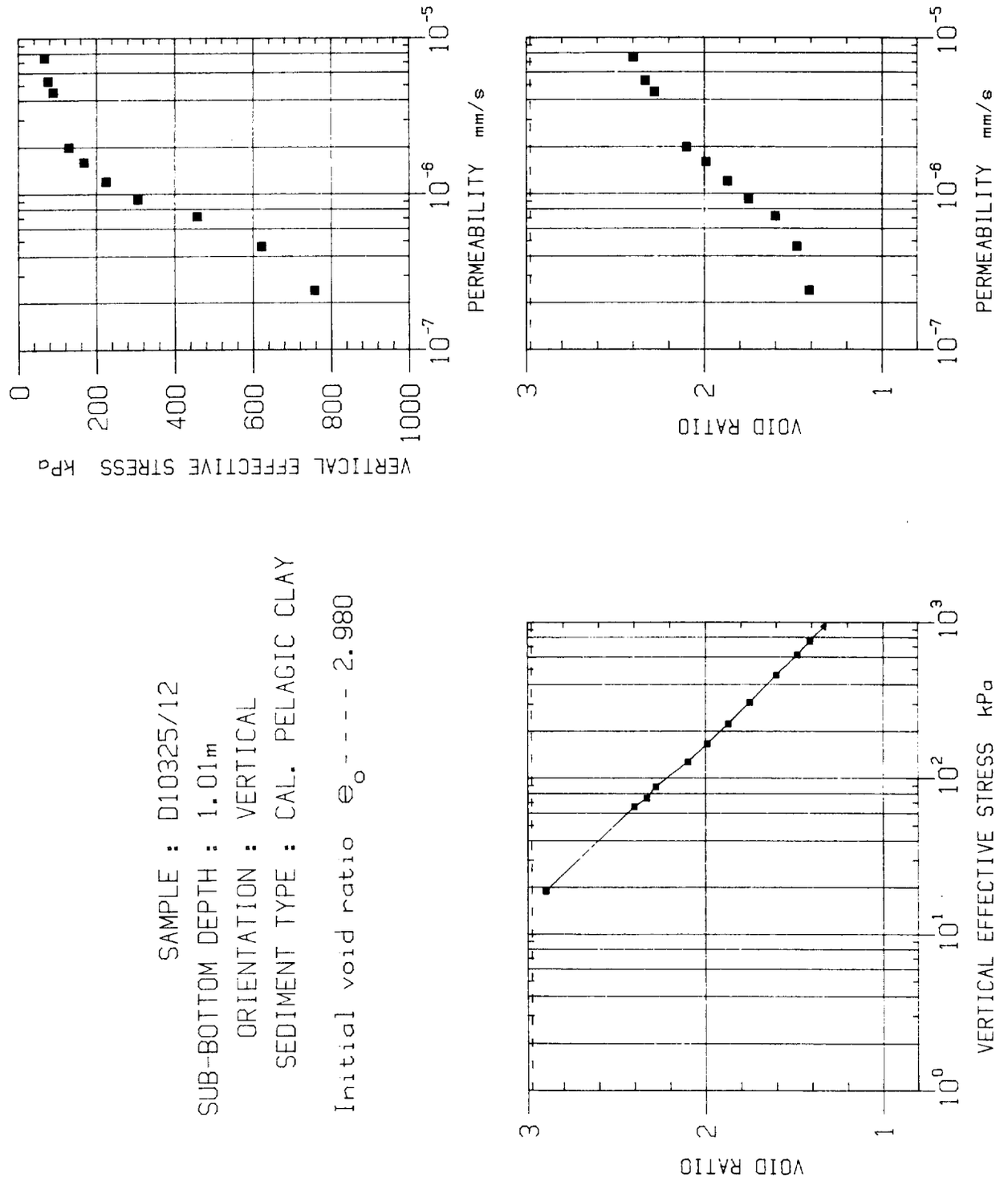
SAMPLE : D10325/12
SUB-BOTTOM DEPTH : 1.01m
ORIENTATION : VERTICAL
SEDIMENT TYPE : CAL. PELAGIC CLAY
Initial void ratio e_o - - - - 2.980
VERTICAL EFFECTIVE STRESS kP_a
0
200
400
600
800
1000
PERMEABILITY mm/s
10^{-5}
10^{-6}
10^{-7}
VOID RATIO
3
2
1
VERTICAL EFFECTIVE STRESS kPa
10^0
10^1
10^2
10^3

Fig. 34

Fig. 35

SAMPLE : D10333/2
SUB-BOTTOM DEPTH : 0.28m
ORIENTATION : VERTICAL
SEDIMENT TYPE : FORAM NANNO OOZE

Initial void ratio e_o - - - - 2.660

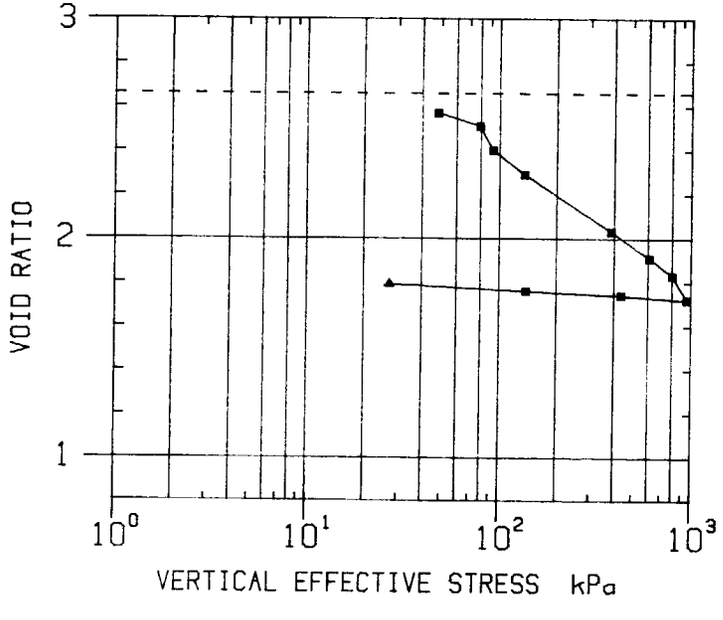

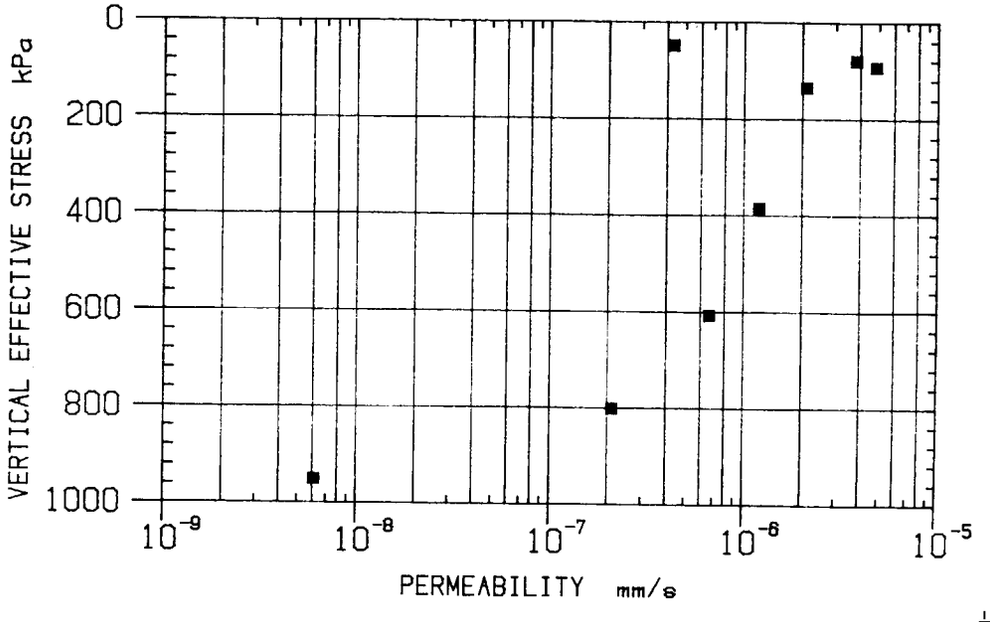

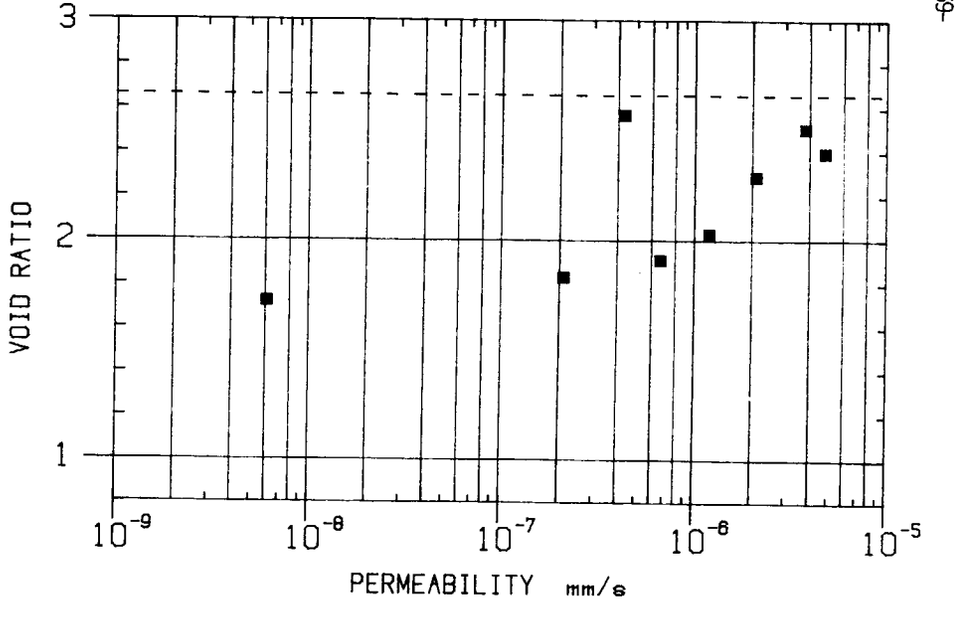

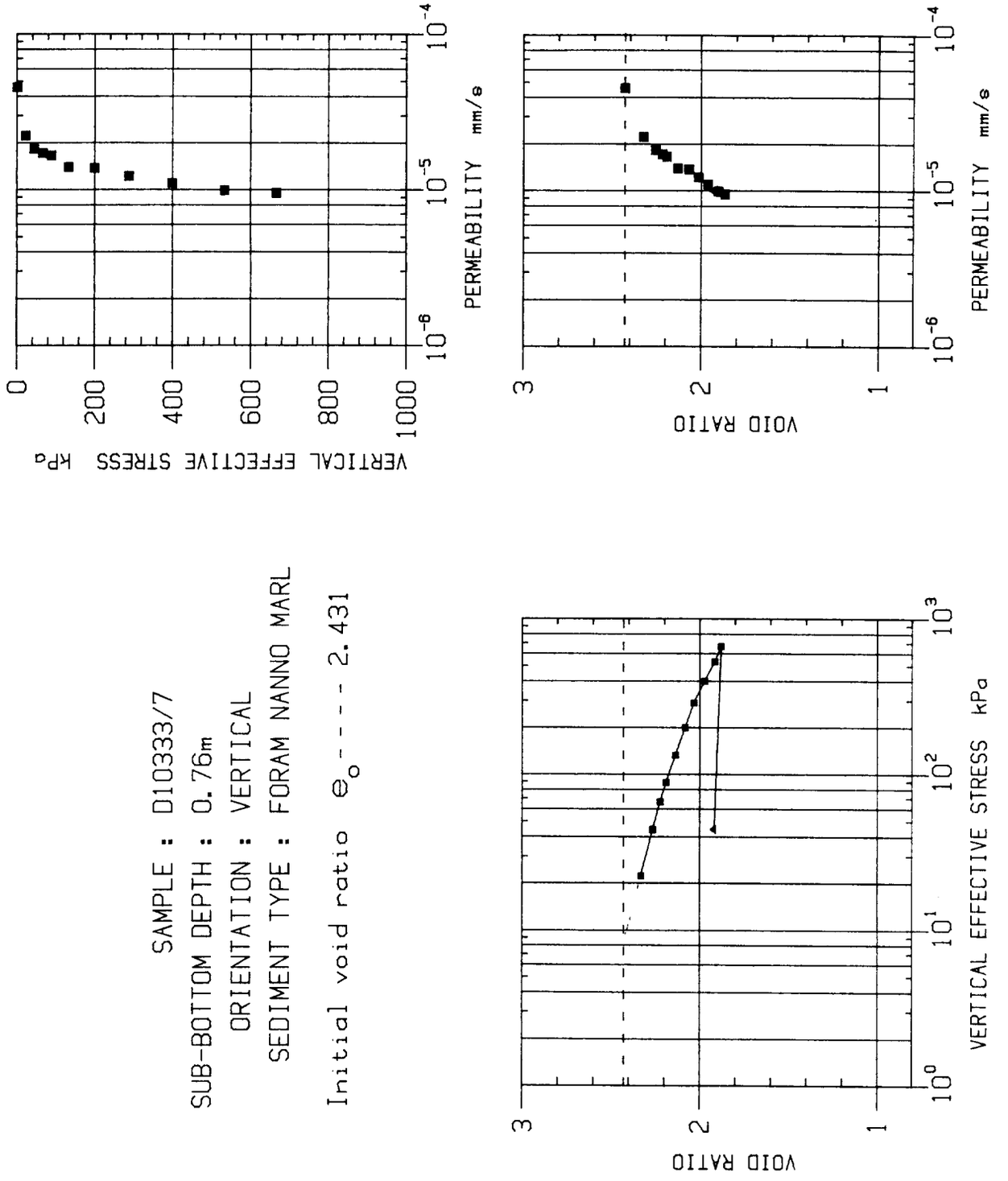
SAMPLE : D10333/7
SUB-BOTTOM DEPTH : 0.76m
ORIENTATION : VERTICAL
SEDIMENT TYPE : FORAM NANNO MARL
Initial void ratio e_o - - - - 2.431
VERTICAL EFFECTIVE STRESS kPa
0
200
400
600
800
1000
PERMEABILITY mm/s
10^{-4}
10^{-5}
10^{-6}
VOID RATIO
3
2
1
VERTICAL EFFECTIVE STRESS kPa
10^0
10^1
10^2
10^3

Fig. 36

Fig. 37

SAMPLE : D10333/9
SUB-BOTTOM DEPTH : 0.92m
ORIENTATION : VERTICAL
SEDIMENT TYPE : FORAM NANNO MARL

Initial void ratio e_o - - - - 2.250

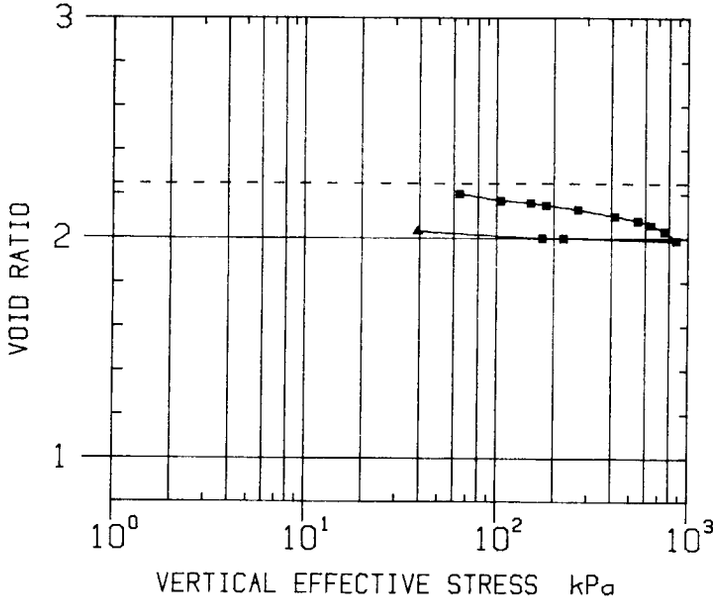

SAMPLE : D10333/10
SUB-BOTTOM DEPTH : 1.08m
ORIENTATION : VERTICAL
SEDIMENT TYPE : FORAM NANNO OOZE

Initial void ratio e_o - - - - 2.210

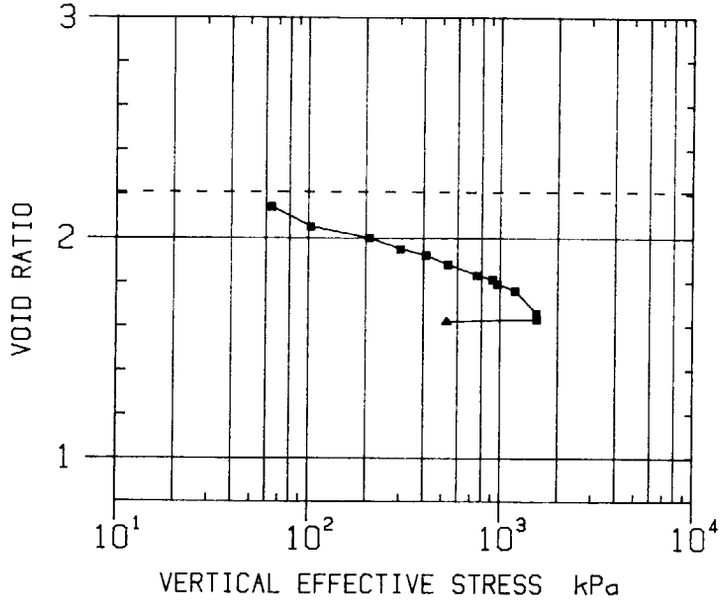

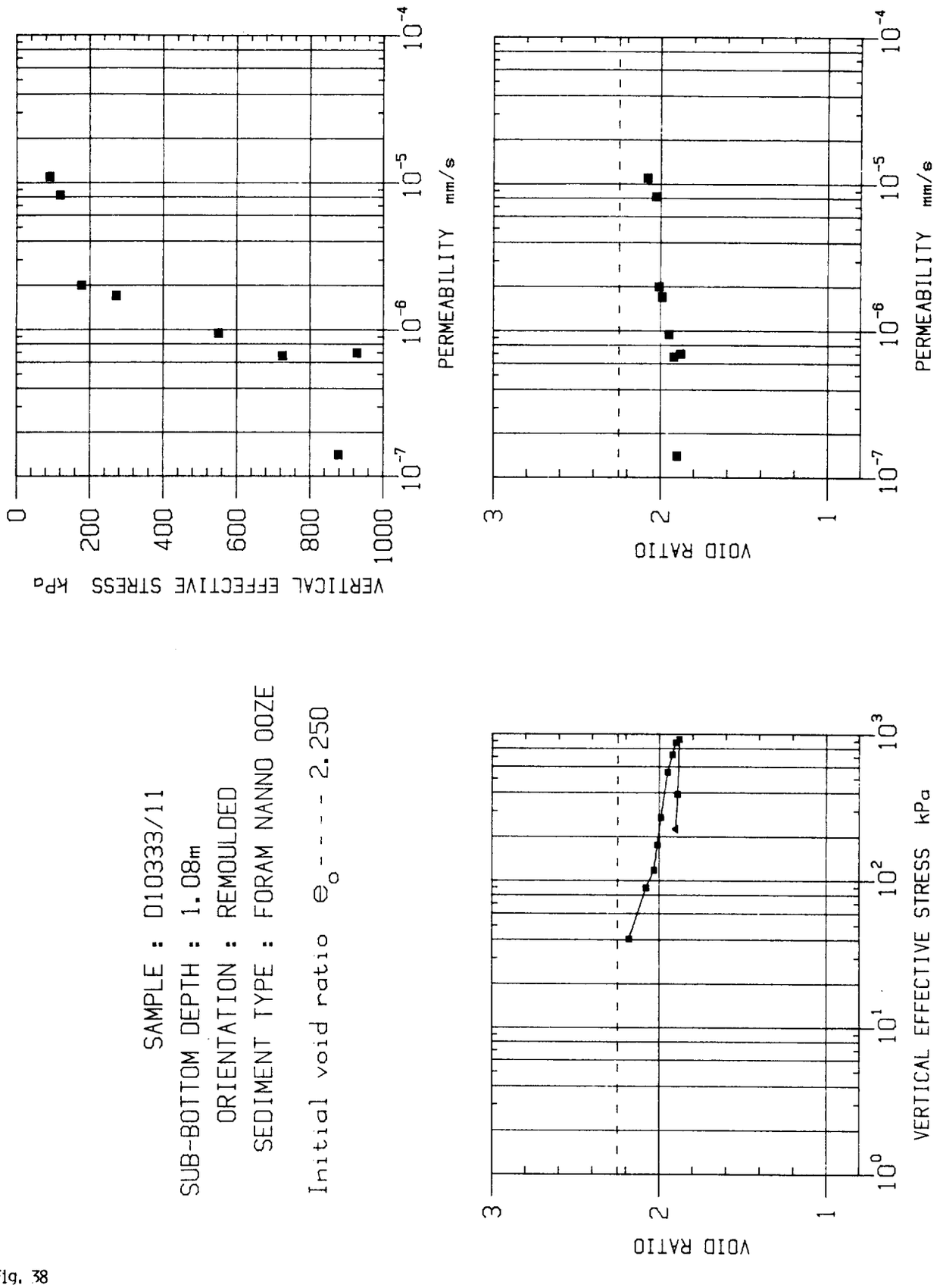
SAMPLE : D10333/11
SUB-BOTTOM DEPTH : 1.08m
ORIENTATION : REMOULDED
SEDIMENT TYPE : FORAM NANNO OOZE
Initial void ratio e_o - - - - 2.250
VERTICAL EFFECTIVE STRESS kPa
0
200
400
600
800
1000
PERMEABILITY mm/s
10^{-4}
10^{-5}
10^{-6}
10^{-7}
VOID RATIO
3
2
1
VERTICAL EFFECTIVE STRESS kPa
10^{0}
10^{1}
10^{2}
10^{3}

Fig. 38

Fig. 39

SAMPLE : D10333/12
SUB-BOTTOM DEPTH : 1.24m
ORIENTATION : VERTICAL
SEDIMENT TYPE : FORAM NANNO OOZE

Initial void ratio e_o - - - - 2.430

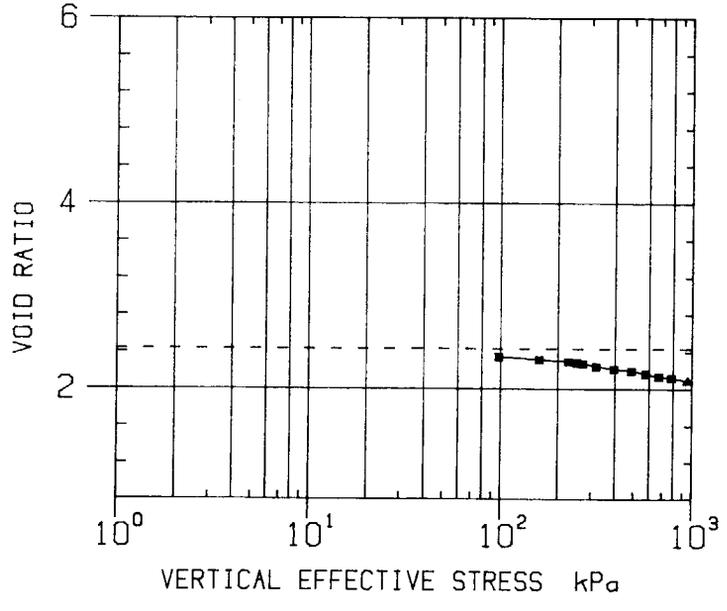

SAMPLE : D10406/1
SUB-BOTTOM DEPTH : 0.21m
ORIENTATION : VERTICAL
SEDIMENT TYPE : FORAM NANNO MARL

Initial void ratio e_o - - - - 5.190

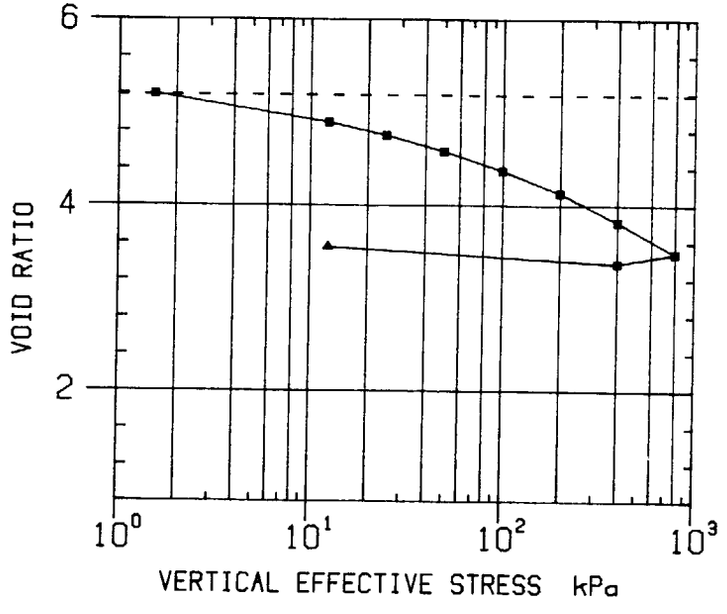

Fig. 40

SAMPLE : D10406/3
SUB-BOTTOM DEPTH : 0.51m
ORIENTATION : VERTICAL
SEDIMENT TYPE : NANNO MARL

Initial void ratio e_o - - - - 4.600

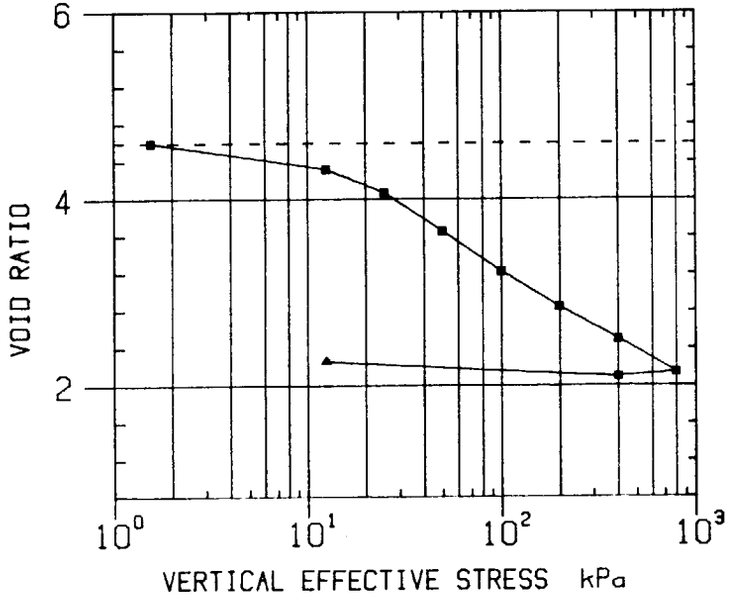

SAMPLE : D10406/7
SUB-BOTTOM DEPTH : 1.04m
ORIENTATION : VERTICAL
SEDIMENT TYPE : NANNO MARL

Initial void ratio e_o - - - - 5.340

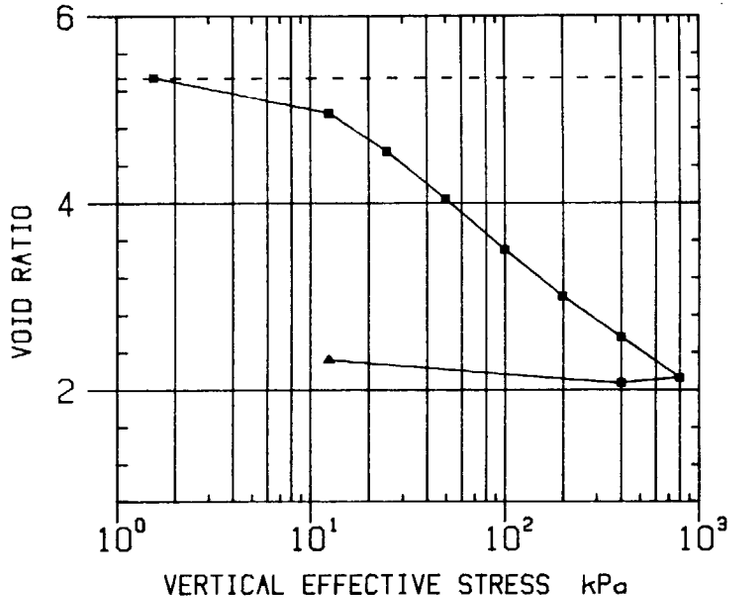

Fig. 41

SAMPLE : D10406/11
SUB-BOTTOM DEPTH : 1.86m
ORIENTATION : VERTICAL
SEDIMENT TYPE : FORAM NANNO OOZE

Initial void ratio e_o - - - - 3.210

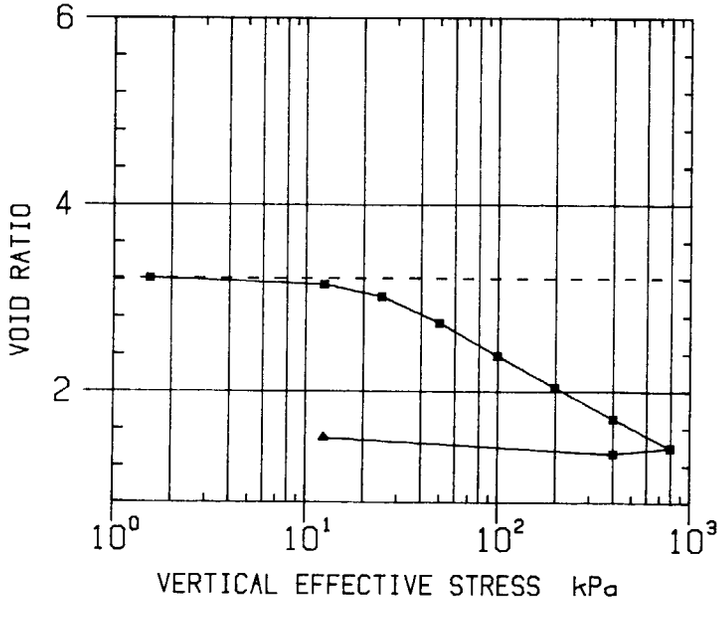

SAMPLE : D10406/20
SUB-BOTTOM DEPTH : 3.04m
ORIENTATION : VERTICAL
SEDIMENT TYPE : FORAM NANNO MARL

Initial void ratio e_o - - - - 2.100

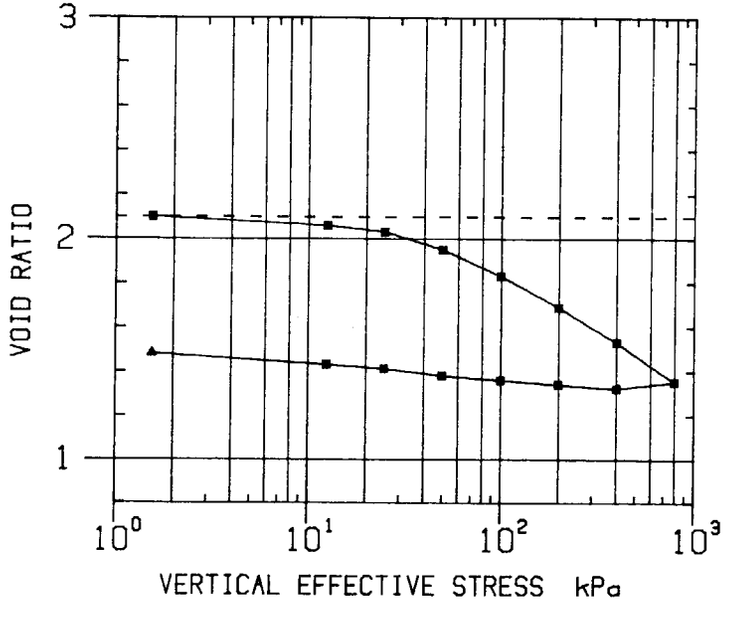

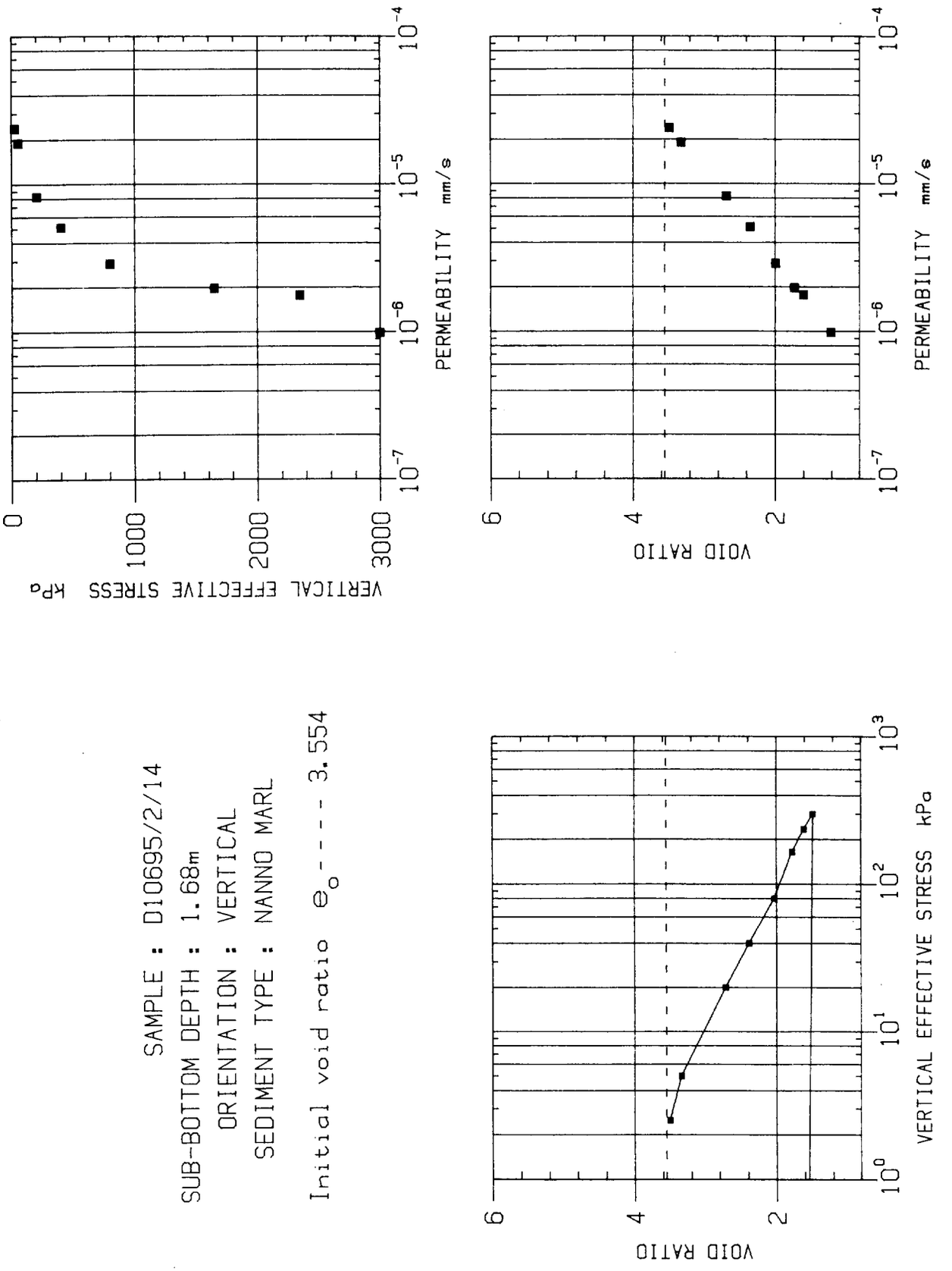
SAMPLE : D10695/2/14
SUB-BOTTOM DEPTH : 1.68m
ORIENTATION : VERTICAL
SEDIMENT TYPE : NANNO MARL
Initial void ratio e_o - - - - 3.554
VERTICAL EFFECTIVE STRESS kPa
0
1000
2000
3000
PERMEABILITY mm/s
10^{-4}
10^{-5}
10^{-6}
10^{-7}
VOID RATIO
2
4
6
VERTICAL EFFECTIVE STRESS kPa
10^{0}
10^{1}
10^{2}
10^{3}

Fig. 42

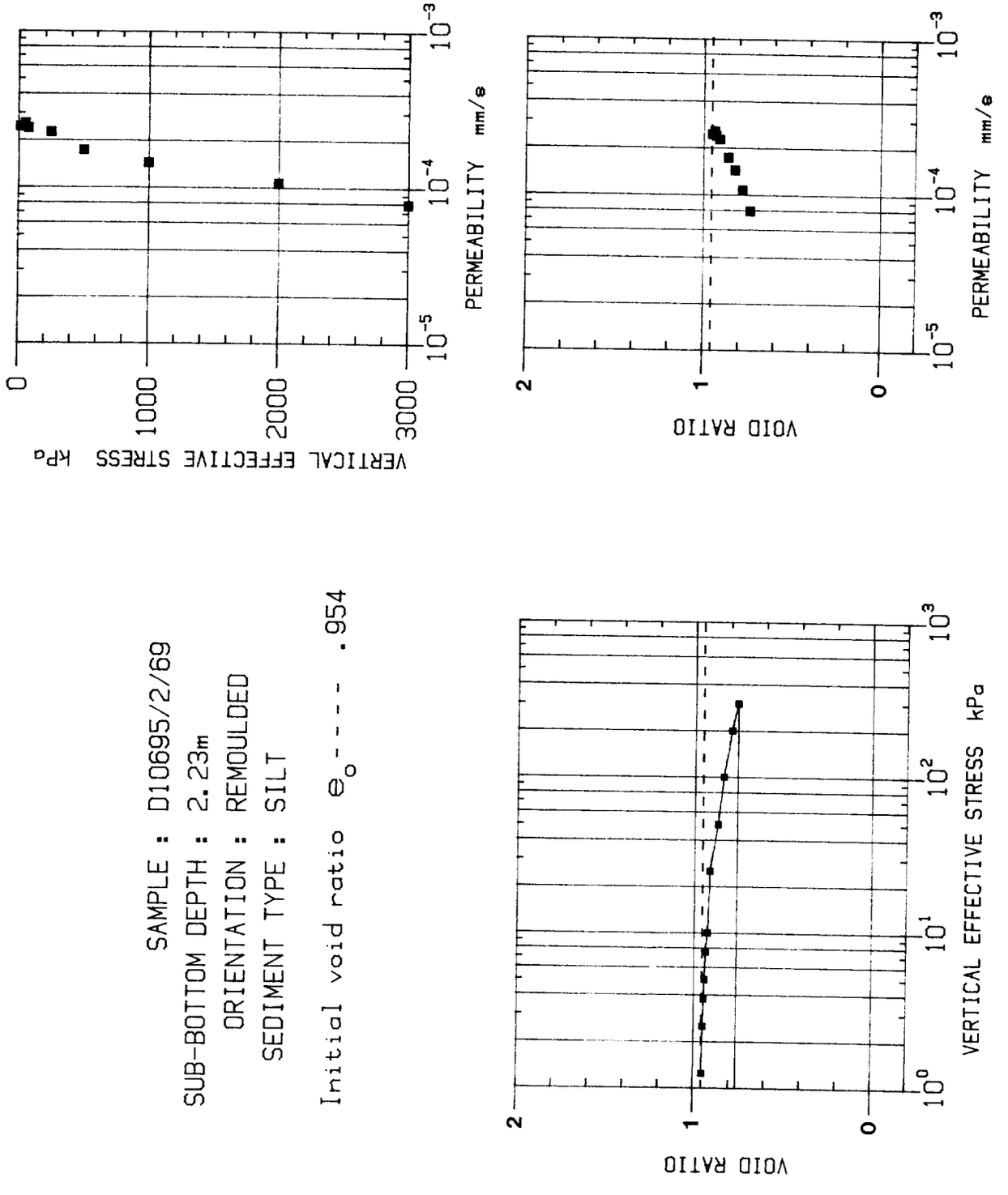
SAMPLE : D10695/2/69
SUB-BOTTOM DEPTH : 2.23m
ORIENTATION : REMOULDED
SEDIMENT TYPE : SILT
Initial void ratio e_o - - - - .954
VERTICAL EFFECTIVE STRESS kPa
0
1000
2000
3000
10^{-3}
10^{-4}
10^{-5}
PERMEABILITY mm/s
VOID RATIO
2
1
0
10^{0}
10^{1}
10^{2}
10^{3}

Fig. 43

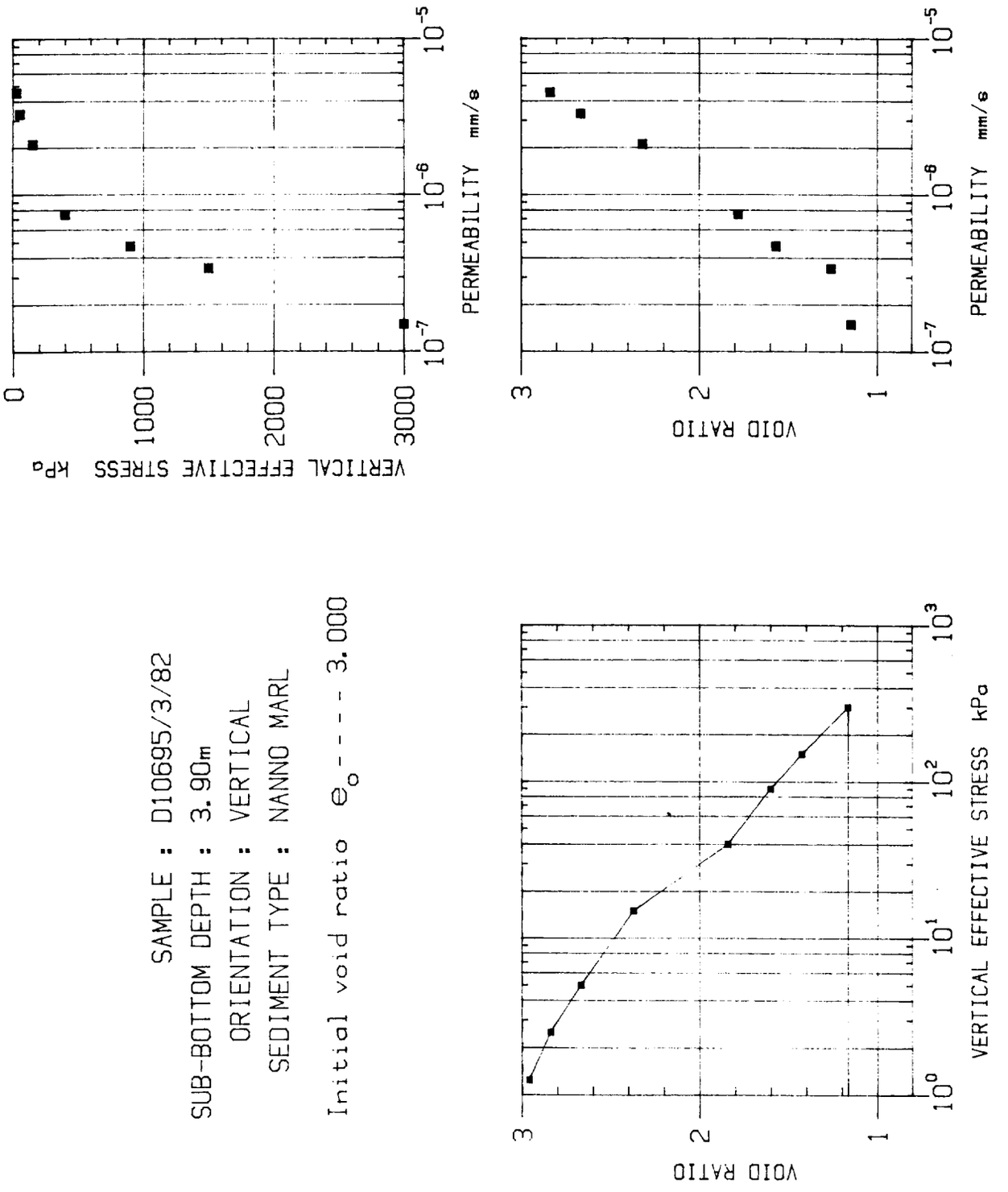
SAMPLE : D10695/3/82
SUB-BOTTOM DEPTH : 3.90m
ORIENTATION : VERTICAL
SEDIMENT TYPE : NANNO MARL
Initial void ratio e_o - - - - 3.000
VERTICAL EFFECTIVE STRESS kPa
0
1000
2000
3000
PERMEABILITY mm/s
10^{-5}
10^{-6}
10^{-7}
VOID RATIO
3
2
1
VERTICAL EFFECTIVE STRESS kPa
10^{0}
10^{1}
10^{2}
10^{3}

Fig. 44

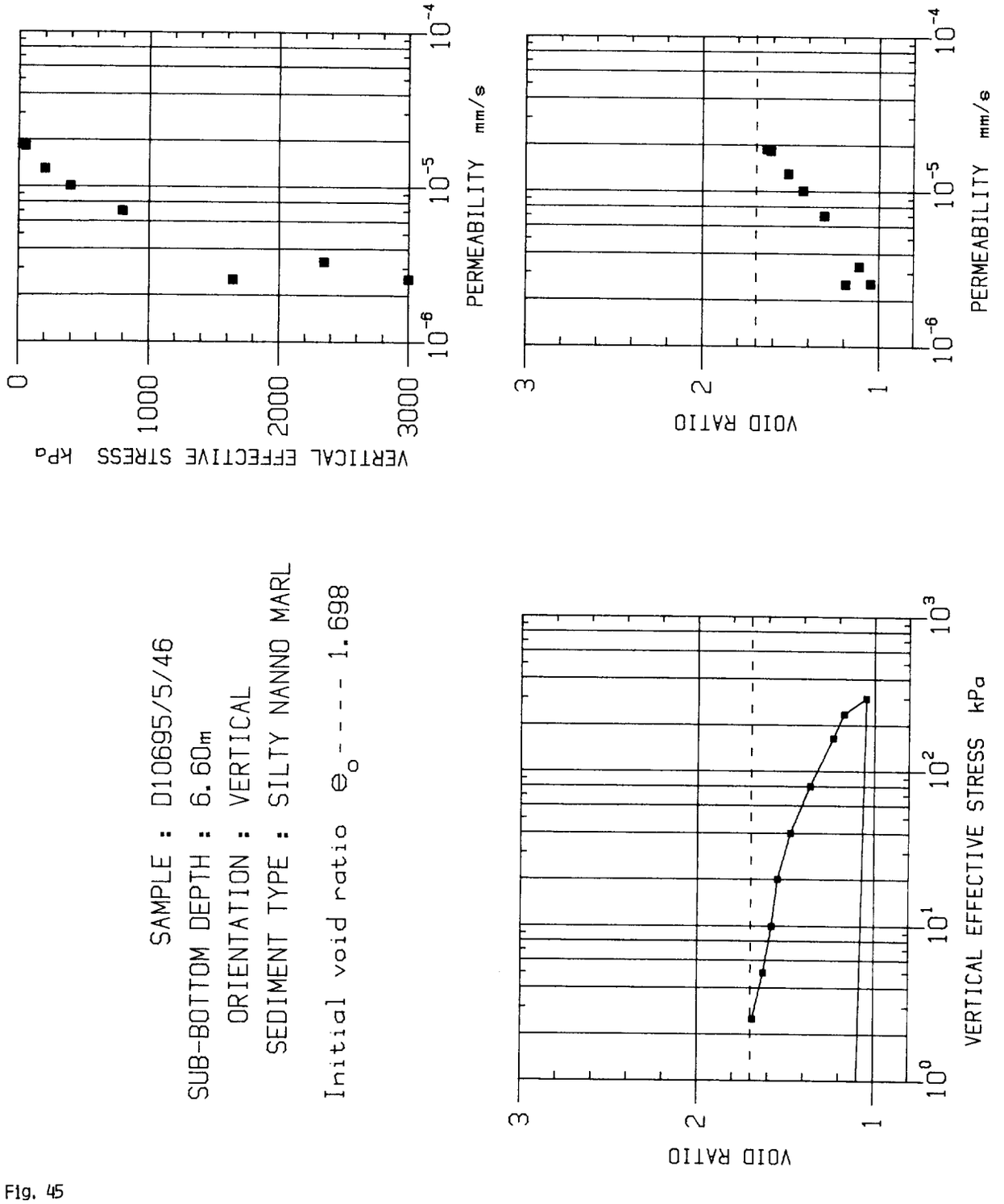
SAMPLE : D10695/5/46
SUB-BOTTOM DEPTH : 6.60m
ORIENTATION : VERTICAL
SEDIMENT TYPE : SILTY NANNO MARL
Initial void ratio e_o ---- 1.698
VERTICAL EFFECTIVE STRESS kPa
0
1000
2000
3000
10^{-6}
10^{-5}
10^{-4}
PERMEABILITY mm/s
VOID RATIO
1
2
3
VERTICAL EFFECTIVE STRESS kPa
10^{0}
10^{1}
10^{2}
10^{3}

Fig. 45

Fig. 46

SAMPLE : D10695/6/28
SUB-BOTTOM DEPTH : 7.94m
ORIENTATION : VERTICAL
SEDIMENT TYPE : NANNO MARL

Initial void ratio e_o - - - - 3.680

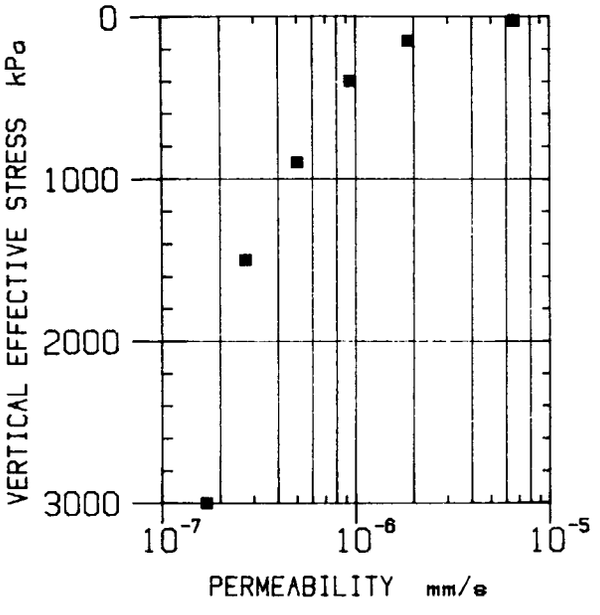

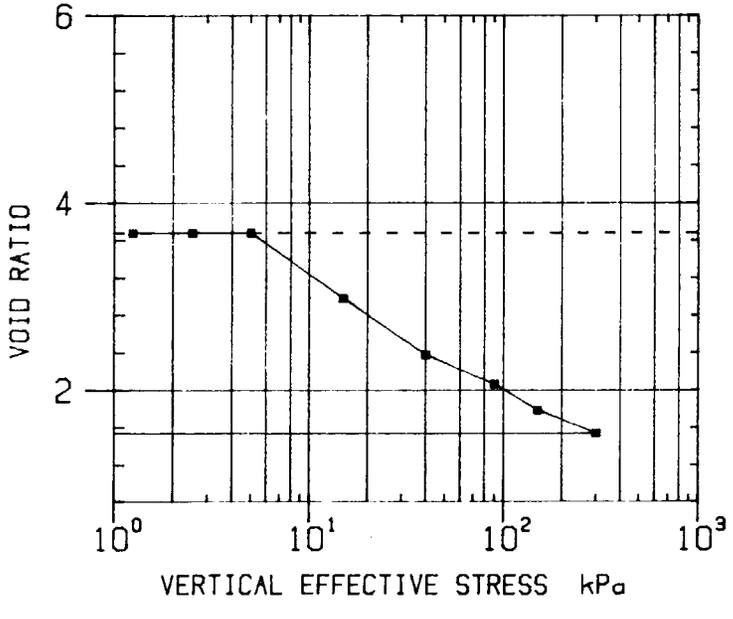

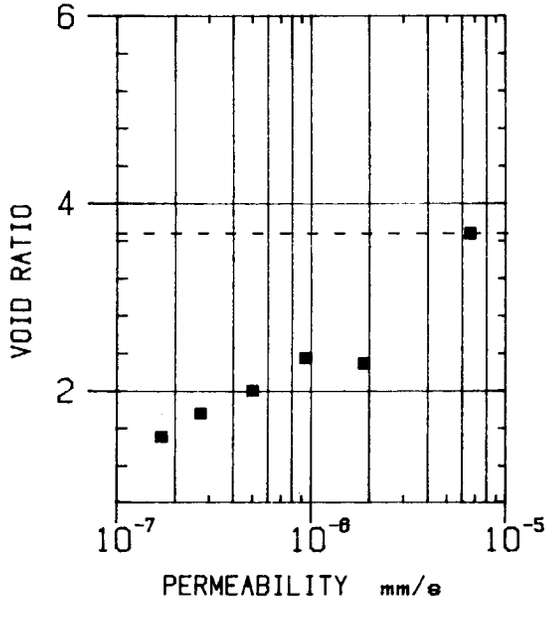

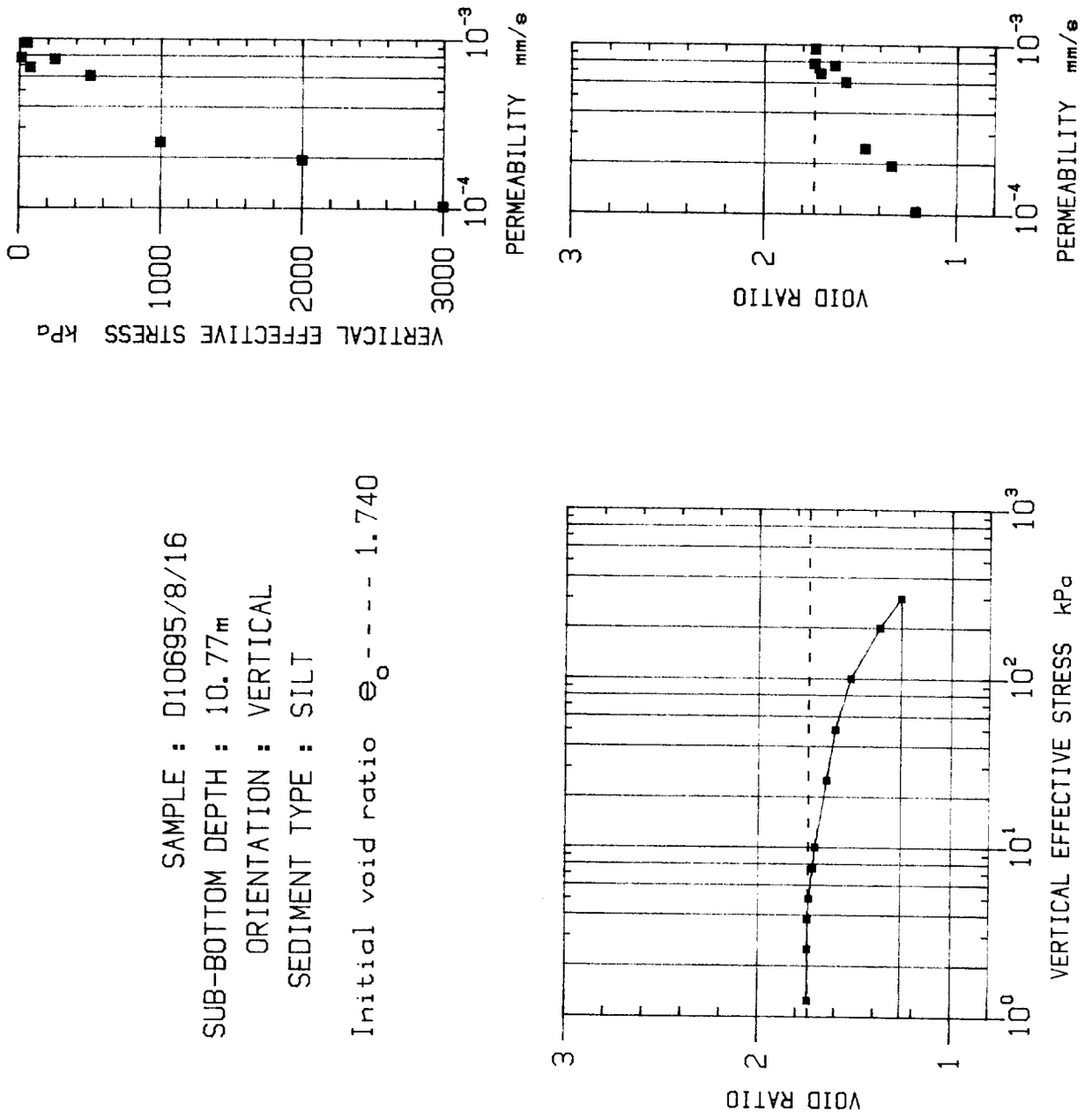
SAMPLE : D10695/8/16
SUB-BOTTOM DEPTH : 10.77m
ORIENTATION : VERTICAL
SEDIMENT TYPE : SILT
Initial void ratio e_o - - - - 1.740
VERTICAL EFFECTIVE STRESS kPa
0
1000
2000
3000
PERMEABILITY mm/s
10^{-3}
10^{-4}
VOID RATIO
1
2
3
VERTICAL EFFECTIVE STRESS kPa
10^0
10^1
10^2
10^3

Fig. 47

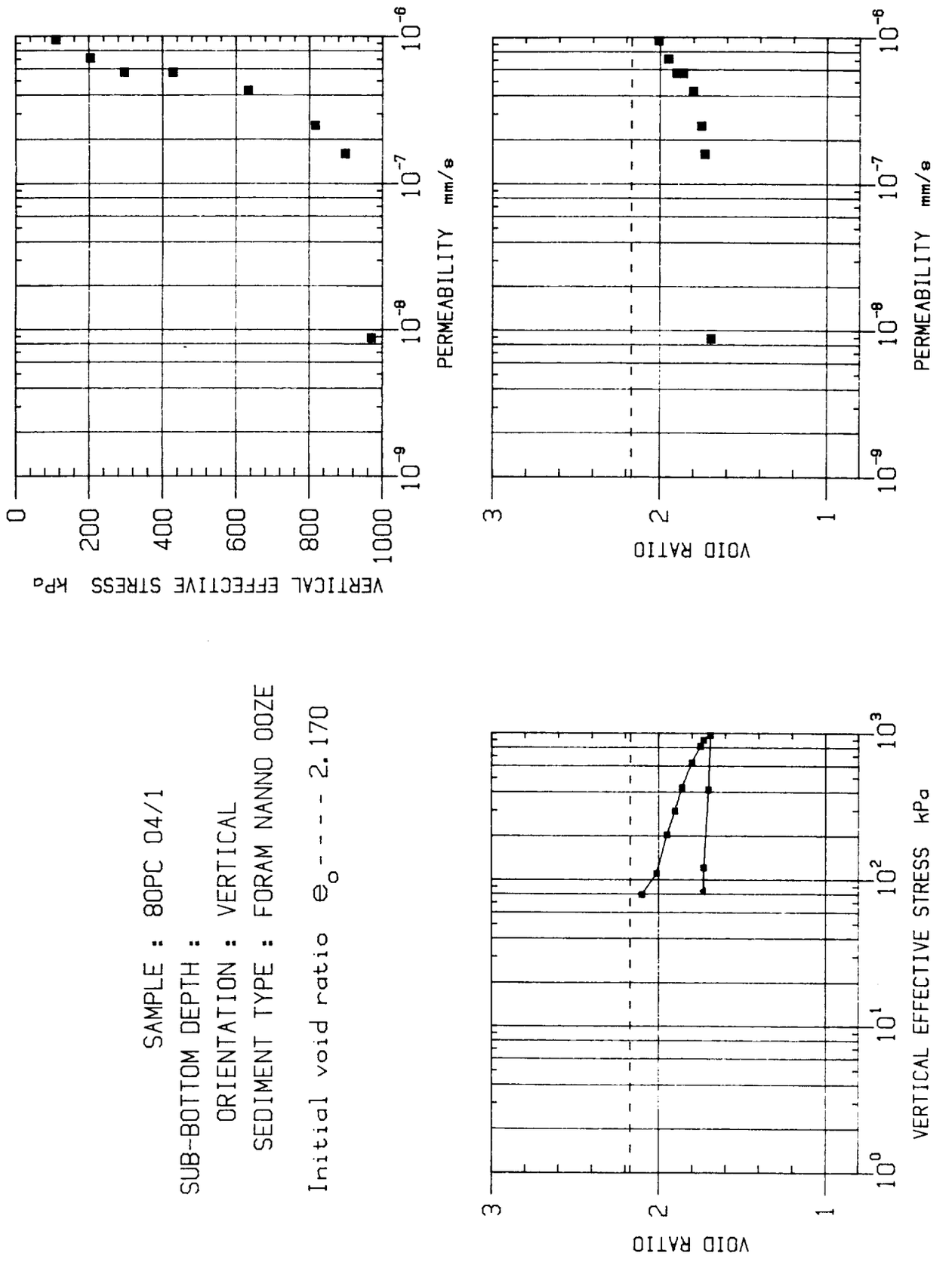
SAMPLE : 80PC 04/1
SUB-BOTTOM DEPTH :
ORIENTATION : VERTICAL
SEDIMENT TYPE : FORAM NANNO OOZE
Initial void ratio e_o - - - - 2.170
VERTICAL EFFECTIVE STRESS kPa
0
200
400
600
800
1000
PERMEABILITY mm/s
10^{-6}
10^{-7}
10^{-8}
10^{-9}
VOID RATIO
3
2
1
VERTICAL EFFECTIVE STRESS kPa
10^{0}
10^{1}
10^{2}
10^{3}

Fig. 48

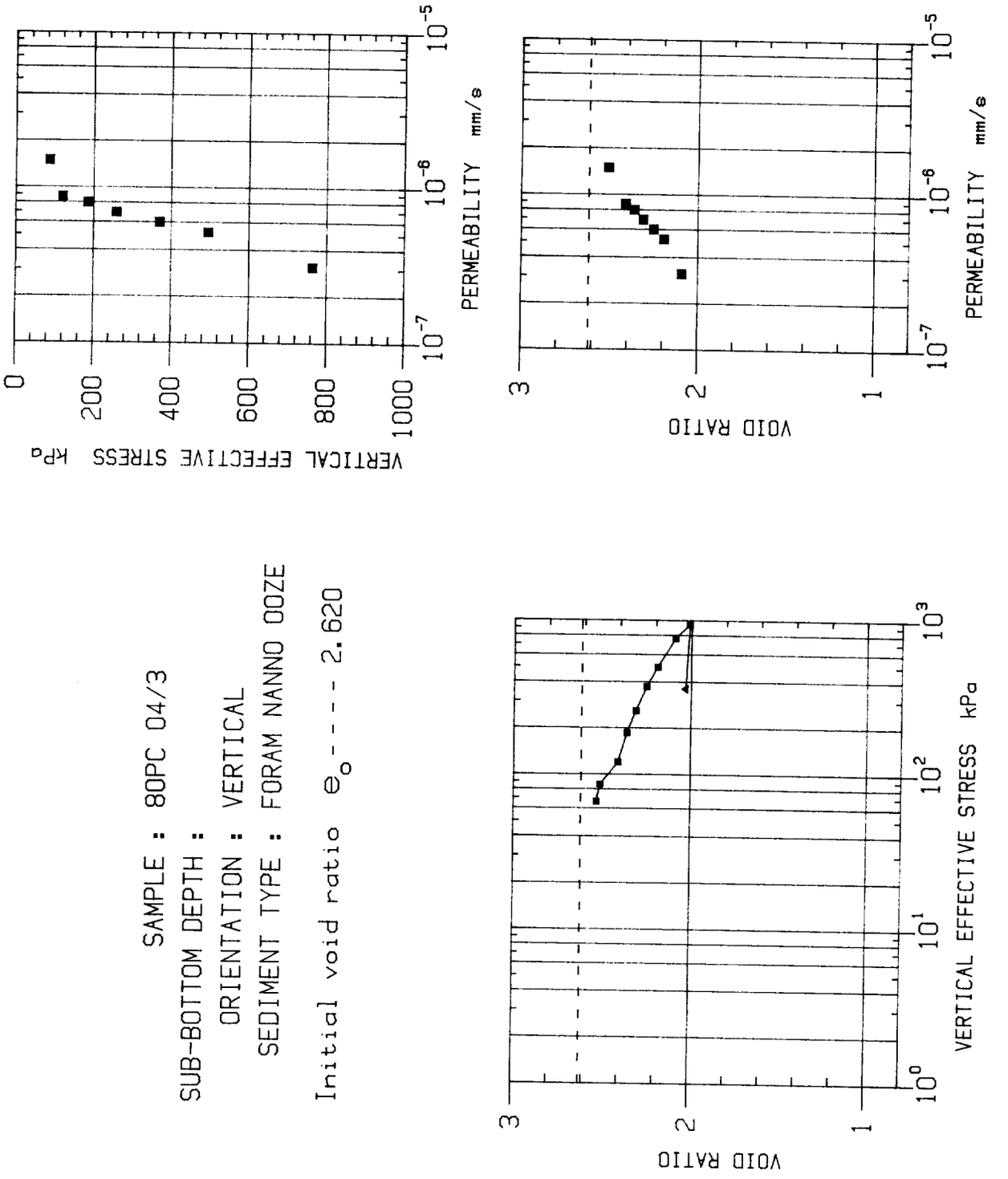
SAMPLE : 80PC 04/3
SUB-BOTTOM DEPTH :
ORIENTATION : VERTICAL
SEDIMENT TYPE : FORAM NANNO OOZE
Initial void ratio e_o ---- 2.620
VERTICAL EFFECTIVE STRESS kPa
0
200
400
600
800
1000
PERMEABILITY mm/s
10^{-5}
10^{-6}
10^{-7}
VOID RATIO
3
2
1
VERTICAL EFFECTIVE STRESS kPa
10^{0}
10^{1}
10^{2}
10^{3}

Fig. 49

Fig. 50

SAMPLE : S126/2-1
SUB-BOTTOM DEPTH : 0.44m
ORIENTATION : VERTICAL
SEDIMENT TYPE : NANNO MARL

Initial void ratio e_o - - - - 5.430

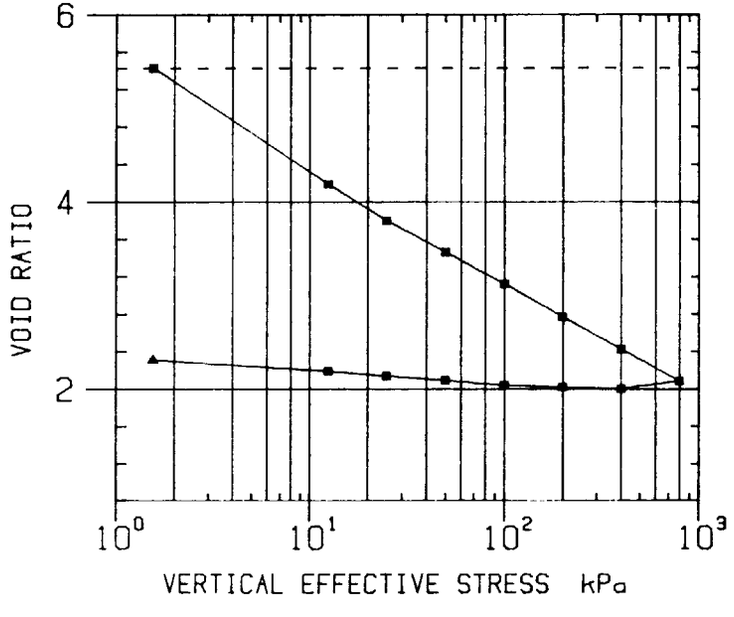

SAMPLE : S126/2-4
SUB-BOTTOM DEPTH : 0.70m
ORIENTATION : VERTICAL
SEDIMENT TYPE : FORAM NANNO MARL

Initial void ratio e_o - - - - 3.440

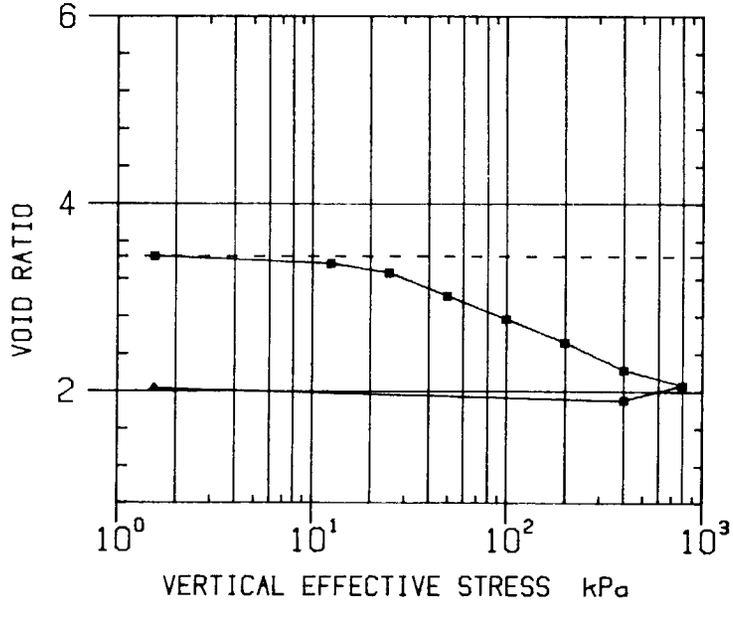

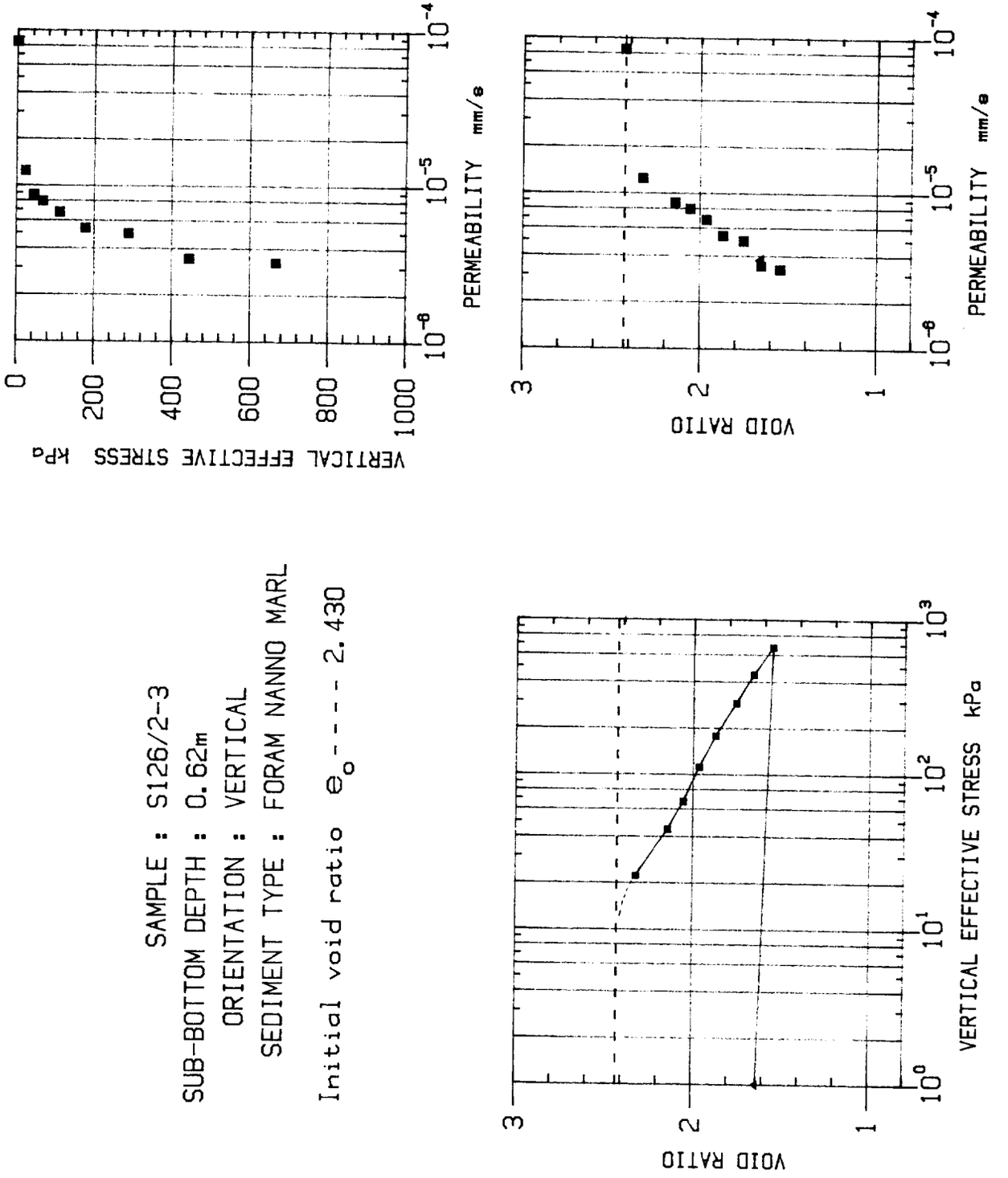
SAMPLE : S126/2-3
SUB-BOTTOM DEPTH : 0.62m
ORIENTATION : VERTICAL
SEDIMENT TYPE : FORAM NANNO MARL
Initial void ratio e_o - - - - 2.430
VERTICAL EFFECTIVE STRESS kPa
0
200
400
600
800
1000
PERMEABILITY mm/s
10^{-4}
10^{-5}
10^{-6}
VOID RATIO
3
2
1
VERTICAL EFFECTIVE STRESS kPa
10^{0}
10^{1}
10^{2}
10^{3}

Fig. 51

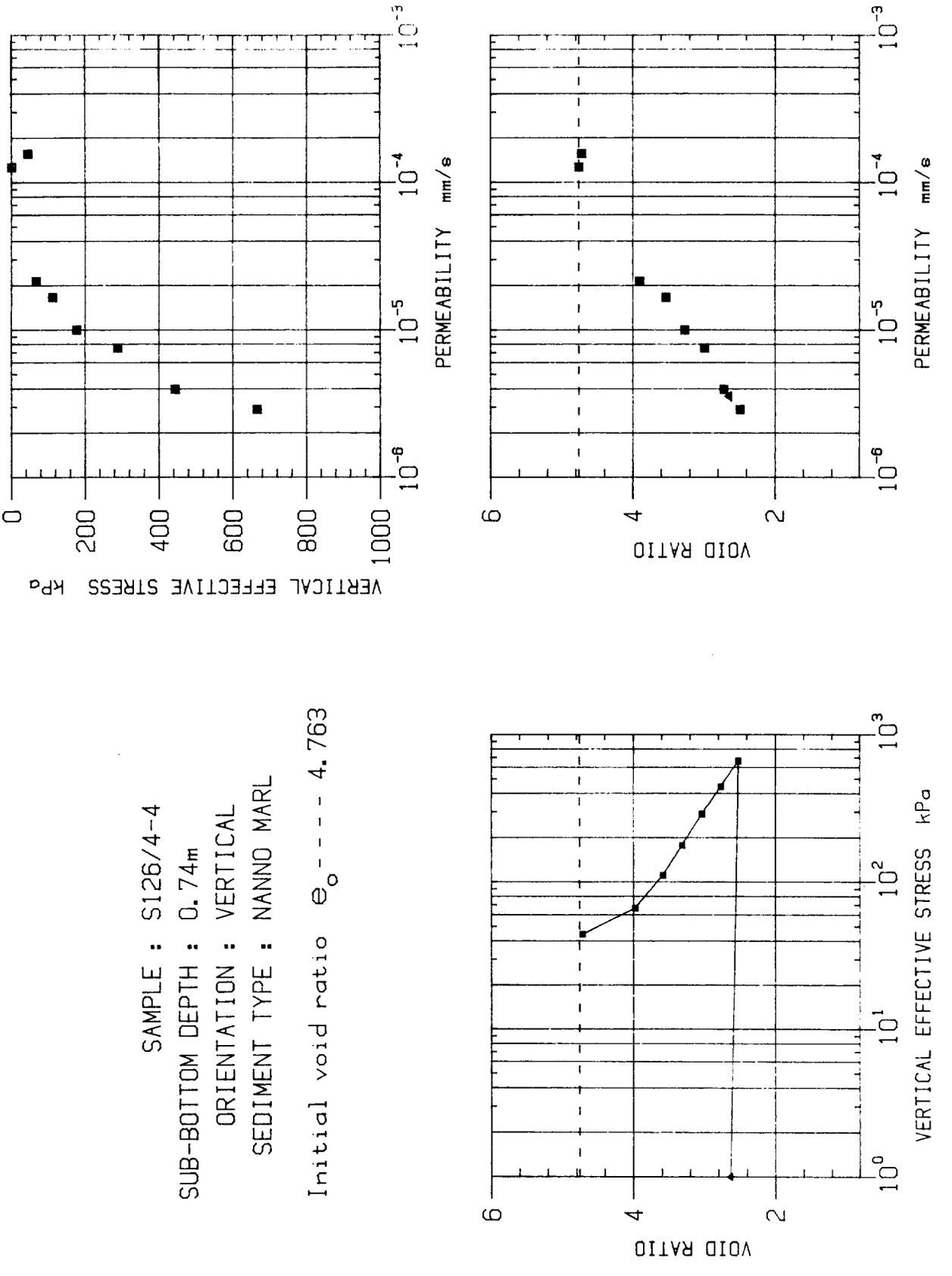
SAMPLE : S126/4-4
SUB-BOTTOM DEPTH : 0.74m
ORIENTATION : VERTICAL
SEDIMENT TYPE : NANNO MARL
Initial void ratio e_o ---- 4.763
VERTICAL EFFECTIVE STRESS kPa
0
200
400
600
800
1000
PERMEABILITY mm/s
10^{-3}
10^{-4}
10^{-5}
10^{-6}
VOID RATIO
2
4
6
VERTICAL EFFECTIVE STRESS kPa
10^{0}
10^{1}
10^{2}
10^{3}

Fig. 52

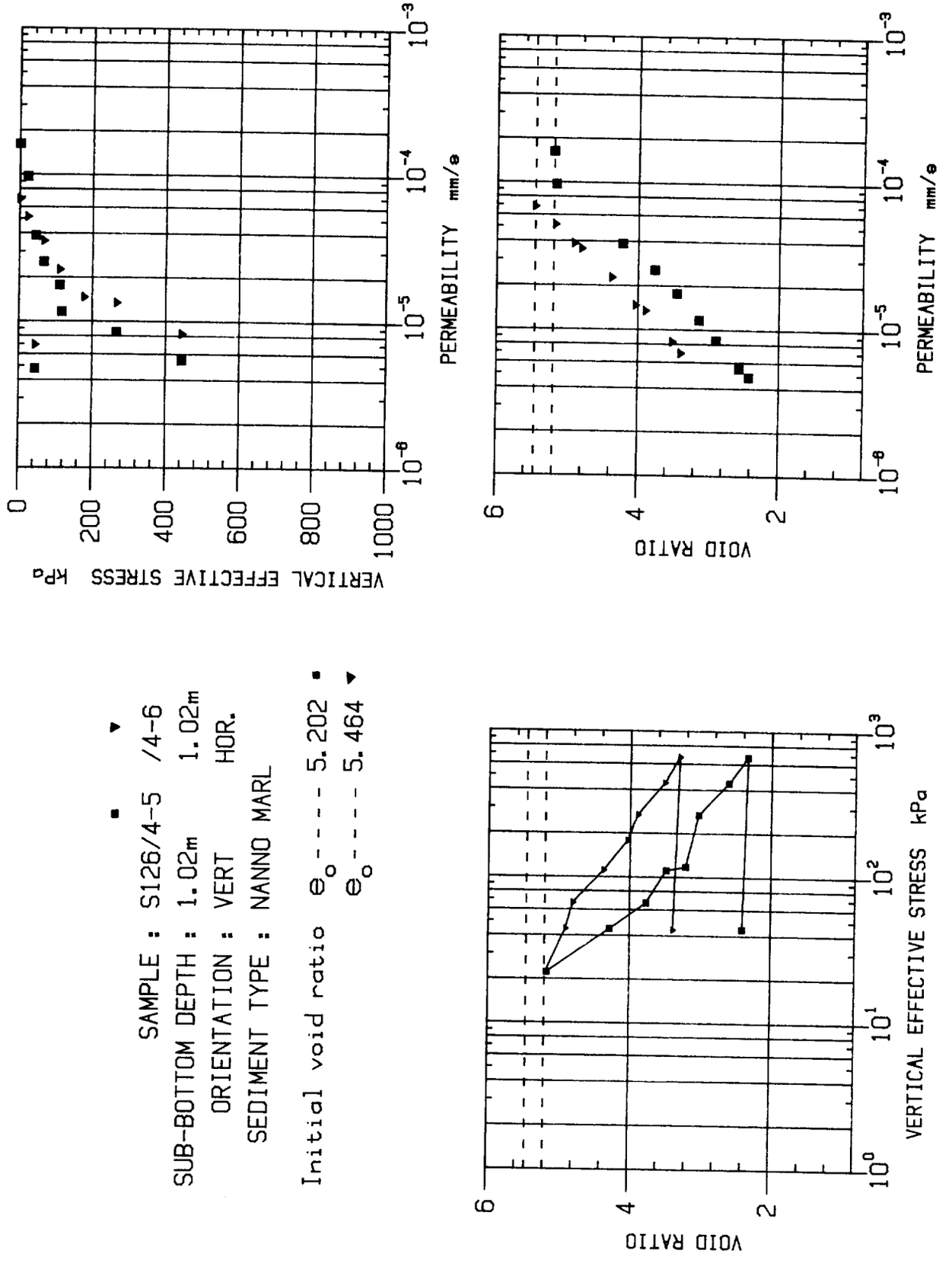
SAMPLE : S126/4-5 /4-6
SUB-BOTTOM DEPTH : 1.02m 1.02m
ORIENTATION : VERT HOR.
SEDIMENT TYPE : NANNO MARL
Initial void ratio e_o ---- 5.202
e_o ---- 5.464
VERTICAL EFFECTIVE STRESS kPa
VOID RATIO
PERMEABILITY mm/s

Fig. 53

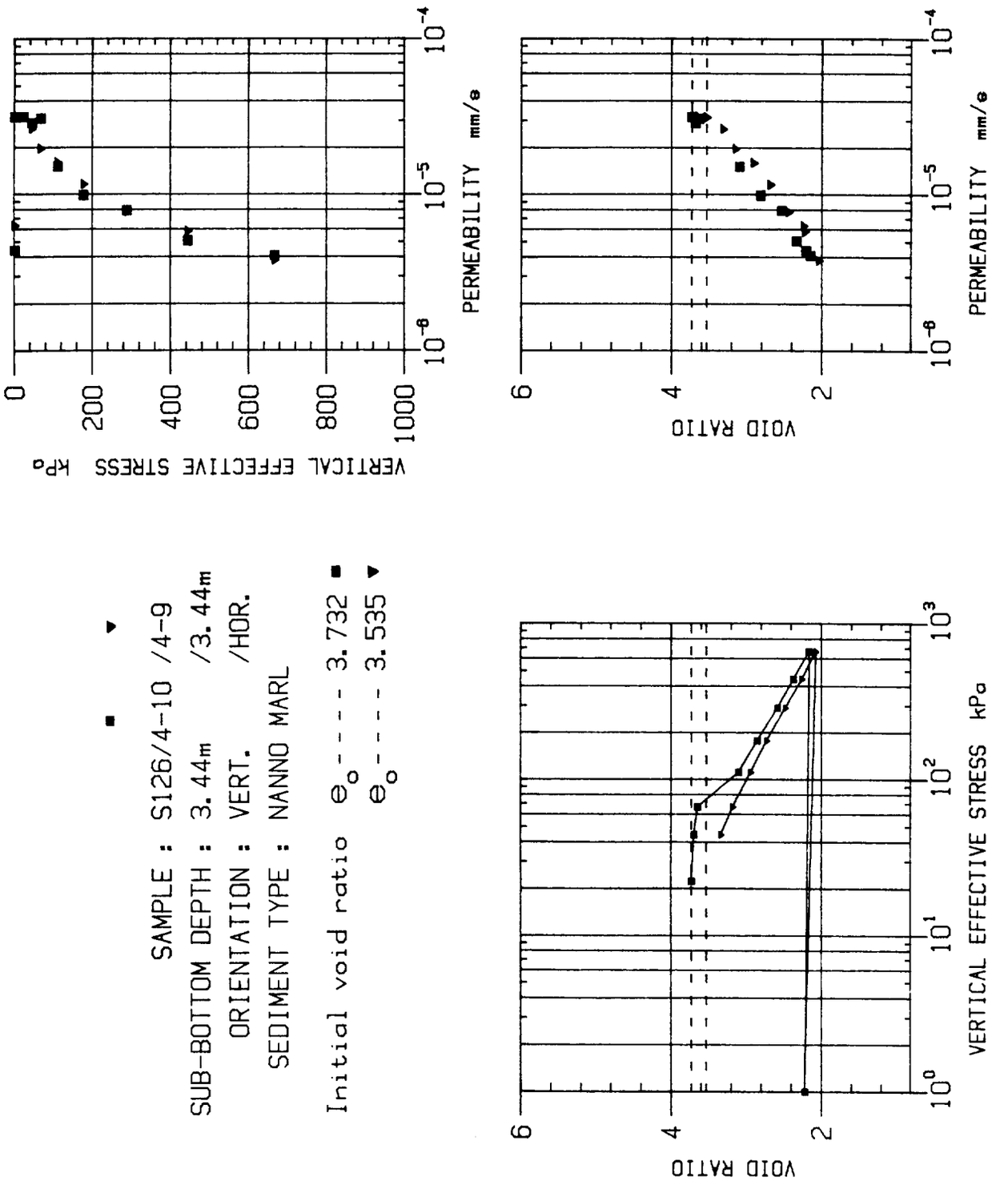
SAMPLE : S126/4-10 /4-9
SUB-BOTTOM DEPTH : 3.44m /3.44m
ORIENTATION : VERT. /HOR.
SEDIMENT TYPE : NANNO MARL
Initial void ratio e_o ---- 3.732
e_o ---- 3.535
VERTICAL EFFECTIVE STRESS kPa
VOID RATIO
PERMEABILITY mm/s

Fig. 54

Fig. 55

SAMPLE : S126/15-4
SUB-BOTTOM DEPTH : 1.66m
ORIENTATION : VERTICAL
SEDIMENT TYPE : CAL. PELAGIC CLAY

Initial void ratio e_o - - - - 2.220

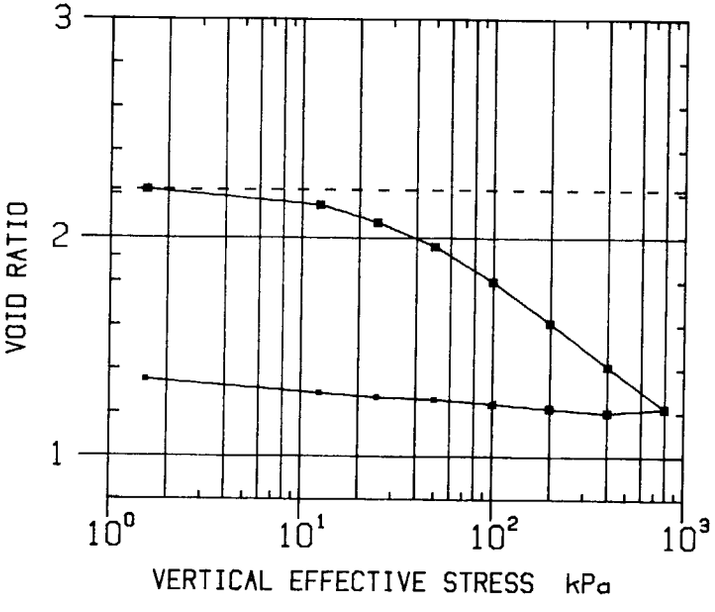

SAMPLE : S126/15-11
SUB-BOTTOM DEPTH : 1.79m
ORIENTATION : VERTICAL
SEDIMENT TYPE : CAL. PELAGIC CLAY

Initial void ratio e_o - - - - 2.540

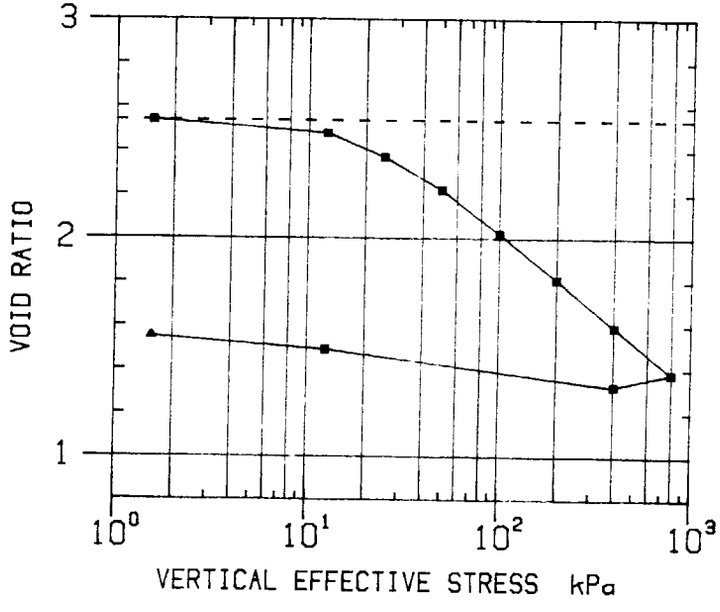

Fig. 56

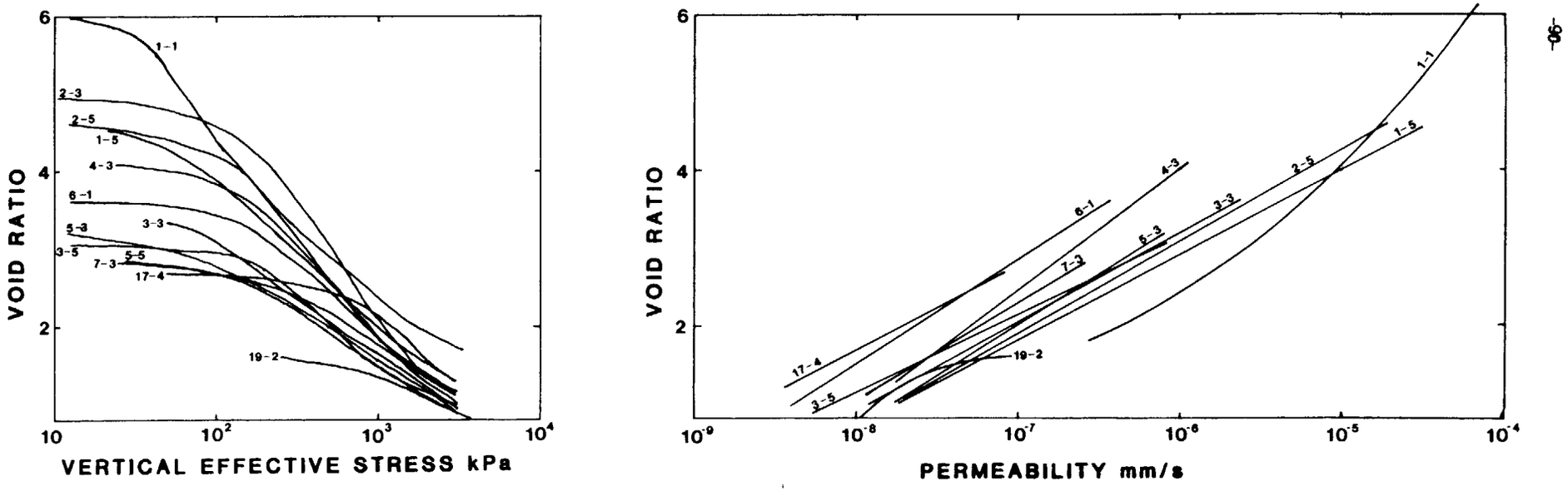

Consolidation and permeability data from DSDP sites 576 and 578.

Fig. 57

SAMPLE : GC577A-4-6
SUB-BOTTOM DEPTH : 37.4m
ORIENTATION : VERTICAL
SEDIMENT TYPE : FORAM NANNO OOZE

Initial void ratio e_o - - - - 1.590

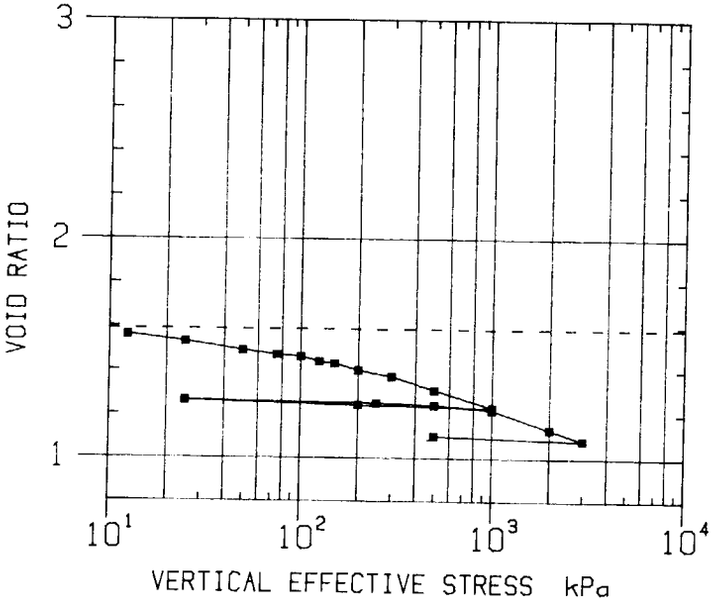

SAMPLE : GC577A-3-4
SUB-BOTTOM DEPTH : 24.9m
ORIENTATION : VERTICAL
SEDIMENT TYPE : FORAM NANNO OOZE

Initial void ratio e_o - - - - 1.840

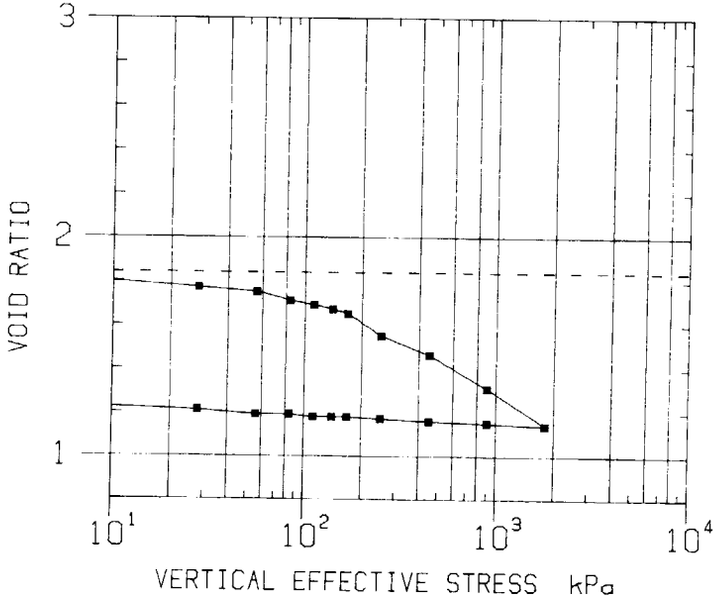

Fig. 58

SAMPLE : GC577A-8-4
SUB-BOTTOM DEPTH : 72.4m
ORIENTATION : VERTICAL
SEDIMENT TYPE : FORAM NANNO OOZE

Initial void ratio e_o - - - - 1.329

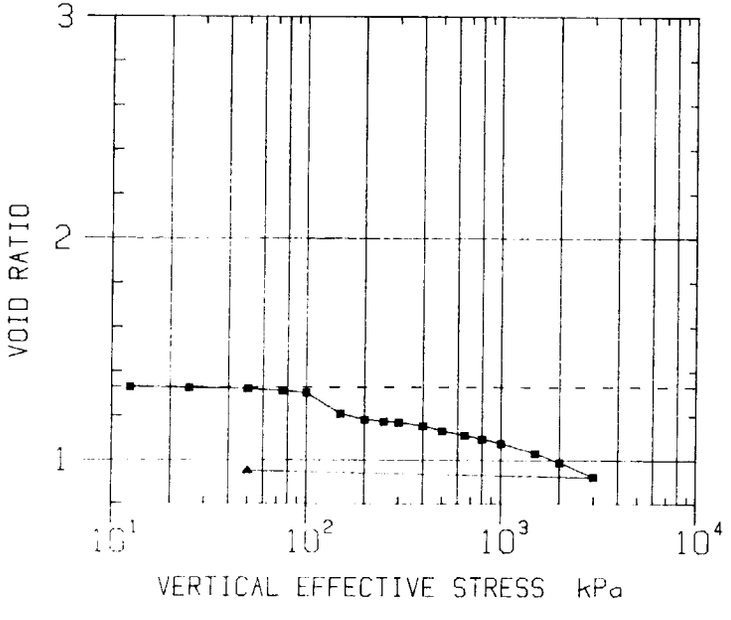

SAMPLE : GC577A-9-2
SUB-BOTTOM DEPTH : 78.9m
ORIENTATION : VERTICAL
SEDIMENT TYPE : FORAM NANNO OOZE

Initial void ratio e_o - - - - 1.240

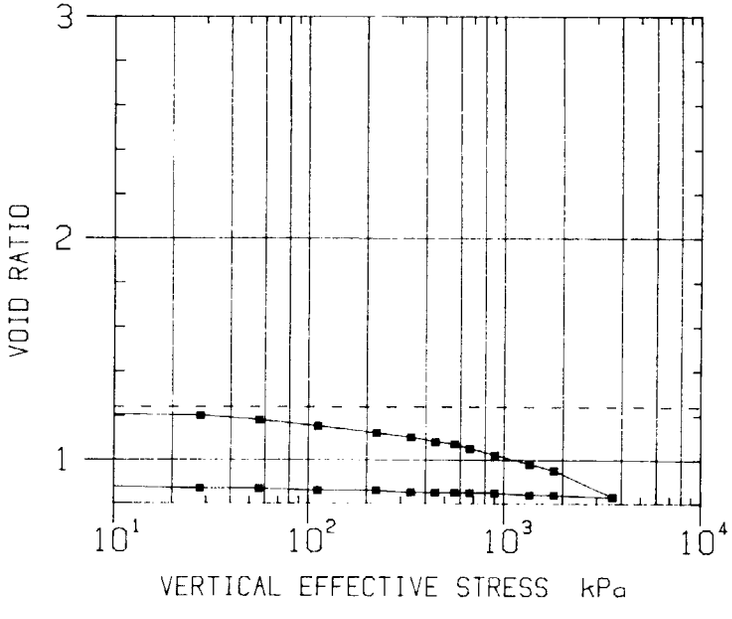

FIG. 59.

1	GC576A 3-5	PACIFIC RED CLAY
2	D10314/15	ATLANTIC RED CLAY
3	D10321/11	CAL. PELAGIC CLAY
4	D10333/7	FORAM/NANNO OOZE
5	D10695/2-14	NANNO FOSSIL MARL
6	D10695/8-16	SILT

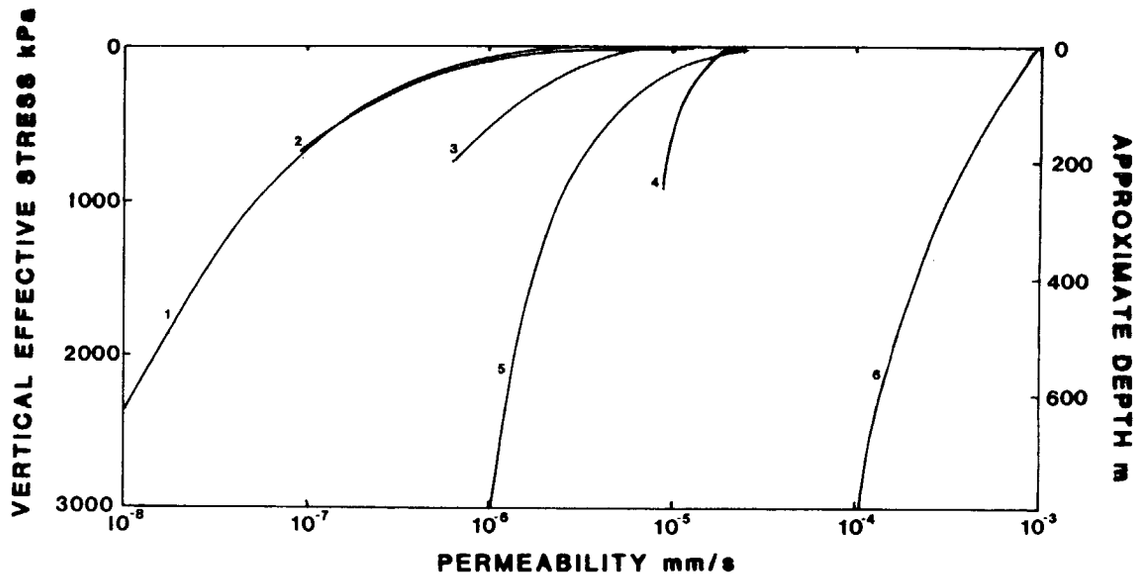

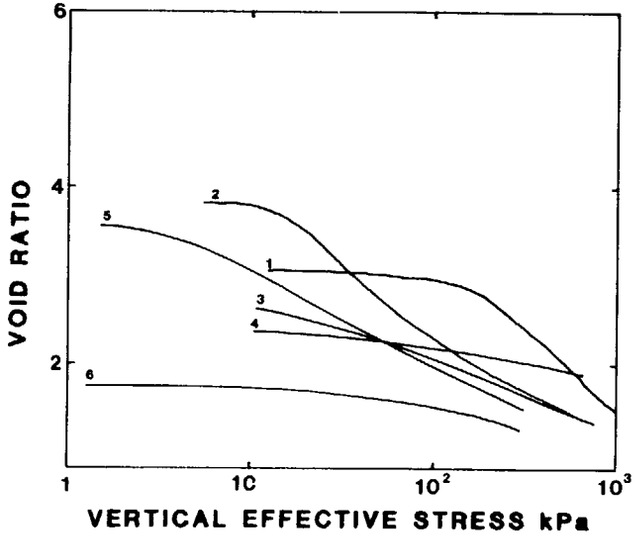

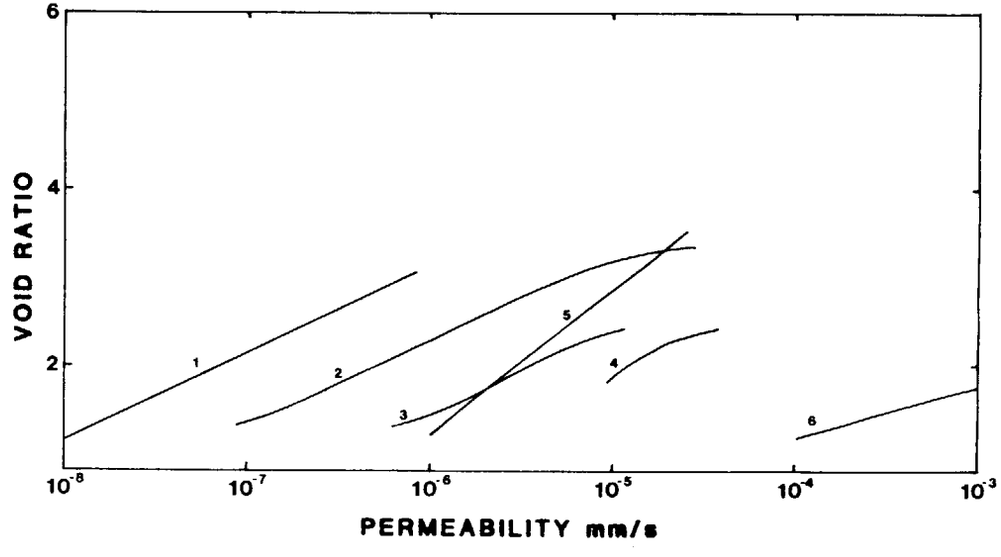

A comparison of the consolidation and permeability characteristics of different sediment types

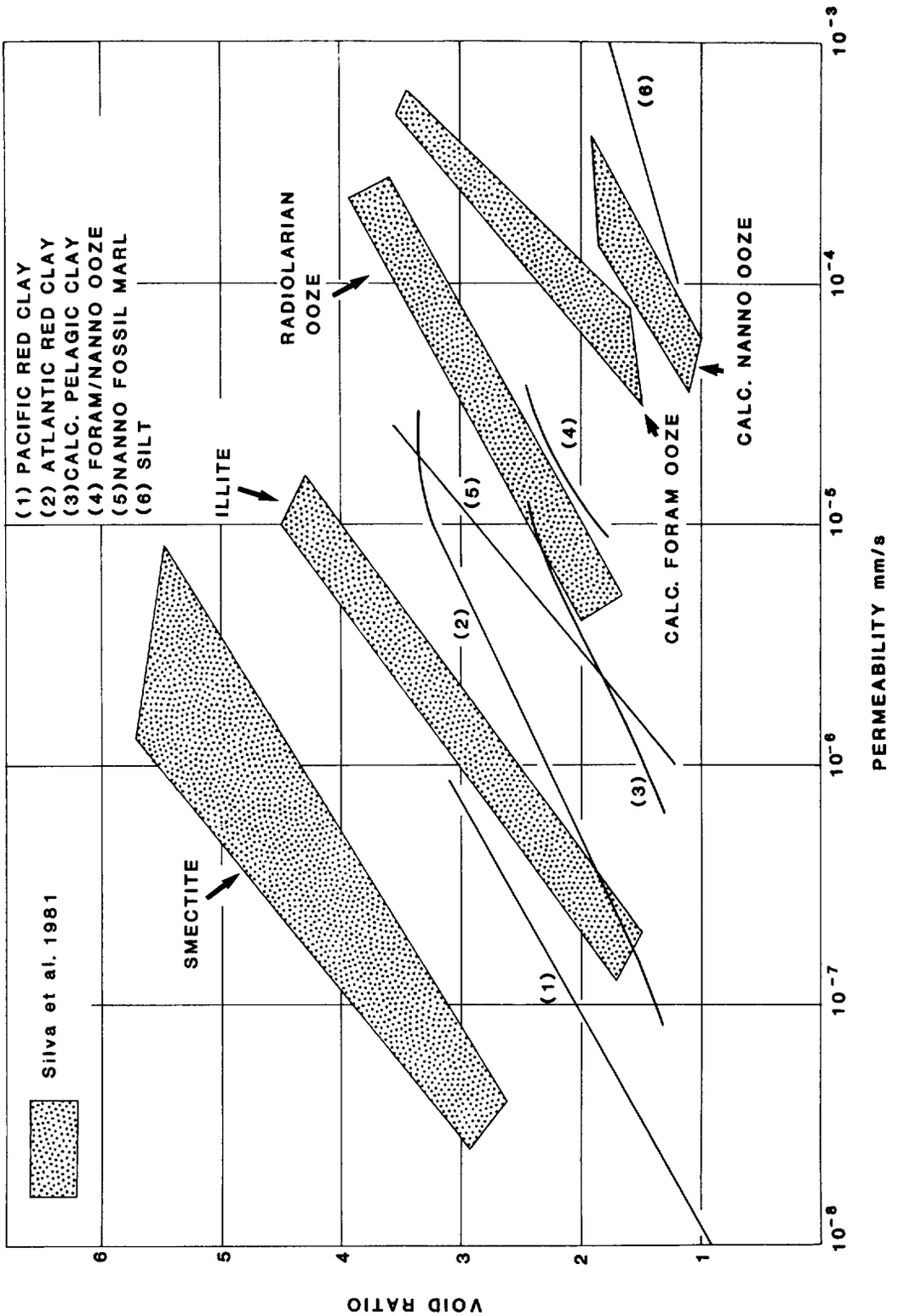

FIG. 60. Void ratio permeability plot showing data presented in this report compared with the data presented by Silva et al. (1981).